

Kirthikaa Balapattabi., Regulation of Supraoptic Vasopressin Neurons during Hypernatremia and Hyponatremia. Doctor of Philosophy (Biomedical Sciences), April 2019

This dissertation addresses the regulatory mechanisms of arginine vasopressin (AVP) secretion during salt loading (SL) and liver failure. The experiments focused on AVP neurons located in the supraoptic nucleus (SON) of hypothalamus that, along with other hypothalamic neurons, secrete AVP. This dissertation has two sections. The first section, specific aims 1a and 1b, examines AVP secretion with SL. Salt loading is associated with increased AVP release and mean arterial pressure. The male SL (2% NaCl for 7 days) rats secrete AVP despite increase in mean arterial pressure and were used as an animal model for this aim to study altered AVP neuron regulation. Previous work has shown that SL impairs baroreceptor mediated inhibition of rat AVP neurons through brain derived neurotrophic factor (BDNF) dependent activation of tyrosine receptor kinase B (TrkB) and downregulation of K⁺/Cl⁻ co-transporter (KCC2). This mechanism diminishes the GABA_A mediated inhibition of SON AVP neurons by increasing intracellular chloride ([Cl]_i). However, the source of BDNF leading to this ionic plasticity is unknown. In specific aim 1a, adeno-associated viral vectors with shRNA against BDNF were used to test if the SON is the source of BDNF contributing to increased AVP release and elevated mean arterial pressure in SL rats. In specific aim 1b, virally mediated chloride imaging with ClopHensorN was combined with single cell Western blot analysis by capillary based Simple Wes technology to verify the expression of KCC2 in the SON AVP neurons and to determine the role of TrkB-KCC2 mechanism in increased [Cl]_i in SL male rats.

In Aim 2, a more clinically relevant animal model was used to study regulatory mechanism leading to inappropriate increase in AVP secretion. Chronic bile duct ligated (BDL) rats were

used as animal model of liver failure induced hyponatremia due to inappropriate AVP release.

The findings and approaches from specific aim 1 were used to test the role of BDNF-TrkB-

KCC2 signaling in increased AVP secretion and hyponatremia during liver failure.

The experiments in this dissertation advance our understanding about the pathophysiology of AVP secretion. There are several novel findings from this work. First, SON was identified as the source of BDNF contributing to increase in $[Cl]_i$ of SON AVP neurons and AVP secretion in SL rats. Additionally, this is the first study to correlate the KCC2 protein expression in individual AVP neurons with its function using chloride imaging. Finally, these results are the first to demonstrate a mechanism that contributes to the increase in AVP secretion resulting in hyponatremia during liver failure.

Regulation of Supraoptic Vasopressin Neurons during
Hypernatremia and Hyponatremia

Kirthikaa Balapattabi

APPROVED:

Major Professor (J. Thomas Cunningham, Ph.D.)

Committee Member (Steve W. Mifflin, Ph.D.)

Committee Member (Ann M. Schreihof, Ph.D.)

Committee Member (Rong Ma, Ph.D.)

Committee Member (Rebecca L. Cunningham, Ph.D.)

University Member (Gulab Zode, Ph.D.)

Chair, Department of Physiology & Anatomy (Steve W. Mifflin, Ph.D.)

Dean (J. Michael Mathis, Ph.D., EdD), Graduate School of Biomedical Sciences

REGULATION OF SUPRAOPTIC VASOPRESSIN NEURONS DURING
HYPERNATREMIA AND HYPONATREMIA

DISSERTATION

Presented to the Graduate Council of the
Graduate School of Biomedical Sciences
University of North Texas
Health Science Center at Fort Worth
in Partial Fulfillment of the Requirements

For the Degree of

DOCTOR OF PHILOSOPHY

By

Kirthikaa Balapattabi

Fort Worth, Texas

April 2019

ACKNOWLEDGEMENTS

My foremost sincere thanks to my mentor, Dr. J. Thomas Cunningham for his willingness and patience to train me to be an independent scientist. I am very grateful to have Dr. Cunningham as my mentor, who is so invested in me and for all the valuable lessons from insightful discussions. All I have accomplished is only possible because of his careful guidance and heartfelt encouragement. In future I hope to mentor students with the care and dedication in which he mentored me.

The scope of my thesis was broadened immensely by the questions, insightful comments and encouragement by my dissertation committee, Drs. Rebecca Cunningham, Rong Ma, Steve Mifflin, Ann Schreihofner and Gulab Zode. I thank my committee members for taking an active interest in my project and their support at committee and progress meetings.

I thank Mr. Joel T. Little, Mrs. Martha Bachelor, Dr. George Farmer and Dr. Lei Wang for their generosity in helping me learn various scientific techniques. Dr. George Farmer played integral role in chloride imaging experiments. This dissertation work was funded by R01 grant from National Institute of Health and predoctoral fellowship from American Heart Association.

I am forever indebted to the University of North Texas Health Science Center community and all the professors who took the time to educate me. Thanks to all my friends, colleagues, staff and associates for their support and assistance.

Most importantly I would like to thank my beloved husband, Rangabhasyam for making this endeavor possible. My family: parents and sisters for their love and support from halfway around the world. So much gratitude to Almighty for all the opportunities and heartbreaks that contributed to my growth.

TABLE OF CONTENTS

ACKNOWLEDGEMENTS	ii
LIST OF TABLESvi
LIST OF FIGURES	vii
ABBREVIATIONSix
CHAPTER I.....	1
OVERVIEW OF DISSERTATION	1
REFERENCES	4
LITERATURE REVIEW.....	.8
CHRONIC OSMOTIC STRESS INDUCED VASOPRESSIN SECRETION8
REFERENCES	21
SPECIFIC AIMS AND HYPOTHESES.....	39
REFERENCES	40
CHAPTER II.....	43
HIGH SALT LOADING INCREASES BRAIN DERIVED NEUROTROPHIC FACTOR IN SUPRAOPTIC VASOPRESSIN NEURONS.....	43
ABSTRACT	44
INTRODUCTION	45
MATERIALS AND METHODS	47

RESULTS	53
DISCUSSION.....	57
REFERENCES.....	62
FIGURES & TABLES	67
CHAPTER III.....	78
INTRACELLULAR CHLORIDE REGULATION OF SUPRAOPTIC VASOPRESSIN	
NEURONS FROM SALT LOADED RATS.....	78
ABSTRACT.....	79
INTRODUCTION.....	81
MATERIALS AND METHODS	83
RESULTS	92
DISCUSSION.....	97
REFERENCES	102
FIGURES & TABLES	108
CHAPTER IV.....	119
BRAIN DERIVED NEUROTROPHIC FACTOR IN THE REGULATION OF SUPRAOPTIC	
VASOPRESSIN NEURONS IN DEVELOPMENT OF HYPONATREMIA.....	
ABSTRACT.....	120
INTRODUCTION.....	122
MATERIALS AND METHODS.....	123

RESULTS.....	128
DISCUSSION.....	133
REFERENCES.....	138
FIGURES.....	144
CHAPTER V.....	150
OVERALL DISCUSSION.....	151
REFERENCES.....	154
PERSPECTIVES & SIGNIFICANCE.....	159
FUTURE DIRECTIONS.....	165
REFERENCES.....	168
APPENDIX I.....	172
SEX DIFFERENCE AND HORMONES IN THE REGULATION OF VASOPRESSIN SECRETION DURING DILUTIONAL HYPONATREMIA.....	172
ABSTRACT.....	173
MATERIALS AND METHODS.....	175
RESULTS.....	179
REFERENCES	184
FIGURES.....	186

LIST OF TABLES

CHAPTER II – TABLE II-2 Primer sequences for qRT-PCR... ..	75
CHAPTER II – TABLE II-2 Plasma osmolality, hematocrit and AVP concentration... ..	76
CHAPTER II – TABLE II-3 Telemetry values: MAP and HR... ..	77
CHAPTER III – TABLE III-1 Plasma osmolality, hematocrit and CPP concentration... ..	118

LIST OF FIGURES

CHAPTER I - Figure I-1 – Increase in Vasopressin secretion during osmotic stress	7
CHAPTER I - Figure I-2 – Linear relationship between plasma AVP and osmolality	37
CHAPTER I - Figure I-3 – GABA Switch during development	38
CHAPTER I - Figure I-4 – Schematic representation of specific aims	42
CHAPTER II - Figure II-1 - LCM and gene expression of hits	67
CHAPTER II - Figure II-2 - LCM and gene expression of non-hits	69
CHAPTER II - Figure II-3 - Western blot images and protein expression	70
CHAPTER II - Figure II-4 - Fluid intake, urine excretion, food intake and body weight	72
CHAPTER II - Figure II-5 - Urine sodium excretion.....	73
CHAPTER II - Figure II-6 - Telemetry recordings: MAP & HR.....	74
CHAPTER III - Figure III-1 Immunofluorescence of AAV2-0VP1-GFP virus	108
CHAPTER III - Figure III-2 Fluid intake and body weight	109
CHAPTER III - Figure III-3 ClopHensorN images; CsCl and KGlu chloride recordings	110
CHAPTER III - Figure III-4- Responder - Protein expression of Eu SON AVP neuron.....	111
CHAPTER III - Figure III-5- Responder - Protein expression of SL SON AVP neuron.....	112
CHAPTER III - Figure III-6 - Non-Responder - Protein expression of SL SON AVP neuron .	113
CHAPTER III - Figure III-7 – Chloride imaging control experiment.....	114
CHAPTER III - Figure III-8 – Chloride imaging with KCC2 antagonists.....	115
CHAPTER III - Figure III-9 – Chloride imaging with NKCC1 antagonists	116
CHAPTER III - Figure III-10 – Chloride imaging with TrkB antagonists.....	117
CHAPTER IV - Figure IV-1 – Parameters of male BDL rats without stereotaxic injections	144
CHAPTER IV - Figure IV-2 –Protein expression of male BDL rats	145

CHAPTER IV - Figure IV-3 – BDL shBDNF Metabolic cage parameters	146
CHAPTER IV - Figure IV-4 – Plasma parameters and liver weight of BDL shBDNF rats	147
CHAPTER IV - Figure IV-5 –Protein expression of BDL shBDNF rats.....	148
CHAPTER V - Figure V-1 – Schematic representation of specific aims with results	163
APPENDIX I - Figure I-1 – Parameters of male and female sham/BDL rats	186
APPENDIX I - Figure I-2 – Immunohistochemistry of FosB and AVP expression in SON	187
APPENDIX I - Figure I-3 – Parameters of female and OVX sham/BDL rats	188
APPENDIX I - Figure I-4 – Adrenal steroid concentration in OVX sham/BDL rats	189

ABBREVIATIONS

AAV	Adeno-associated virus
aCSF	Artificial cerebrospinal fluid
ACT	Activity
ANP	Atrial natriuretic peptide
AT1aR	Ang II receptor type 1 subtype a
AVP	Arginine vasopressin
BDNF	Brain Derived Neurotrophic Factor
BCA	Bicinchoninic acid
BDL	Bile duct ligation
BDL SCR	BDL rats injected with SCR virus
BDLshBDNF	BDL rats injected with shBDNF virus
BSA	Bovine serum albumin
CCC	Chloride co-transporters
[Cl] _i	Intracellular chloride concentration
CNS	Central nervous system
CPP	Copeptin
CsCl	Cesium chloride
Ct	cycle threshold
CVO	Circumventricular organ
DAB	3,3' Diaminobenzidine
DMSO	Dimethyl sulfoxide
DTT	Dithiothreitol
E2GFP	Enhanced green fluorescent protein

ECF	Extracellular fluid
ELISA	Enzyme Linked Immunosorbent Assay
Eu	Euhhydrated
Eu SCR	Euhhydrated rats injected with SCR virus
Eu shBDNF	Euhhydrated rats injected with shBDNF virus
4-PL	Four parametric logistic analysis
PNZ	Perinuclear zone
GABA	Gamma aminobutyric acid
GAPDH	Glyceraldehyde 3-phosphate dehydrogenase
GFP	Green fluorescent protein
hnRNA	heteronuclear Ribonucleic Acid
HR	Heart Rate
IHC	Immunohistochemistry
KCC2	K ⁺ /Cl ⁻ Co-transporter 2
KGlu	Potassium Gluconate
LCM	Laser capture microdissection
MAP	Mean Arterial Pressure
MNC	Magnocellular Neurosecretory Cells
MnPO	Median preoptic nucleus
NaCl	Sodium Chloride
NT	Neurotrophin
NKCC1	Na ⁺ /K ⁺ /Cl ⁻ Co-transporter 1
OVLT	Organum vasculosum of Lamina Terminalis
OVX	Ovariectomized

OXT	Oxytocin
PBS	Phosphate-buffered saline
pKCC2	Phosphorylated K ⁺ -Cl ⁻ co-transporter 2
pTrkB	Phosphorylated tyrosine receptor kinase B
PVDF	Polyvinylidene difluoride
PVN	Paraventricular nucleus of hypothalamus
mRNA	messenger Ribonucleic Acid
RAS	Renin-Angiotensin system
RIPA	Radioimmunoprecipitation assay buffer
RT - PCR	Real time - Polymerase chain reaction
Salt SCR	Salt loaded rats injected with SCR virus
Salt shBDNF	Salt loaded rats injected with shBDNF virus
SCR	Short-hairpin RNA-scramble sequence
SDS	Sodium dodecyl sulphate
SEM	Standard error mean
SFO	Subfornical Organ
shBDNF	Short-hairpin RNA against BDNF
Sham SCR	Sham rats injected with SCR virus
Sham shBDNF	Sham rats injected with shBDNF virus
SL	Salt Loading
SON	Supraoptic nucleus of hypothalamus
TrkB	Tyrosine receptor kinase B
TRPV	Transient receptor potential channels of vanilloid subtype
WB	Western blotting

CHAPTER I

OVERVIEW OF DISSERTATION

Arginine Vasopressin (AVP) is synthesized in Magnocellular Neurosecretory Cells (MNCs) located in Supraoptic Nucleus (SON) and Paraventricular Nucleus (PVN) of the hypothalamus⁽¹⁻³⁾. This peptide hormone produced in the hypothalamus is axonally transported through the hypothalamic hypophyseal tract to the posterior pituitary. The AVP hormone is stored and systemically released from posterior pituitary in response to action potential from MNCs^(1,2). Release of AVP is highly regulated by plasma osmolality, blood pressure, and blood volume to maintain body fluid homeostasis⁽⁴⁻⁶⁾. Increased plasma osmolality activates hypothalamic MNCs increasing circulating AVP which acts at the kidneys to increase water reabsorption and maintain homeostasis. Conversely, decreased plasma osmolality is associated with inhibition of AVP MNCs, reduced plasma AVP, and diuresis. In normal conditions, a linear relationship between plasma AVP and osmolality is maintained by highly coordinated excitatory and inhibitory synaptic responses^(3,7). Altered synaptic homeostasis of vasopressinergic MNCs could contribute to disease conditions in which circulating AVP is abnormally elevated^(7,8). Despite vast existing knowledge about the regulation of AVP neurons^(4,6,9-12) the pathophysiology of inappropriate AVP secretion remains unknown.

SALT LOADING – AVP SECRETION

Salt loading (SL), giving rats only 2% NaCl to drink, increases AVP release from MNCs into systemic circulation due to increase in plasma osmolality. High salt intake causes hypernatremia leading to AVP release as a way to maintain plasma osmolality. The increase in mean arterial pressure during SL is partly mediated by AVP through the elevation of vascular resistance and renal water retention. However, the increased AVP secretion sustains despite elevated mean arterial pressure due to changes in the excitability of AVP neurons⁽¹³⁻¹⁵⁾.

Previous studies have shown that sustained AVP release in SL rats is due to impairment of GABA_A mediated inhibition of AVP neurons⁽¹³⁻¹⁵⁾. This study is focused on SON as it is less heterogeneous than PVN and we previously observed SL-mediated changes in GABA inhibition of SON MNCs.

The inhibitory effect of GABA depends on a low intracellular chloride concentration ($[Cl^-]_i$). Increases in $[Cl^-]_i$ can reverse the direction of chloride movement across the cell membrane and prevent GABA_A -mediated inhibition⁽¹⁶⁻¹⁸⁾. The balance between neural excitation and inhibition is crucial to maintain the concentration of circulating AVP within normal limits^(17, 18). In most neurons, $[Cl^-]_i$ is regulated by cation chloride cotransporters such as K⁺/Cl⁻ co-transporter 2 (KCC2), which causes efflux of Cl⁻ ions, and Na⁺/K⁺/Cl⁻ cotransporter 1 (NKCC1), which causes influx of Cl⁻ ions^(19, 20). Previous studies have shown that SL downregulates KCC2 through Brain derived Neurotrophic Factor (BDNF) dependent activation of tyrosine receptor kinase B (TrkB). This regulatory mechanism in the SON create a feed forward loop causing sustained AVP release. This dissertation is focused on determining the source of BDNF leading to increase in AVP secretion and mean arterial pressure in SL rats. Also, to determine the role of

the proposed mechanism in increase in $[Cl^-]_i$ leading to impairment of GABA_A mediated inhibition in SL male rats.

LIVER FAILURE - AVP SECRETION

Similar increases in AVP secretion are observed during liver failure which leads to hyponatremia. Dilutional hyponatremia is the most frequent electrolyte abnormality and is characterized by serum sodium <135 mEq/L. The cost of its treatment in the US has been estimated to be \$1.6-\$3.6 billion per year ⁽²¹⁻²³⁾. Hyponatremia often is related to congestive heart failure or liver failure. Hyponatremia caused by liver failure leads to ascites, seizures, pulmonary and cerebral edema due to inappropriate vasopressin release ⁽²¹⁾. The treatment of hyponatremia in the setting of liver failure is a challenge as conventional therapies are frequently inefficacious ^(24, 25). The development of effective therapeutic approaches for dilutional hyponatremia may require a better understanding of the molecular mechanisms behind the abnormality. This study contributes to this understanding by using chronic bile duct ligated rats, a model of dilutional hyponatremia due to increased AVP secretion associated with liver failure. In this study, we test the role of BDNF-TrkB signaling in the regulation of the main chloride extruder, KCC2, in the loss the GABA mediated inhibition of AVP neurons in male bile duct ligated rats.

REFERENCES

1. Cunningham JT, Penny ML, Murphy D. Cardiovascular regulation of supraoptic neurons in the rat: synaptic inputs and cellular signals. *Prog Biophys Mol Biol.* 2004; 84: 183-96.
2. Armstrong WE. Morphological and electrophysiological classification of hypothalamic supraoptic neurons. *Progress in Neurobiology.* 1995; 47: 291-339.
3. Di S, Tasker JG. Dehydration-induced synaptic plasticity in magnocellular neurons of the hypothalamic supraoptic nucleus. *Endocrinology.* 2004; 145: 5141-9.
4. Bourque CW. Central mechanisms of osmosensation and systemic osmoregulation. *Nat Rev Neurosci.* 2008; 9: 519-31.
5. Gizowski C, Bourque CW. The neural basis of homeostatic and anticipatory thirst. *Nature Reviews Nephrology.* 2017; 14: 11.
6. Verbalis JG. Osmotic Inhibition of Neurohypophysial Secretion. *Annals of the New York Academy of Sciences.* 1993; 689: 146-60.
7. Leng G, Brown CH, Bull PM, Brown D, Scullion S, Currie J, Blackburn-Munro RE, Feng J, Onaka T, Verbalis JG, Russell JA, Ludwig M. Responses of magnocellular neurons to osmotic stimulation involves coactivation of excitatory and inhibitory input: an experimental and theoretical analysis. *J Neurosci.* 2001; 21: 6967-77.
8. Potapenko ES, Biancardi VC, Zhou Y, Stern JE. Astrocytes modulate a postsynaptic NMDA-GABAA-receptor crosstalk in hypothalamic neurosecretory neurons. *J Neurosci.* 2013; 33: 631-40.
9. Carreño FR, Ji LL, Cunningham JT. Altered central TRPV4 expression and lipid raft association related to inappropriate vasopressin secretion in cirrhotic rats. *American Journal of Physiology - Regulatory, Integrative and Comparative Physiology.* 2009; 296: R454-R66.

10. Cunningham JT, Nedungadi TP, Walch JD, Nestler EJ, Gottlieb HB. Δ FosB in the supraoptic nucleus contributes to hyponatremia in rats with cirrhosis. *American Journal of Physiology - Regulatory, Integrative and Comparative Physiology*. 2012; 303: R177-R85.
11. Cunningham JT, Nissen R, Renaud LP. Norepinephrine injections in diagonal band of Broca selectively reduced the activity of vasopressin supraoptic neurons in the rat. *Brain research*. 1993; 610: 152-5.
12. Nedungadi TP, Cunningham JT. Differential regulation of TRPC4 in the vasopressin magnocellular system by water deprivation and hepatic cirrhosis in the rat. *American Journal of Physiology - Regulatory, Integrative and Comparative Physiology*. 2014; 306: R304-R14.
13. Choe KY, Han SY, Gaub P, Shell B, Voisin DL, Knapp BA, Barker PA, Brown CH, Cunningham JT, Bourque CW. High salt intake increases blood pressure via BDNF-mediated downregulation of KCC2 and impaired baroreflex inhibition of vasopressin neurons. *Neuron*. 2015; 85: 549-60.
14. Choe KY, Prager-Khoutorsky M, Farmer WT, Murai KK, Bourque CW. Effects of Salt Loading on the Morphology of Astrocytes in the Ventral Glia Limitans of the Rat Supraoptic Nucleus. *Journal of Neuroendocrinology*. 2016; 28.
15. Choe KY, Trudel E, Bourque CW. Effects of Salt Loading on the Regulation of Rat Hypothalamic Magnocellular Neurosecretory Cells by Ionotropic GABA and Glycine Receptors. *J Neuroendocrinol*. 2016; 28.
16. Rinehart J, Maksimova YD, Tanis JE, Stone KL, Hodson CA, Zhang J, Risinger M, Pan W, Wu D, Colangelo CM, Forbush B, Joiner CH, Gulcicek EE, Gallagher PG, Lifton RP. Sites of regulated phosphorylation that control K-Cl cotransporter activity. *Cell*. 2009; 138: 525-36.

17. Rivera C, Voipio J, Payne JA, Ruusuvuori E, Lahtinen H, Lamsa K, Pirvola U, Saarma M, Kaila K. The K⁺/Cl⁻ co-transporter KCC2 renders GABA hyperpolarizing during neuronal maturation. *Nature*. 1999; 397: 251-5.
18. Rivera C, Voipio J, Thomas-Crusells J, Li H, Emri Z, Sipila S, Payne JA, Minichiello L, Saarma M, Kaila K. Mechanism of activity-dependent downregulation of the neuron-specific K-Cl cotransporter KCC2. *J Neurosci*. 2004; 24: 4683-91.
19. Chamma I, Chevy Q, Poncer JC, Levi S. Role of the neuronal K-Cl co-transporter KCC2 in inhibitory and excitatory neurotransmission. *Frontiers in cellular neuroscience*. 2012; 6: 5.
20. Kim YB, Kim YS, Kim WB, Shen FY, Lee SW, Chung HJ, Kim JS, Han HC, Colwell CS, Kim YI. GABAergic excitation of vasopressin neurons: possible mechanism underlying sodium-dependent hypertension. *Circulation research*. 2013; 113: 1296-307.
21. Verbalis JG. Disorders of body water homeostasis. *Best Pract Res Clin Endocrinol Metab*. 2003; 17: 471-503.
22. Boscoe A, Paramore C, Verbalis JG. Cost of illness of hyponatremia in the United States. *Cost Effectiveness and Resource Allocation*. 2006; 4: 10-.
23. Braun MM, Barstow CH, Pyzocha NJ. Diagnosis and management of sodium disorders: hyponatremia and hypernatremia. *American family physician*. 2015; 91: 299-307.
24. Cardenas A, Arroyo V. Mechanisms of water and sodium retention in cirrhosis and the pathogenesis of ascites. *Best Pract Res Clin Endocrinol Metab*. 2003; 17: 607-22.
25. John S, Thuluvath PJ. Hyponatremia in cirrhosis: Pathophysiology and management. *World Journal of Gastroenterology : WJG*. 2015; 21: 3197-205.

CHAPTER I - Figure I-1 – Increase in Vasopressin secretion during osmotic stress

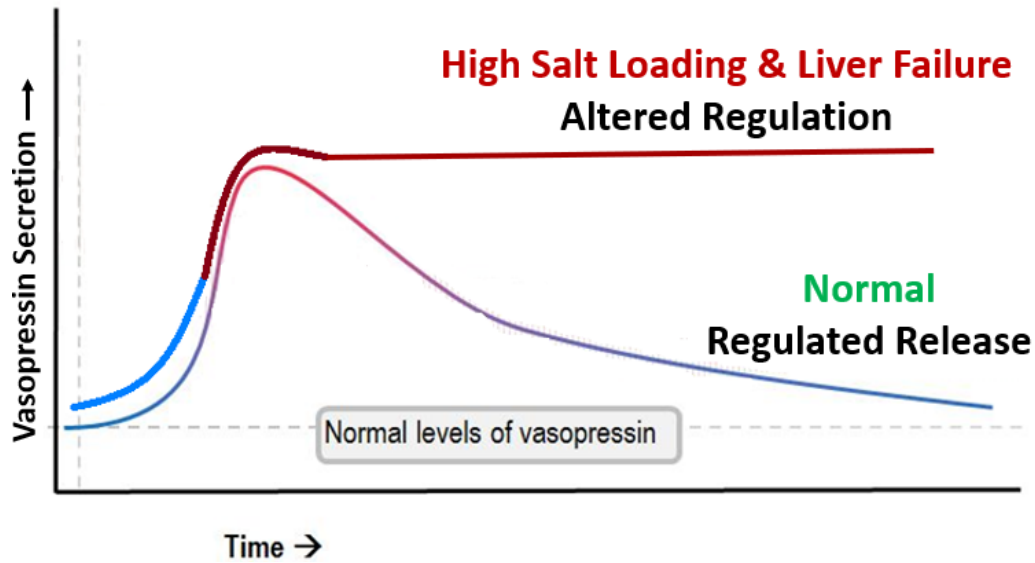


Figure 1: Arginine vasopressin (AVP) secretion with time is highly regulated during normal conditions that helps in maintaining normal levels of AVP. Altered regulation of AVP neurons leads to sustained increase in AVP secretion during high salt loading and liver failure.

LITERATURE REVIEW

CHRONIC OSMOTIC STRESS INDUCED VASOPRESSIN SECRETION

ARGININE VASOPRESSIN (AVP)

The first evidence of vasopressor activity of posterior pituitary extracts was shown by Oliver and Schäfer in 1895^(1,2) of which the active peptide was later identified as AVP. In 1913, Farini and von den Velden discovered the antidiuretic property of pituitary extract and used the extracts to successfully treat patients with diabetes insipidus, a condition marked by polydipsia and polyuria^(2,3). By 1928, the terms vasopressin and oxytocin were coined after they were separately purified⁽⁴⁾ and made available for physiological and clinical studies. The nine amino acid sequence and structure of AVP was not known until the work of du Vigneaud in 1950s which won the Nobel Prize for chemistry^(5,6). This work attributed the pressor and anti-diuretic properties of posterior pituitary extract to a single nonapeptide hormone, AVP.

The presence of arginine at the eighth position structurally distinguishes AVP from other forms of mammalian vasopressin. The AVP differs from oxytocin by only two amino acids at positions three and eight⁽⁷⁾. By 1947, Verney established that AVP release is controlled by central osmoreceptors located in or near the supraoptic nucleus of hypothalamus⁽⁸⁾. In late 1950s, Bargmann and Scharrer reported that the hormones of the posterior pituitary were produced by neurons in the hypothalamus. This moved the attention from the posterior pituitary products to the hypothalamus.

AVP SYNTHESIS AND SECRETION

Following the discovery by Bargmann and Scharrer⁽⁹⁾, AVP was demonstrated to be synthesized in magnocellular neurosecretory cells (MNCs) concentrated in the supraoptic nucleus (SON) and paraventricular nucleus (PVN) of hypothalamus using electron microscopy⁽²⁾. The SON is located behind blood-brain-barrier superior to the optic chiasm in the anterior region of

hypothalamus. The SON contains a homogenous composition of MNCs and acts as a primary source of circulating AVP and oxytocin ⁽¹⁰⁾. In the rat SON, AVP MNCs are clustered in the caudal portion of the nuclei and make up the majority (~60 – 70%) of cells ^(11, 12). The studies performed in the SON contributes to most available knowledge on AVP secretion.

The AVP is synthesized as a pre-prohormone, which includes an N-terminal signal peptide, vasopressin, neurophysin, and a C-terminal glycoprotein called copeptin ^(13, 14). After post-translational modifications in the Golgi apparatus, the hormone is stored in the vesicles of magnocellular cell bodies. AVP is axonally transported to replenish the store in neurosecretory vesicles located in Herring bodies of the posterior pituitary ^(13, 15-20). The hormone is released from posterior pituitary into systemic circulation in response to action potentials propagated from MNCs to axon terminals in the neurohypophysis ^(21, 22).

ACTIVITY DEPENDENT RELEASE OF AVP

The frequency of action potentials from MNCs determines the quantity of AVP hormone released ⁽²³⁾. Additionally, the basal firing frequency of MNCs establishes the osmotic set point ^(24, 25). The MNC action potential frequency (Hz) in rat with normal plasma osmolality (~ 294 mOsm/kg) is ~ 3 Hz ⁽²⁶⁻²⁸⁾, to maintain normal circulating AVP concentration ⁽²⁹⁾. Dehydration, hemorrhage, and hyperosmotic stimuli in rats, increases the MNC firing rate above basal frequencies up to ~ 15 Hz. The increase in frequency is shown to linearly correlate with increased AVP secretion ^(26-28, 30-32). It was shown by Douglas (1963) that the release of AVP from neurosecretory terminals occurs through exocytosis and is calcium dependent.

The depolarization of MNC axon terminals causes voltage-gated calcium channels (VGCC) mediated influx of calcium ions (Ca²⁺). The increase in Ca²⁺ fuses vesicles with the membrane

and release AVP into extracellular space from where it is released into peripheral circulation through fenestrated neurohypophyseal capillaries ^(19, 33-35).

REGULATION OF AVP SECRETION

Several intrinsic and extrinsic mechanisms regulate the activity of AVP MNCs and AVP release.

The activity of MNCs is regulated by non-osmotic and osmotic mechanisms through synaptic inputs from neuronal projections. Hemodynamic influences, hypotension and hypovolemia are the important non-osmotic factors that can potentially stimulate AVP release. Non-osmotic regulation is predominantly mediated by baroreceptor (BR) activation and is controlled by projections from various brainstem centers to the hypothalamus. It is well established that the ascending inputs from arterial BRs reach the nucleus of the tractus solitarius in the brainstem via cranial nerves IX and X ^(36, 37). It is from nucleus of the tractus solitarius the inputs are relayed to the locus coeruleus ⁽³⁷⁻³⁹⁾. The ascending relay of information between the BRs and the SON involves both neurons located in the nucleus of the diagonal band of Broca (DBB) and inhibitory interneurons located in the perinuclear zone (PNZ) that surrounds the SON ⁽⁴⁰⁻⁴⁵⁾. Several studies have shown that GABAergic neurons in the PNZ project into the SON ^(37, 40, 42).

The osmoreceptors are very sensitive to small (1-2%) increases in plasma osmolality. This causes linear graded secretion of AVP with osmotic stimulation (Figure 1). In normal conditions, the osmoregulatory set point or threshold at which AVP release is increased is 285mOsm/L in humans and 290mOsm/L in rats to maintain the osmolality within the normal range of 280-290mOsm/L ^(46, 47). The MNCs get afferent inputs from osmoreceptors located in the median preoptic nucleus (MnPO) and the circumventricular organs (CVOs): subfornical organ (SFO) and organum vasculosum of the laminae terminalis (OVLT) ^(19, 24, 48). In addition to controlling

AVP release, these hypothalamus regions also mediate the effects of angiotensin and collectively control thirst and centrally mediated natriuresis ⁽⁴⁹⁾.

Unlike the baroreceptor signaling, the neural projections for osmoregulation are controversial. But it is known that both the increase in arterial pressure detected by BRs and decrease in osmolality detected by osmoreceptors inhibit AVP MNCs through complex polysynaptic pathways leading to the activation of PNZ GABAergic neurons ⁽⁵⁰⁻⁵²⁾. The brainstem innervation to diagonal band of Broca through locus coeruleus appear to be involved in hypervolemia mediated inhibition of AVP release. The ventral median preoptic nucleus plays important role in osmoregulatory control of both thirst and AVP secretion and is shown to have possible inhibitory GABAergic innervation to the SON ^(51, 52).

The AVP neurons are also auto regulated by intrinsic osmosensory mechanisms or by somato-dendritic release of AVP ^(53, 54). These processes collectively alter the action potential firing rate of MNCs and subsequently AVP secretion from posterior pituitary. The evidence for osmoreceptors in SON MNCs was first provided by Mason in 1980 by recording the dissociated SON neurosecretory cells ⁽⁵⁵⁾. They increased the osmolality of the perfusate gradually which created correlating increase in firing rate of SON neurons independent of synaptic transmission ⁽⁵⁵⁾. The increase in cation conductance was observed in these neurons in addition to depolarization in the presence of hyperosmotic fluid ^(48, 55). Inversely, perfusing the acutely isolated SON neurons with hypoosmotic solution, hyperpolarize and inhibit cation conductance ⁽⁵⁶⁻⁵⁸⁾. The changes in cell volume and cation conductance of these neurons suggested the role of mechanosensitive non-selective cation channels in osmosensory transduction ⁽⁵⁶⁻⁵⁹⁾.

The subsequent studies provided evidence of the co-existence of TRPV1-4 in AVP MNCs of SON ^(60, 61). Mouse knockout studies have shown the role of TRPV1 during hyperosmotic

stimulation. The TRPV1 channels are activated by its interaction with microtubules during cellular shrinkage ^(62, 63). Both TRPV4 and TRPV2 are activated by hypoosmotic stimulation ^(60, 61). In contrary to these findings, few studies using TRPV 1 knockout rats suggest that TRPV1 channels are not necessary for AVP secretion and thirst stimulated by hypernatremia ⁽⁶⁴⁾. These studies also show that deletion of the TRPV1 and/or TRPV4 gene in mice do not disrupt thirst stimulated by acute hypernatremia or hyperosmolality ⁽⁶⁵⁾. The role of TRPV 1 and TRPV 4 in osmotransduction remains controversial.

Additionally, during hyponatremia the glial cells within SON release taurine which acts as an agonist for glycine receptor and activates glycine mediated inhibitory mechanism in the AVP neurons ^(22, 66, 67). The glial cells were reported to reversibly withdrawn from MNCs during hypernatremia induced by salt loading and dehydration ⁽⁶⁸⁻⁷⁰⁾.

OSMOREGULATORY FUNCTION OF AVP

The AVP secreted into systemic circulation acts on guanine nucleotide-binding (G) protein-coupled V2 and V1a receptors to maintain hydromineral and hemodynamic homeostasis respectively ^(7, 29). The vasoconstrictor effect was the first recognized functional characteristic of AVP, but its predominant function is traditionally described as osmoregulation ^(71, 72). The effect of AVP on function of renal AVP type 2 (V2) receptors alters tubular reabsorption and therefore plasma osmolality ⁽⁷⁾. Anti-diuresis occurs when AVP binds to V2 receptors located in the late distal tubules and collecting ducts of the kidneys ⁽⁷⁾. The binding of AVP to V2 receptors activates protein kinase A which in turn mobilizes aquaporin-2 channels to the surface. The surface expression of aquaporin-2 increases water reabsorption from the renal filtrate and concentrates the urine ^(52, 73). Urine concentration and excreted volume are linearly proportional to serum AVP in humans and rats ^(52, 73, 74).

HEMODYNAMIC FUNCTION OF AVP

AVP contributes to hemodynamic homeostasis by regulating vascular tone through the AVP type 1a (V1a) receptor pathways⁽⁷⁾. The smooth muscle of various blood vessels express V1a receptors^(75, 76). The V1a receptor is phosphorylated and activated upon binding of AVP. This results in the release of intracellular Ca²⁺ stores through sequential activation of second messengers, phospholipase C and inositol trisphosphate⁽⁷⁾. The increase in Ca²⁺ contracts the smooth muscle by interacting with the myosin. Few studies have shown that AVP blocks ATP-sensitive potassium (K_{ATP}) channels. K_{ATP} channels regulate vascular tone by inhibiting voltage-sensitive Ca²⁺ channels in smooth muscle cells⁽⁷⁷⁾. Similar to osmoregulation, the release of AVP to maintain arterial blood pressure occurs in a dose-dependent manner^{(7) (78, 79)}. The role of AVP in maintaining mean arterial pressure has been demonstrated by pharmacologically blocking V1 receptors during experimental hypovolemia and hypervolemia^(79, 80).

CHRONIC OSMOTIC STRESS INDUCED VASOPRESSIN SECRETION

Several chronic osmotic stresses have been shown to cause increased AVP release in rats: salt loading, liver failure, hemorrhage, and dehydration. This dissertation examines increased AVP secretion during salt loading and liver failure. Increase in circulating AVP associated with salt loading and liver failure was measured using ELISA to verify the animal models⁽⁸¹⁾.

SALT LOADING (SL)

Osmotic stress affects the action potential firing rate of MNCs in addition to their structural and functional properties. Salt loading (SL) by replacing drinking water with 2% NaCl leads to hypernatremia in male rats by increasing plasma osmolality. In SL male rats, MNCs continue to release AVP into systemic circulation despite elevated blood pressure⁽⁸²⁾. This makes SL rats a model to study changes in neuronal regulation of AVP release due to chronic osmotic stress.

Hypertremia caused by high salt intake leads to increased AVP release as a feedback mechanism to maintain plasma osmolality. Increased mean arterial pressure in SL rats is partly mediated by AVP, likely due to the elevation of vascular resistance and renal water retention. Previous studies have reported morphological and structural modification in both the SON and in the neurohypophysis during salt loading^(30, 83). The glial-neuron interaction in the SON undergo a structural change in response to salt loading. Previous studies have reported coordinated astrocytic withdrawal from the SON neurons^(37, 83, 84). Additionally, the functional plasticity induced by salt loading results in decrease in GABAergic and taurine input and increases translocation of transporters from the membrane^(24, 85). Furthermore, cellular processes such as signal transduction and gene expression are also modulated in the MNCs during salt loading, leading to an increase in AVP gene expression^(37, 69, 81, 82, 86). The mechanisms of these changes are not completely understood.

LIVER FAILURE

Liver failure induced hyponatremia results mainly from a decrease in plasma osmolality due to increased AVP secretion. The decrease in plasma volume and vasodilation in response to portal hypertension disturb the normal circulatory physiology during liver failure and are reported to increase AVP secretion as a compensatory mechanism^(60, 87-89). In liver failure patients, the secretion of AVP is not suppressed relative to plasma osmolality leading to hyponatremia that increases morbidity and mortality of these patients^(52, 90). The traditional treatment involves diuretics, hypertonic saline, V1a/V2 nonselective inhibitor conivaptan and selective V2 antagonist tolvaptan^(91, 92). These treatments are mostly inefficacious and have several limitations^(52, 90). The most important limitations are hypotension and thirst with administration of vaptans^(91, 92). Dilutional hyponatremia due to inappropriate AVP release is a common

electrolyte disorder in the clinic, but the mechanisms leading to increases in AVP secretion have not been investigated.

Common animal models of liver failure include chronic bile duct ligation, total or partial hepatectomy, and D-galactosamine induced biliary fibrosis. In addition, toxic agents such as carbon tetrachloride (CCl₄), thioacetamide (TAA), dimethylnitrosamine (DMN), and diethylnitrosamine (DEN) are used to induce liver failure^(93, 94). The development and severity of some of these models depend on the dosage, frequency, and route of administration^(93, 94). Chronic bile duct ligated rat model develops hyponatremia due to increased AVP secretion related to liver failure^(60, 61, 88). This model is widely used as it is reproducible and the survival rate associated with this model is higher compared to other liver failure animal models. Several studies using bile duct ligated male rats have shown AVP neuron activation accompanied by increased AVP hnRNA expression and elevated circulating AVP concentration^(88, 95, 96). The bile duct ligation for four weeks leads to hyponatremia as indicated by the decrease in plasma osmolality and hematocrit values^(60, 88, 95, 96).

INTRACELLULAR CHLORIDE CONCENTRATION AND GABA SWITCH

The intracellular chloride concentration [Cl]_i in SON neurons is primarily regulated by cation chloride co-transporters (CCC), Na⁺/ K⁺/ Cl⁻ cotransporter (NKCC1) and K⁺/ Cl⁻ cotransporter (KCC2). The KCC2 cotransporter was first identified in neurons by Payne in 1996^(97, 98).

NKCC1 and KCC2 have been strongly implicated in the maturation of GABAergic transmission^(99, 100). The later studies by Claudio Rivera and collaborators demonstrated that the [Cl]_i in developing immature neurons is higher than the mature neurons due to a high NKCC1 and low KCC2 expression⁽¹⁰⁰⁾. The movement of chloride ions through the GABA_A receptor is determined by the concentration gradient across the cell membrane. This leads to chloride efflux

and a depolarization of the neuron during GABA_AR-mediated synaptic activity. In mature neurons, the activity of KCC2 is higher than NKCC1 which primarily contributes to maintaining low [Cl]_i. This predominant KCC2 activity accounts for the hyperpolarizing response upon synaptic GABA_AR activation by changing the flux of chloride ion through GABA receptor⁽¹⁰¹⁾. The [Cl]_i mediated GABA switch in developing and mature neurons is shown in Figure 2. Hence, changes in the activity of these transporters directly impact synaptic transmission and have been involved in various pathological conditions^(37, 81, 82).

MEMBRANE EXPRESSION OF KCC2

The KCC2 is expressed throughout the CNS. However, KCC2 expression and localization at the membrane is tightly regulated by neuronal activity and during brain development. The posttranslational modifications of amino acid residues of KCC2 are involved in both membrane expression and transport function. The protein kinase C (PKC) mediated phosphorylation of Ser940 residue has been shown to decrease endocytosis resulting in increased KCC2 activity and membrane stability⁽¹⁰²⁻¹⁰⁴⁾. The phosphorylation and dephosphorylation of Ser940 parallels the maturation of GABAergic transmission^(105, 106). The Thr906 and Thr1007 residues are involved in cellular volume regulation through With No Lysine (WNK) Kinases and/or Ste20p-related proline/Alanine-rich kinase (SPAK) - oxidative stress-responsive kinase-1 (OSR1) pathway⁽¹⁰⁷⁾. The phosphorylation of Tyr1087 is not completely understood. It is thought to inactivates KCC2 in heterologous systems^(108, 109) or neurons⁽¹¹⁰⁻¹¹²⁾ without affecting its membrane expression.

BDNF-TrkB MECHANISM

One important mechanism that contributes to the downregulation of KCC2 involves Brain-Derived Neurotrophic Factor (BDNF) dependent activation of tyrosine receptor kinase B (TrkB)

^(81, 82). The BDNF belongs to the family of neurotrophins that includes nerve growth factor (NGF), neurotrophin 3 (NT-3), and neurotrophin 4 (NT-4). Neurotrophins are known to play significant roles in proliferation, differentiation and survival of neurons present in both central and peripheral nervous systems during embryogenesis ^(113, 114).

The BDNF has varied and complicated functions in various regions of CNS from early stages of development throughout the life span ⁽¹¹⁵⁾. In the mature animals, BDNF is known to be expressed in hippocampus, hypothalamus, cortex, cerebellum, and in few regions of the brain stem ⁽¹¹⁶⁻¹¹⁸⁾. The BDNF plays role in synaptic plasticity in the hippocampus but its function is less well defined in the hypothalamus ⁽¹¹⁹⁾. Previous studies have shown that BDNF expression can be regulated by several neurotransmitters such as serotonin, glutamate, acetylcholine and GABA ⁽¹¹⁶⁾. Additionally, the modulation of neuronal activity due to osmotic or immobilization stress can increase the expression of BDNF.

BDNF SYNTHESIS AND SIGNALING

The BDNF is synthesized as proBDNF of 30–35 kDa size. It is proteolytically cleaved by proconvertases or proteinases at a highly conserved dibasic amino acid motif site resulting in proBDNF, which is then converted to mature BDNF ^(120, 121). The structure of mature BDNF is 50% identical to the proBDNF. The BDNF packaged into vesicles and undergoes activity-dependent release from neuronal cells ^{(122) (123, 124)}.

Neurotrophins recognize and bind with high affinity to a complex receptor system consisting of transmembrane tyrosine kinase receptors belonging to the tropomyosine- related kinase (Trk) family. These neurotrophins bind equally to the pan neurotrophin receptor 75 (p75) but have differing affinities for the various subtypes of Trk receptors. There are three different kinds of Trk receptors, which serve as the receptors for the neurotrophins. TrkA is bound by NGF, TrkB

is bound by BDNF and NT-4, and TrkC is bound by NT-3⁽¹²⁵⁾. Most neuronal effects of BDNF are mediated by the TrkB receptor. The binding of BDNF to TrkB induces phosphorylation and dimerization of the intracellular tyrosine kinase domain of receptor resulting in activation⁽¹¹⁵⁾. These events initiate several complex intracellular signal transduction cascades including those controlled by Ras, MAPK, PI3K, PLC- γ and the Cdc42/Rac/RhoG protein family^(126, 127). Additionally, during neuronal development, the BDNF- TrkB complex can be internalized and transported retrogradely to the neuron cell body to regulate gene expression^{(128) (129)}.

BDNF MEDIATED MECHANISM AND AVP SECRETION

The first evidence of BDNF expression in the SON of adult rat was reported in 1998 by Marmigere⁽¹³⁰⁾. Further studies by Aliaga showed increased expression of BDNF in the SON with hypertonic saline injection⁽¹³¹⁾. This study also showed a correlation between increases in BDNF and AVP along with morphological co-localization of BDNF in SON AVP neurons. The studies done by Ohbuchi in 2009 provided the first evidence that BDNF reduces the frequency and amplitude of postsynaptic inhibitory GABA_A receptor-mediated currents⁽¹³²⁾. The consecutive studies used TrkB-Fc as a BDNF scavenger to show activation of TrkB receptor and downregulation of KCC2 in the SON associated with increase in mean arterial pressure in SL rats. These studies showed that the weakening of baroreceptor mediated inhibition of AVP MNCs during SL is mediated through BDNF-TrkB-KCC2 mechanism^(37, 69, 81, 82, 86, 125).

In conclusion, the abovementioned vast contributions to the understanding of AVP regulation indicates that highly regulated release of AVP is crucial to maintain body fluid homeostasis. Nevertheless, the altered AVP neuron regulation leading to sustained AVP release is not completely understood. This dissertation addresses the gaps in existing knowledge by examining

the role of BDNF-TrkB- KCC2 mechanism in impairment of GABA inhibition in AVP neurons,
leading to sustained AVP secretion using salt loading and liver failure rat models.

REFERENCES

1. Oliver G, Schäfer EA. On the Physiological Action of Extracts of Pituitary Body and certain other Glandular Organs: Preliminary Communication. *The Journal of physiology*. 1895; 18: 277-9.
2. Russell JA, Leng G. Veni, vidi, vici: the neurohypophysis in the twentieth century. *Experimental Physiology*. 2000; 85: 1s-6s.
3. Qureshi S, Galiveeti S, Bichet DG, Roth J. Diabetes insipidus: celebrating a century of vasopressin therapy. *Endocrinology*. 2014; 155: 4605-21.
4. Kamm O, Aldrich TB, Grote IW, Rowe LW, Bugbee EP. The active principles of the posterior lobe of the pituitary gland. I. The demonstration of the presence of two active principles. II. The separation of the two principles and their concentration in the form of potent solid preparations. *Journal of the American Chemical Society*. 1928; 50: 573-601.
5. Vigneaud Vd, Lawler HC, Popenoe EA. Enzymatic cleavage of glycinamide from vasopressin and a proposed structure for this pressor-antidiuretic hormone of the posterior pituitary. *Journal of the American Chemical Society*. 1953; 75: 4880-1.
6. Turner RA, Pierce JG, du VV. The purification and the amino acid content of vasopressin preparations. *The Journal of biological chemistry*. 1951; 191: 21-8.
7. Koshimizu TA, Nakamura K, Egashira N, Hiroyama M, Nonoguchi H, Tanoue A. Vasopressin V1a and V1b receptors: from molecules to physiological systems. *Physiological reviews*. 2012; 92: 1813-64.
8. Verney EB. The antidiuretic hormone and the factors which determine its release. *Proceedings of the Royal Society of London Series B, Biological sciences*. 1947; 135: 25-106.

9. Bargmann W. Neurosecretion. In: Bourne GH, Danielli JF, eds. *International Review of Cytology*: Academic Press 1966: 183-201.
10. Gross PM, Sposito NM, Pettersen SE, Fenstermacher JD. Differences in function and structure of the capillary endothelium in the supraoptic nucleus and pituitary neural lobe of rats. Evidence for the supraoptic nucleus as an osmometer. *Neuroendocrinology*. 1986; 44: 401-7.
11. Swaab DF, Pool CW, Nijveldt F. Immunofluorescence of vasopressin and oxytocin in the rat hypothalamo-neurohypophyseal system. *Journal of Neural Transmission*. 1975; 36: 195-215.
12. Rhodes CH, Morrell JI, Pfaff DW. Immunohistochemical analysis of magnocellular elements in rat hypothalamus: distribution and numbers of cells containing neurophysin, oxytocin, and vasopressin. *The Journal of comparative neurology*. 1981; 198: 45-64.
13. Sachs H, Takabatake Y. Evidence for a precursor in vasopressin biosynthesis. *Endocrinology*. 1964; 75: 943-8.
14. Sachs H. Biosynthesis and release of vasopressin. *The American journal of medicine*. 1967; 42: 687-700.
15. Takabatake Y, Sachs H. Vasopressin biosynthesis. 3. in vitro studies. *Endocrinology*. 1964; 75: 934-42.
16. Sachs H, Fawcett P, Takabatake Y, Portanova R. Biosynthesis and release of vasopressin and neurophysin. *Recent progress in hormone research*. 1969; 25: 447-91.
17. Gainer H, Sarne Y, Brownstein MJ. Biosynthesis and axonal transport of rat neurohypophysial proteins and peptides. *J Cell Biol*. 1977; 73: 366-81.
18. Brownstein MJ, Russell JT, Gainer H. Synthesis, transport, and release of posterior pituitary hormones. *Science (New York, NY)*. 1980; 207: 373-8.

19. Leng G, Brown CH, Russell JA. Physiological pathways regulating the activity of magnocellular neurosecretory cells. *Prog Neurobiol.* 1999; 57: 625-55.
20. Brown CH, Bains JS, Ludwig M, Stern JE. Physiological regulation of magnocellular neurosecretory cell activity: integration of intrinsic, local and afferent mechanisms. *J Neuroendocrinol.* 2013; 25: 678-710.
21. Pickford M. Neural control of the pituitary gland. By G. W. Harris, F.R.S., Sc.D., M.D., Fitzmary Professor of Physiology, Institute of Psychiatry, Maudsley Hospital. Edward Arnold (Publishers) Ltd. 1955. Pp. 298. 30s. *Quarterly Journal of Experimental Physiology and Cognate Medical Sciences.* 1956; 41: 355-6.
22. Dreifuss JJ, Kalnins I, Kelly JS, Ruf KB. Action potentials and release of neurohypophysial hormones in vitro. *The Journal of physiology.* 1971; 215: 805-17.
23. J Bicknell R. *Optimizing release from peptide hormone secretory nerve terminals*, 1988.
24. Bourque CW. Central mechanisms of osmosensation and systemic osmoregulation. *Nat Rev Neurosci.* 2008; 9: 519-31.
25. Poulain DA, Wakerley JB. Electrophysiology of hypothalamic magnocellular neurones secreting oxytocin and vasopressin. *Neuroscience.* 1982; 7: 773-808.
26. Wakerley JB, Poulain DA, Brown D. Comparison of firing patterns in oxytocin- and vasopressin-releasing neurones during progressive dehydration. *Brain research.* 1978; 148: 425-40.
27. Brimble MJ, Dyball RE. Characterization of the responses of oxytocin- and vasopressin-secreting neurones in the supraoptic nucleus to osmotic stimulation. *J Physiol.* 1977; 271: 253-71.

28. Bourque CW. Osmoregulation of vasopressin neurons: a synergy of intrinsic and synaptic processes. *Progress in brain research*. 1998; 119: 59-76.
29. Dunn FL, Brennan TJ, Nelson AE, Robertson GL. The role of blood osmolality and volume in regulating vasopressin secretion in the rat. *The Journal of clinical investigation*. 1973; 52: 3212-9.
30. Walters JK, Hatton GI. Supraoptic neuronal activity in rats during five days of water deprivation. *Physiology & Behavior*. 1974; 13: 661-7.
31. B Wakerley J, A Poulain D, Dyball R, A Cross B. *Activity of phasic neurosecretory cells during hemorrhage*, 1975.
32. Dutton A, Dyball RE. Phasic firing enhances vasopressin release from the rat neurohypophysis. *J Physiol*. 1979; 290: 433-40.
33. Fisher TE, Bourque CW. The function of Ca(2+) channel subtypes in exocytotic secretion: new perspectives from synaptic and non-synaptic release. *Prog Biophys Mol Biol*. 2001; 77: 269-303.
34. Fisher TE, Bourque CW. Voltage-gated calcium currents in the magnocellular neurosecretory cells of the rat supraoptic nucleus. *The Journal of physiology*. 1995; 486 (Pt 3): 571-80.
35. Lim NF, Nowycky MC, Bookman RJ. Direct measurement of exocytosis and calcium currents in single vertebrate nerve terminals. *Nature*. 1990; 344: 449-51.
36. Lipski J, McAllen RM, Spyer KM. The sinus nerve and baroreceptor input to the medulla of the cat. *The Journal of physiology*. 1975; 251: 61-78.

37. Choe KY, Trudel E, Bourque CW. Effects of Salt Loading on the Regulation of Rat Hypothalamic Magnocellular Neurosecretory Cells by Ionotropic GABA and Glycine Receptors. *J Neuroendocrinol.* 2016; 28.
38. Sakai K, Touret Mn, Salvert D, Léger L, Jouvet M. *Afferent projections to the cat locus coeruleus as visualized by the horseradish peroxidase technique*, 1977.
39. Banks D, Harris MC. Lesions of the locus coeruleus abolish baroreceptor-induced depression of supraoptic neurones in the rat. *The Journal of physiology.* 1984; 355: 383-98.
40. Renaud LP, Jhamandas JH, Buijs R, Raby W, Randle JC. Cardiovascular input to hypothalamic neurosecretory neurons. *Brain research bulletin.* 1988; 20: 771-7.
41. Jhamandas JH, Raby W, Rogers J, Buijs RM, Renaud LP. Diagonal band projection towards the hypothalamic supraoptic nucleus: light and electron microscopic observations in the rat. *The Journal of comparative neurology.* 1989; 282: 15-23.
42. Jhamandas JH, Renaud LP. Neurophysiology of a central baroreceptor pathway projecting to hypothalamic vasopressin neurons. *The Canadian journal of neurological sciences / Le journal canadien des sciences neurologiques.* 1987; 14: 17-24.
43. Jhamandas JH, Renaud LP. Diagonal band neurons may mediate arterial baroreceptor input to hypothalamic vasopressin-secreting neurons. *Neuroscience letters.* 1986; 65: 214-8.
44. Grindstaff RR, Cunningham JT. Cardiovascular regulation of vasopressin neurons in the supraoptic nucleus. *Exp Neurol.* 2001; 171: 219-26.
45. Grindstaff RJ, Grindstaff RR, Cunningham JT. Baroreceptor sensitivity of rat supraoptic vasopressin neurons involves noncholinergic neurons in the DBB. *American journal of physiology Regulatory, integrative and comparative physiology.* 2000; 279: R1934-43.

46. Thompson CJ, Bland J, Burd J, Baylis PH. The osmotic thresholds for thirst and vasopressin release are similar in healthy man. *Clinical science (London, England : 1979)*. 1986; 71: 651-6.
47. Dunn FL, Brennan TJ, Nelson AE, Robertson GL. The role of blood osmolality and volume in regulating vasopressin secretion in the rat. *The Journal of clinical investigation*. 1973; 52: 3212-9.
48. Leng G, Mason WT, Dyer RG. The supraoptic nucleus as an osmoreceptor. *Neuroendocrinology*. 1982; 34: 75-82.
49. Johnson AK. The periventricular anteroventral third ventricle (AV3V): Its relationship with the subfornical organ and neural systems involved in maintaining body fluid homeostasis. *Brain research bulletin*. 1985; 15: 595-601.
50. Jhamandas JH, Renaud LP. Bicuculline blocks an inhibitory baroreflex input to supraoptic vasopressin neurons. *The American journal of physiology*. 1987; 252: R947-52.
51. Verbalis JG. Osmotic Inhibition of Neurohypophysial Secretion. *Annals of the New York Academy of Sciences*. 1993; 689: 146-60.
52. Verbalis JG. Disorders of body water homeostasis. *Best Pract Res Clin Endocrinol Metab*. 2003; 17: 471-503.
53. Ludwig M. Dendritic release of vasopressin and oxytocin. *J Neuroendocrinol*. 1998; 10: 881-95.
54. Brown CH. Rhythmogenesis in Vasopressin Cells. *Journal of Neuroendocrinology*. 2004; 16: 727-39.
55. Mason WT. Supraoptic neurones of rat hypothalamus are osmosensitive. *Nature*. 1980; 287: 154-7.

56. Oliet SH, Bourque CW. Properties of supraoptic magnocellular neurones isolated from the adult rat. *J Physiol*. 1992; 455: 291-306.
57. Oliet SH, Bourque CW. Steady-state osmotic modulation of cationic conductance in neurons of rat supraoptic nucleus. *The American journal of physiology*. 1993; 265: R1475-9.
58. Oliet SH, Bourque CW. Mechanosensitive channels transduce osmosensitivity in supraoptic neurons. *Nature*. 1993; 364: 341-3.
59. Qiu DL, Shirasaka T, Chu CP, Watanabe S, Yu NS, Katoh T, Kannan H. Effect of hypertonic saline on rat hypothalamic paraventricular nucleus magnocellular neurons in vitro. *Neuroscience letters*. 2004; 355: 117-20.
60. Carreño FR, Ji LL, Cunningham JT. Altered central TRPV4 expression and lipid raft association related to inappropriate vasopressin secretion in cirrhotic rats. *American Journal of Physiology - Regulatory, Integrative and Comparative Physiology*. 2009; 296: R454-R66.
61. Nedungadi TP, Cunningham JT. Differential regulation of TRPC4 in the vasopressin magnocellular system by water deprivation and hepatic cirrhosis in the rat. *American Journal of Physiology - Regulatory, Integrative and Comparative Physiology*. 2014; 306: R304-R14.
62. Prager-Khoutorsky M, Bourque CW. Mechanical basis of osmosensory transduction in magnocellular neurosecretory neurones of the rat supraoptic nucleus. *J Neuroendocrinol*. 2015; 27: 507-15.
63. Prager-Khoutorsky M, Khoutorsky A, Bourque CW. Unique interweaved microtubule scaffold mediates osmosensory transduction via physical interaction with TRPV1. *Neuron*. 2014; 83: 866-78.

64. Tucker AB, Stocker SD. Hypernatremia-induced vasopressin secretion is not altered in TRPV1^{-/-} rats. *American journal of physiology Regulatory, integrative and comparative physiology*. 2016; 311: R451-R6.
65. Kinsman B, Cowles J, Lay J, Simmonds SS, Browning KN, Stocker SD. Osmoregulatory thirst in mice lacking the transient receptor potential vanilloid type 1 (TRPV1) and/or type 4 (TRPV4) receptor. *American journal of physiology Regulatory, integrative and comparative physiology*. 2014; 307: R1092-R1100.
66. Hussy N, Deleuze C, Pantaloni A, Desarménien MG, Moos F. Agonist action of taurine on glycine receptors in rat supraoptic magnocellular neurones: possible role in osmoregulation. *The Journal of physiology*. 1997; 502 (Pt 3): 609-21.
67. Deleuze C, Duvoid A, Hussy N. Properties and glial origin of osmotic-dependent release of taurine from the rat supraoptic nucleus. *The Journal of physiology*. 1998; 507 (Pt 2): 463-71.
68. Armstrong WE. Morphological and electrophysiological classification of hypothalamic supraoptic neurons. *Prog Neurobiol*. 1995; 47: 291-339.
69. Choe KY, Prager-Khoutorsky M, Farmer WT, Murai KK, Bourque CW. Effects of Salt Loading on the Morphology of Astrocytes in the Ventral Glia Limitans of the Rat Supraoptic Nucleus. *Journal of Neuroendocrinology*. 2016; 28.
70. Lang F. Mechanisms and significance of cell volume regulation. *Journal of the American College of Nutrition*. 2007; 26: 613s-23s.
71. Mouillac B, Chini B, Balestre MN, Elands J, Trumpp-Kallmeyer S, Hoflack J, Hibert M, Jard S, Barberis C. The binding site of neuropeptide vasopressin V1a receptor. Evidence for a major localization within transmembrane regions. *The Journal of biological chemistry*. 1995; 270: 25771-7.

72. Gizowski C, Bourque CW. The neural basis of homeostatic and anticipatory thirst. *Nature Reviews Nephrology*. 2017; 14: 11.
73. Baylis PH. Osmoregulation and control of vasopressin secretion in healthy humans. *The American journal of physiology*. 1987; 253: R671-8.
74. Robertson GL, Shelton RL, Athar S. The osmoregulation of vasopressin. *Kidney Int*. 1976; 10: 25-37.
75. Share L. Role of vasopressin in cardiovascular regulation. *Physiological reviews*. 1988; 68: 1248-84.
76. Morel A, O'Carroll AM, Brownstein MJ, Lolait SJ. Molecular cloning and expression of a rat V1a arginine vasopressin receptor. *Nature*. 1992; 356: 523-6.
77. Nelson MT, Quayle JM. Physiological roles and properties of potassium channels in arterial smooth muscle. *The American journal of physiology*. 1995; 268: C799-822.
78. Schrier RW, Berl T, Anderson RJ. Osmotic and nonosmotic control of vasopressin release. *The American journal of physiology*. 1979; 236: F321-32.
79. Schwartz J, Reid IA. Effect of vasopressin blockade on blood pressure regulation during hemorrhage in conscious dogs. *Endocrinology*. 1981; 109: 1778-80.
80. Robertson GL, Athar S. The interaction of blood osmolality and blood volume in regulating plasma vasopressin in man. *The Journal of clinical endocrinology and metabolism*. 1976; 42: 613-20.
81. Balapattabi K, Little JT, Farmer GE, Cunningham JT. High salt loading increases brain derived neurotrophic factor in supraoptic vasopressin neurones. *J Neuroendocrinol*. 2018; 30: e12639.

82. Choe KY, Han SY, Gaub P, Shell B, Voisin DL, Knapp BA, Barker PA, Brown CH, Cunningham JT, Bourque CW. High salt intake increases blood pressure via BDNF-mediated downregulation of KCC2 and impaired baroreflex inhibition of vasopressin neurons. *Neuron*. 2015; 85: 549-60.
83. Hatton GI. Oxytocin and vasopressin neurones: vive la difference! *J Physiol*. 1997; 500 (Pt 2): 284.
84. Hatton GI. Function-related plasticity in hypothalamus. *Annual review of neuroscience*. 1997; 20: 375-97.
85. Di S, Tasker JG. Dehydration-induced synaptic plasticity in magnocellular neurons of the hypothalamic supraoptic nucleus. *Endocrinology*. 2004; 145: 5141-9.
86. Marosi K, Mattson MP. Hold the salt: vasopressor role for BDNF. *Cell metabolism*. 2015; 21: 509-10.
87. Cardenas A, Arroyo V. Mechanisms of water and sodium retention in cirrhosis and the pathogenesis of ascites. *Best Pract Res Clin Endocrinol Metab*. 2003; 17: 607-22.
88. Cunningham JT, Nedungadi TP, Walch JD, Nestler EJ, Gottlieb HB. Δ FosB in the supraoptic nucleus contributes to hyponatremia in rats with cirrhosis. *American Journal of Physiology - Regulatory, Integrative and Comparative Physiology*. 2012; 303: R177-R85.
89. Martin PY, Schrier RW. Sodium and water retention in heart failure: pathogenesis and treatment. *Kidney international Supplement*. 1997; 59: S57-61.
90. Boscoe A, Paramore C, Verbalis JG. Cost of illness of hyponatremia in the United States. *Cost Effectiveness and Resource Allocation*. 2006; 4: 10-.
91. Aditya S, Rattan A. Vaptans: A new option in the management of hyponatremia. *International journal of applied & basic medical research*. 2012; 2: 77-83.

92. D'Auria D, Marinosci GZ, De Benedictis G, Piazza O. Vaptans and hyponatremia in critical patients. *Translational medicine @ UniSa*. 2012; 3: 1-14.
93. Liu Y, Meyer C, Xu C, Weng H, Hellerbrand C, ten Dijke P, Dooley S. Animal models of chronic liver diseases. *American journal of physiology Gastrointestinal and liver physiology*. 2013; 304: G449-68.
94. Rahman TM, Hodgson HJ. Animal models of acute hepatic failure. *International journal of experimental pathology*. 2000; 81: 145-57.
95. Saxena A, Bachelor M, Park YH, Carreno FR, Nedungadi TP, Cunningham JT. Angiotensin II induces membrane trafficking of natively expressed transient receptor potential vanilloid type 4 channels in hypothalamic 4B cells. *American journal of physiology Regulatory, integrative and comparative physiology*. 2014; 307: R945-55.
96. Walch JD, Carreño FR, Cunningham JT. Intracerebroventricular losartan infusion modulates angiotensin type 1 receptor expression in the subfornical organ and drinking behaviour in bile duct ligated rats. *Experimental physiology*. 2013; 98: 922-33.
97. Payne JA, Stevenson TJ, Donaldson LF. Molecular characterization of a putative K-Cl cotransporter in rat brain. A neuronal-specific isoform. *The Journal of biological chemistry*. 1996; 271: 16245-52.
98. Payne JA. Functional characterization of the neuronal-specific K-Cl cotransporter: implications for [K⁺]_o regulation. *The American journal of physiology*. 1997; 273: C1516-25.
99. Plotkin MD, Snyder EY, Hebert SC, Delpire E. Expression of the Na-K-2Cl cotransporter is developmentally regulated in postnatal rat brains: a possible mechanism underlying GABA's excitatory role in immature brain. *J Neurobiol*. 1997; 33: 781-95.

100. Rivera C, Voipio J, Payne JA, Ruusuvuori E, Lahtinen H, Lamsa K, Pirvola U, Saarma M, Kaila K. The K⁺/Cl⁻ co-transporter KCC2 renders GABA hyperpolarizing during neuronal maturation. *Nature*. 1999; 397: 251-5.
101. Rivera C, Voipio J, Thomas-Crusells J, Li H, Emri Z, Sipila S, Payne JA, Minichiello L, Saarma M, Kaila K. Mechanism of activity-dependent downregulation of the neuron-specific K-Cl cotransporter KCC2. *J Neurosci*. 2004; 24: 4683-91.
102. Bos R, Sadlaoud K, Boulenguez P, Buttigieg D, Liabeuf S, Brocard C, Haase G, Bras H, Vinay L. Activation of 5-HT_{2A} receptors upregulates the function of the neuronal K-Cl cotransporter KCC2. *Proceedings of the National Academy of Sciences of the United States of America*. 2013; 110: 348-53.
103. Lee HH, Deeb TZ, Walker JA, Davies PA, Moss SJ. NMDA receptor activity downregulates KCC2 resulting in depolarizing GABA_A receptor-mediated currents. *Nature neuroscience*. 2011; 14: 736-43.
104. Lee HH, Walker JA, Williams JR, Goodier RJ, Payne JA, Moss SJ. Direct protein kinase C-dependent phosphorylation regulates the cell surface stability and activity of the potassium chloride cotransporter KCC2. *The Journal of biological chemistry*. 2007; 282: 29777-84.
105. Kahle KT, Deeb TZ, Puskarjov M, Silayeva L, Liang B, Kaila K, Moss SJ. Modulation of neuronal activity by phosphorylation of the K-Cl cotransporter KCC2. *Trends in neurosciences*. 2013; 36: 726-37.
106. Rinehart J, Maksimova YD, Tanis JE, Stone KL, Hodson CA, Zhang J, Risinger M, Pan W, Wu D, Colangelo CM, Forbush B, Joiner CH, Gulcicek EE, Gallagher PG, Lifton RP. Sites of regulated phosphorylation that control K-Cl cotransporter activity. *Cell*. 2009; 138: 525-36.

107. de Los Heros P, Alessi DR, Gourlay R, Campbell DG, Deak M, Macartney TJ, Kahle KT, Zhang J. The WNK-regulated SPAK/OSR1 kinases directly phosphorylate and inhibit the K⁺-Cl⁻ co-transporters. *The Biochemical journal*. 2014; 458: 559-73.
108. Strange K, Singer TD, Morrison R, Delpire E. Dependence of KCC2 K-Cl cotransporter activity on a conserved carboxy terminus tyrosine residue. *American journal of physiology Cell physiology*. 2000; 279: C860-7.
109. Watanabe M, Wake H, Moorhouse AJ, Nabekura J. Clustering of neuronal K⁺-Cl⁻ cotransporters in lipid rafts by tyrosine phosphorylation. *The Journal of biological chemistry*. 2009; 284: 27980-8.
110. Akerman CJ, Cline HT. Depolarizing GABAergic conductances regulate the balance of excitation to inhibition in the developing retinotectal circuit in vivo. *J Neurosci*. 2006; 26: 5117-30.
111. Chudotvorova I, Ivanov A, Rama S, Hübner CA, Pellegrino C, Ben-Ari Y, Medina I. Early expression of KCC2 in rat hippocampal cultures augments expression of functional GABA synapses. *The Journal of physiology*. 2005; 566: 671-9.
112. Pellegrino C, Gubkina O, Schaefer M, Becq H, Ludwig A, Mukhtarov M, Chudotvorova I, Corby S, Salyha Y, Salozhin S, Bregestovski P, Medina I. Knocking down of the KCC2 in rat hippocampal neurons increases intracellular chloride concentration and compromises neuronal survival. *J Physiol*. 2011; 589: 2475-96.
113. Davies AM. The role of neurotrophins in the developing nervous system. *Journal of Neurobiology*. 1994; 25: 1334-48.
114. McAllister AK. Neurotrophins and neuronal differentiation in the central nervous system. *Cellular and molecular life sciences : CMLS*. 2001; 58: 1054-60.

115. Tapia-Arancibia L, Rage F, Givalois L, Arancibia S. Physiology of BDNF: focus on hypothalamic function. *Frontiers in Neuroendocrinology*. 2004; 25: 77-107.
116. Castren E, Thoenen H, Lindholm D. Brain-derived neurotrophic factor messenger RNA is expressed in the septum, hypothalamus and in adrenergic brain stem nuclei of adult rat brain and is increased by osmotic stimulation in the paraventricular nucleus. *Neuroscience*. 1995; 64: 71-80.
117. Katoh-Semba R, Takeuchi IK, Semba R, Kato K. Distribution of brain-derived neurotrophic factor in rats and its changes with development in the brain. *Journal of neurochemistry*. 1997; 69: 34-42.
118. Nawa H, Carnahan J, Gall C. BDNF protein measured by a novel enzyme immunoassay in normal brain and after seizure: partial disagreement with mRNA levels. *The European journal of neuroscience*. 1995; 7: 1527-35.
119. Kerner SG, Liebl DJ, Parada LF. BDNF regulates eating behavior and locomotor activity in mice. *The EMBO journal*. 2000; 19: 1290-300.
120. Lee R, Kermani P, Teng KK, Hempstead BL. Regulation of cell survival by secreted proneurotrophins. *Science (New York, NY)*. 2001; 294: 1945-8.
121. Seidah NG, Benjannet S, Pareek S, Chretien M, Murphy RA. Cellular processing of the neurotrophin precursors of NT3 and BDNF by the mammalian proprotein convertases. *FEBS letters*. 1996; 379: 247-50.
122. Farhadi HF, Mowla SJ, Petrecca K, Morris SJ, Seidah NG, Murphy RA. Neurotrophin-3 sorts to the constitutive secretory pathway of hippocampal neurons and is diverted to the regulated secretory pathway by coexpression with brain-derived neurotrophic factor. *J Neurosci*. 2000; 20: 4059-68.

123. Lebrun B, Bariohay B, Moyse E, Jean A. Brain-derived neurotrophic factor (BDNF) and food intake regulation: a minireview. *Autonomic neuroscience : basic & clinical*. 2006; 126-127: 30-8.
124. Luo XG, Rush RA, Zhou XF. Ultrastructural localization of brain-derived neurotrophic factor in rat primary sensory neurons. *Neuroscience research*. 2001; 39: 377-84.
125. Rivera C, Li H, Thomas-Crusells J, Lahtinen H, Viitanen T, Nanobashvili A, Kokaia Z, Airaksinen MS, Voipio J, Kaila K, Saarma M. BDNF-induced TrkB activation down-regulates the K⁺-Cl⁻ cotransporter KCC2 and impairs neuronal Cl⁻ extrusion. *J Cell Biol*. 2002; 159: 747-52.
126. Chao MV. Neurotrophins and their receptors: a convergence point for many signalling pathways. *Nat Rev Neurosci*. 2003; 4: 299-309.
127. Kaplan DR, Miller FD. Neurotrophin signal transduction in the nervous system. *Current opinion in neurobiology*. 2000; 10: 381-91.
128. DiStefano PS, Friedman B, Radziejewski C, Alexander C, Boland P, Schick CM, Lindsay RM, Wiegand SJ. The neurotrophins BDNF, NT-3, and NGF display distinct patterns of retrograde axonal transport in peripheral and central neurons. *Neuron*. 1992; 8: 983-93.
129. Oppenheim RW. Cell death during development of the nervous system. *Annual review of neuroscience*. 1991; 14: 453-501.
130. Marmigere F, Rage F, Tapia-Arancibia L, Arancibia S. Expression of mRNAs encoding BDNF and its receptor in adult rat hypothalamus. *Neuroreport*. 1998; 9: 1159-63.
131. Aliaga E, Arancibia S, Givalois L, Tapia-Arancibia L. Osmotic stress increases brain-derived neurotrophic factor messenger RNA expression in the hypothalamic supraoptic nucleus

with differential regulation of its transcripts. Relation to arginine-vasopressin content.

Neuroscience. 2002; 112: 841-50.

132. Ohbuchi T, Yokoyama T, Saito T, Hashimoto H, Suzuki H, Otsubo H, Fujihara H, Suzuki H, Ueta Y. Brain-derived neurotrophic factor inhibits spontaneous inhibitory postsynaptic currents in the rat supraoptic nucleus. *Brain research*. 2009; 1258: 34-42.

FIGURES

CHAPTER I- Figure I-2 – Linear relationship between plasma AVP and osmolality

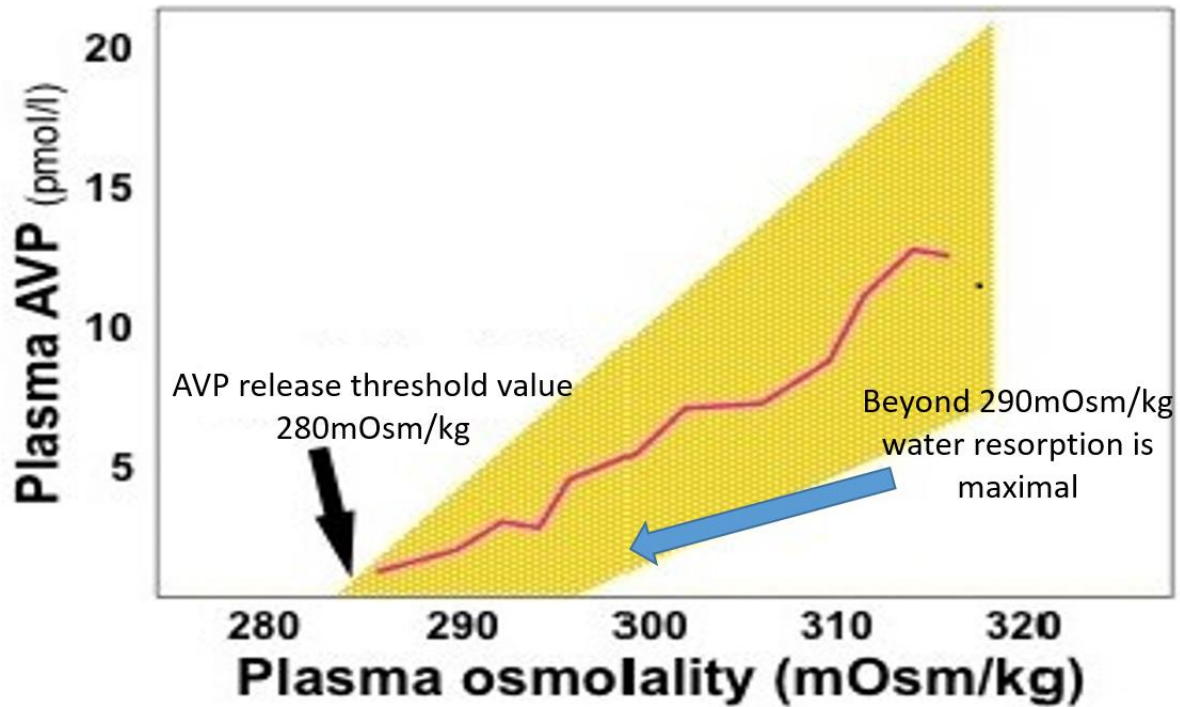


Figure 1: Plasma vasopressin secretion is directly linear with plasma osmolality. The normal physiological range of plasma osmolality is 280-290mOsm/kg with setpoint or threshold for AVP secretion is 285mOsm/kg in humans and 290mOsm/L in rats. *Adapted from Stout et al, 1999, Gerontology; Feingold KR et al., 2000, The Neurohypophysis: Endocrinology of Vasopressin and Oxytocin.*

CHAPTER I- Figure I-3 – GABA Switch during development

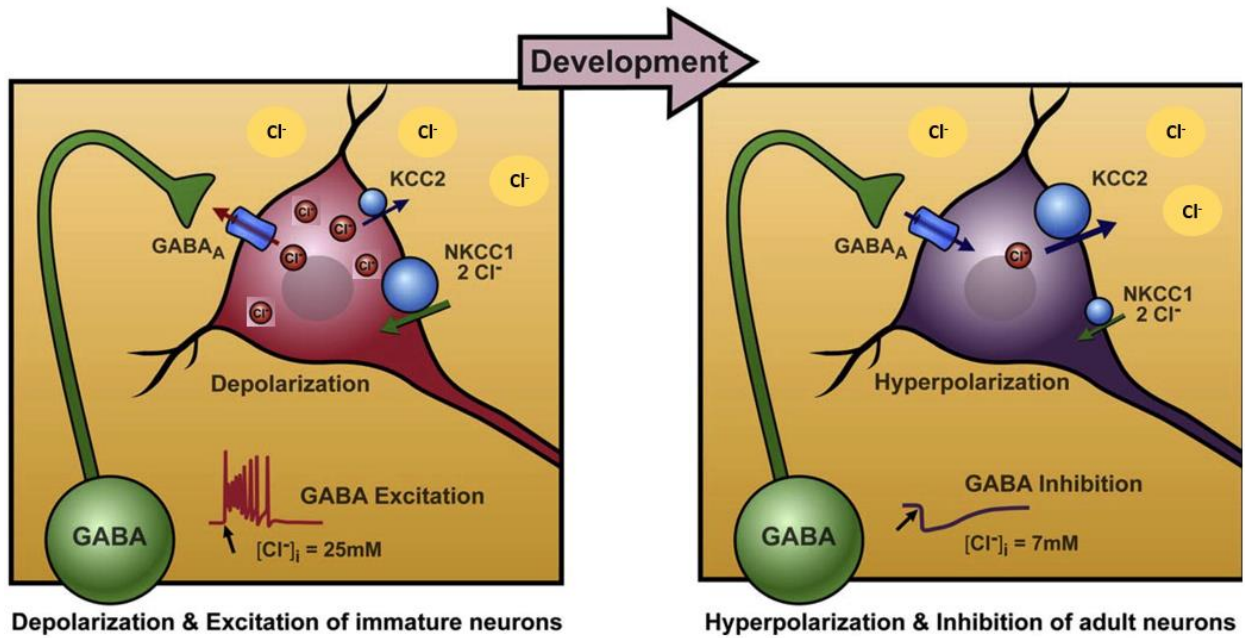


Figure 2: GABA switch from excitation to inhibition during development shows the decrease in intracellular chloride and upregulation of K^+ Cl^- co-transporter 2 (KCC2). Adapted from Y. Ben-Ari, 2014, *Neuroscience*

SPECIFIC AIMS AND HYPOTHESES

The focus of this dissertation is to understand the regulation of supraoptic vasopressin neurons during hypernatremia using high salt loaded rat model and during hyponatremia using liver failure model. Figure 4 is schematic representation of all two specific aims of this dissertation.

Specific Aim 1A

To determine if the Supraoptic Nucleus (SON) is the source of BDNF contributing to increased AVP release and mean arterial pressure in high salt loaded rats

Previous studies have shown that salt loading (SL) upregulates Brain Derived Neurotrophic Factor (BDNF). BDNF diminishes the GABA_A inhibition in vasopressin neurons in the SON by increasing intracellular chloride ([Cl]_i) through Tyrosine kinase receptor B (TrkB) phosphorylation. This produces sustained increase in arginine vasopressin (AVP) release and mean arterial pressure⁽¹⁻³⁾. However, the source of BDNF is not known. We hypothesize that SON is the source of BDNF contributing to increased AVP release in SL rats. We verify this hypothesis using adeno-associated viral vectors with shRNA against BDNF in 2% SL male rats.

Specific Aim 1B

To determine if TrkB-KCC2 mediated mechanism contributes to increased intracellular chloride concentration in SON AVP neurons of high salt loaded rats

Salt loading (SL) increases intracellular chloride concentration [Cl]_i, impairing GABA_A inhibition of SON AVP neurons. But the regulatory mechanisms leading to increased [Cl]_i is not completely understood. Based on previous studies, we hypothesize that SL activates TrkB receptor and downregulates K⁺/Cl⁻ co-transporter 2 (KCC2) co-transporter. Downregulation of

KCC2 decreases the efflux of chloride ion causing increase in $[Cl]_i$ in SON AVP neurons^(2,4). In this aim, we have combined virally mediated ClopHensorN, a relatively new ratiometric chloride imaging technique with capillary based Simple Western technology to record changes in $[Cl]_i$ and specifically detect KCC2 protein expression in individual SON AVP neurons.

Specific Aim 2

To determine if BDNF from the SON contributes to increased AVP secretion and hyponatremia during liver failure in male rats

Based on previous studies^(2,4), we hypothesize that inappropriate AVP release associated with liver failure is due to increased BDNF in the SON. BDNF diminishes GABA_A inhibition in SON AVP neurons by increasing intracellular chloride ($[Cl]_i$) through TrkB activation and downregulation of KCC2. This loss of inhibition could increase AVP secretion. To test this hypothesis, chronic bile duct ligated (BDL) rats, a model of dilutional hyponatremia associated with liver failure, were injected with shRNA to prevent increased BDNF in the SON.

REFERENCES

1. Choe KY, Han SY, Gaub P, Shell B, Voisin DL, Knapp BA, Barker PA, Brown CH, Cunningham JT, Bourque CW. High salt intake increases blood pressure via BDNF-mediated downregulation of KCC2 and impaired baroreflex inhibition of vasopressin neurons. *Neuron*. 2015; 85: 549-60.
2. Choe KY, Trudel E, Bourque CW. Effects of Salt Loading on the Regulation of Rat Hypothalamic Magnocellular Neurosecretory Cells by Ionotropic GABA and Glycine Receptors. *J Neuroendocrinol*. 2016; 28.

3. Marosi K, Mattson MP. Hold the salt: vasopressor role for BDNF. *Cell metabolism*. 2015; 21: 509-10.
4. Balapattabi K, Little JT, Farmer GE, Cunningham JT. High salt loading increases brain derived neurotrophic factor in supraoptic vasopressin neurones. *J Neuroendocrinol*. 2018; 30: e12639.

CHAPTER I- Figure I-4 – Schematic representation of specific aims

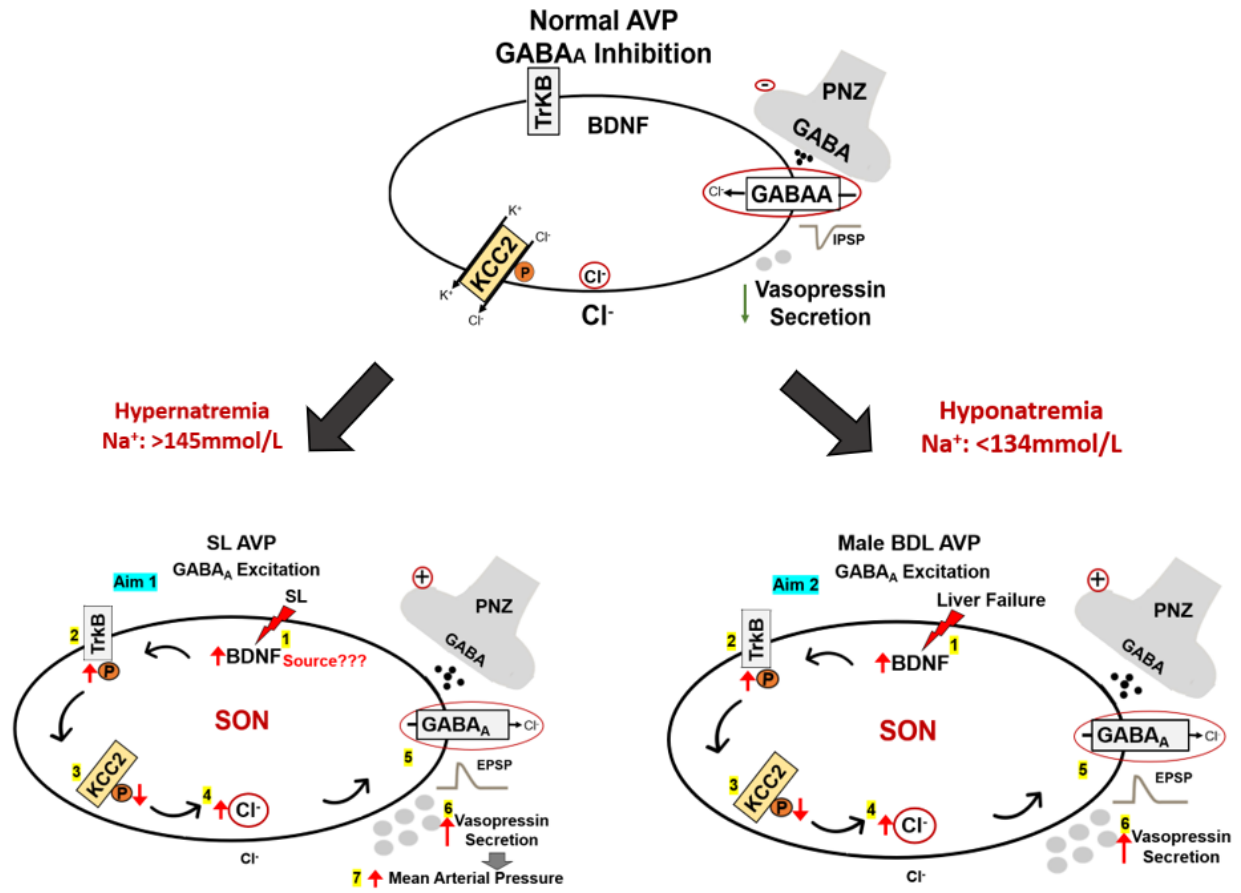


Figure 4: Schematic representation of specific aims. Regulatory mechanism in normal vasopressin neuron (top); Regulatory mechanism in salt loaded male rats (bottom, left; specific aim 1a and 1b); bile duct ligation (BDL) in male rats leading to dilutional hyponatremia (bottom, right; specific aim 2).

PUBLISHED ORIGINAL RESEARCH ARTICLE

CHAPTER II

HIGH SALT LOADING INCREASES BRAIN DERIVED NEUROTROPHIC FACTOR IN
SUPRAOPTIC VASOPRESSIN NEURONS

Kirthikaa Balapattabi, Joel T. Little, George E. Farmer, and J. Thomas Cunningham

J Neuroendocrinol. 2018 30(11): e12639. PMID: 30129982

ABSTRACT

High salt loading (SL) is associated with inappropriate arginine vasopressin (AVP) release and increased mean arterial pressure. Previous work has shown that chronic high salt intake impairs baroreceptor inhibition of rat AVP neurons through Brain-Derived Neurotrophic Factor (BDNF) dependent activation of tyrosine receptor kinase B (TrkB) and downregulation of K⁺/Cl⁻ co-transporter KCC2. This mechanism diminishes the GABA_A inhibition of AVP neurons in the supraoptic nucleus (SON) by increasing intracellular chloride ([Cl]_i). However, the source of BDNF leading to this ionic plasticity is unknown. Here we used adeno-associated viral vectors with shRNA against BDNF to test if SON is the source of BDNF contributing to increased AVP release and elevated mean arterial pressure in high salt loaded rats. Virally mediated BDNF knockdown (shBDNF) in the SON of salt loaded rats significantly blocked the increases in BDNF mRNA and AVP hnRNA expression. The observed increase in the activation of TrkB receptor during salt loading is consistent with previous studies. Western blot analysis of SON punches revealed that tyrosine phosphorylation of TrkB (pTrkB^{Y515}) was significantly decreased in Salt shBDNF rats compared to the Salt SCR rats. Injections of shBDNF in the SON also significantly prevented the increase in plasma AVP concentration associated with salt loading. However, the salt loading induced increase in mean arterial pressure was not decreased with BDNF knockdown in the SON. Average daily fluid intake and urine output were significantly elevated in both Salt SCR and Salt shBDNF rats compared to the euhydrated controls. Daily average urine sodium concentration was significantly higher in shBDNF injected Salt rats than the other groups. These findings indicate that BDNF produced in the SON contributes to the increased AVP secretion during high salt loading but not for the subsequent increase in mean arterial pressure.

INTRODUCTION

Arginine vasopressin (AVP) is a peptide hormone that is synthesized in Magnocellular Neurosecretory Cells (MNCs) present in Supraoptic Nucleus (SON) and Paraventricular Nucleus (PVN) of the hypothalamus ⁽¹⁻³⁾. Arginine vasopressin is axonally transported through hypothalamic hypophyseal tract from hypothalamus to the posterior pituitary where it is released into systemic circulation ^(1, 2). Release of AVP is regulated primarily by plasma osmolality, blood pressure, and blood volume ⁽⁴⁻⁶⁾. Increased plasma osmolality activates hypothalamic MNCs increasing circulating AVP which acts at the kidneys to increase water reabsorption and maintain homeostasis. Conversely, decreased plasma osmolality is associated with inhibition of AVP MNCs, reduced plasma AVP, and diuresis. A linear relationship between plasma AVP and osmolality is observed during normal conditions and requires highly coordinated excitatory and inhibitory postsynaptic responses ^(3, 7).

Altered synaptic homeostasis of vasopressinergic MNCs could contribute to disease conditions in which circulating AVP is abnormally elevated ^(7, 8). For example, congestive heart failure and decompensated cirrhosis can be associated with dilutional hyponatremia ⁽⁹⁻¹¹⁾. The development of hyponatremia is associated with increased morbidity and mortality in these diseases ⁽¹²⁻¹⁴⁾.

Despite vast existing knowledge about the regulation of AVP neurons ^(5, 6, 15-18) the pathophysiology of inappropriate AVP secretion remains unknown. Increased AVP release into systemic circulation from MNCs despite elevated mean arterial pressure is reported during high salt loading (SL; i.e. giving rats only 2% NaCl to drink) ⁽¹⁹⁾. This makes salt loaded rats a model to study changes in neuronal regulation of AVP release due to chronic osmotic stress.

High salt intake causes hypernatremia leading to AVP release as a feedback to maintain plasma osmolality. Salt - induced increases in mean arterial pressure is partly mediated by AVP through

the elevation of vascular resistance and renal water retention. Previous studies have shown that salt loading upregulates Brain Derived Neurotrophic Factor (BDNF)⁽¹⁹⁻²²⁾. Increases in BDNF diminish or reverse the GABA_A mediated inhibition in AVP neurons by increasing intracellular chloride ([Cl]_i). This disturbance in the chloride homeostasis is mediated by BDNF - dependent activation of tyrosine receptor kinase B (TrkB) and downregulation of potassium chloride co-transporter (KCC2). The changes in regulatory mechanisms creates a feed forward loop causing sustained release of AVP and an increase in mean arterial pressure^(19, 21, 22). However, the source of BDNF is yet to be elucidated. We hypothesize that the SON is the source of BDNF contributing to increased AVP release and mean arterial pressure in salt loaded rats. In this study, we used adeno-associated viral vectors with shRNA against BDNF to test our hypothesis by knocking down BDNF in the SON. This study will address several critical gaps in the literature by determining the source of BDNF that contribute to neural adaptations resulting in pathophysiology of inappropriate AVP release in the high salt loaded rats.

MATERIALS AND METHODS

ANIMALS

All the experiments were conducted on outbred adult male Sprague-Dawley rats with body weight of 200-250 g (Charles River, Wilmington, MA). Rats were individually housed due to the use of survival surgery and individual fluid intake measurements in the protocol. All animals were maintained in a temperature-controlled environment on a 12/12h light dark cycle with *ad libitum* access to food and water unless otherwise indicated. Experimental protocols involving animals were approved by the UNT Health Science Center IACUC and conducted in accordance to the National Institute of Health *Guide for the Care and Use of Laboratory Animals*. Survival surgeries were conducted using aseptic techniques. All rats were given procaine penicillin G (30,000 U, sc) and non-steroidal anti-inflammatory drug, carprofen (Rimadyl, 2 mg po), was given before and after surgery for pain management.

AAV-MEDIATED KNOCKDOWN OF BDNF IN THE SUPRAOPTIC NUCLEUS

Rats were bilaterally injected in the SON (300 nl/side) with an Adeno-associated virus (AAV) serotype 2 conjugated with a shRNA directed against BDNF, a mCherry reporter, and a U6 promoter (shBDNF). Another group of rats received bilateral SON injections of equal titer and amount of AAV2 conjugated with a scrambled (SCR) sequence of shRNA (Vector Biolabs, Malvern, PA) as controls. The vectors were injected at a titer of 1.0×10^{13} GC/ml (Vector Biolabs). Each rat was anaesthetized with isoflurane (2-3%) and placed in stereotaxic frame. Their skulls were exposed and leveled between lambda and bregma⁽²³⁾. A micromanipulator was oriented to lower the probe to the targeted coordinates of SONs (1.4 mm posterior, 9.1 mm

ventral, and ± 1.4 mm lateral from bregma). Each construct was injected in both the SONs over a 10-min period. After 5 min, the injector was removed, and the incision was closed with sutures.

METABOLIC CAGE STUDY

After two weeks of recovery from surgery, rats were moved into metabolic cages (Lab Products, Seaford, DE) for measurement of daily food intake, fluid intake, and urine excretion. The rats were provided with *ad libitum* access to food and water for first 7 days to record baseline parameters. Following the baseline measurements, a subset of shBDNF and SCR rats had their water replaced with 2% salt (NaCl) to drink for 7 days as previously described⁽¹⁹⁾. Food and fluid intake were measured by filling the containers up to a predetermined weight in grams and subtracting the remaining weight 24 h later. Mineral oil was added to the urine collection vials to prevent evaporation of water from urine. Urine excretion volume was recorded, and urine samples were collected for measuring daily sodium excretion.

MEASUREMENT OF ELECTROLYTE CONCENTRATION

Urine from each rat was collected in 50-ml centrifuge tubes and a 1 to 2 ml aliquot was taken from each daily sample and centrifuged (20 min; 10,000 g). Sodium concentration in each of the urine samples was determined at 1:500 dilution using flame photometer (Jenway PFP7, VWR International, Radnor PA). Final sodium concentration in mmol/l was calculated from linear calibration curve derived from sodium standards.

LASER CAPTURE MICRODISSECTION (LCM) AND QUANTITATIVE REAL TIME PCR (qRT-PCR)

At the end of the 7-day salt loading protocol, the rats were anesthetized with inactin (100 mg/kg ip, Millipore Sigma, Burlington, MA) and decapitated. Their brains were collected and flash

frozen using precooled 2- Methyl butane. Fresh frozen brains were prepared for LCM^(18, 20) by cutting 10µm thick coronal sections through the hypothalamus at the level of the SON. The sections were mounted onto poly(p-phenylene) sulfide membrane coated slides (Leica Microsystems, Buffalo Grove, IL). Separate sets of sections with 40µm thickness were mounted on gel coated slides to verify histology of other nuclei in hypothalamus. A Leica Microsystems Laser Capture Microdissection instrument which utilizes an UV cutting laser to dissect the region of interest into collection tube, was used to verify the accuracy of the injection sites by visualizing the mCherry reporter and to specifically collect the SON neurons. Minimum of 7-9 SON regions were laser captured and collected from each rat for RNA extraction and amplification. The SONs collected from LCM were used to measure changes in BDNF mRNA and AVP hnRNA using qRT-PCR. The RNA was extracted and purified from each sample using ArrayPure Nano-Scale RNA Purification Kit reagents (Epicentre Biotechnologies, Madison, WI). The concentration and quality of each RNA sample was evaluated using a Nanodrop Spectrophotometer (Thermo Scientific, Waltham, MA) and reverse transcribed to cDNA with Sensiscript RT Kit reagents (Qiagen, Valencia, CA)⁽²⁰⁾. Real-time PCR was performed on an CFX96 C1000 Cycler (Bio-Rad, Hercules, CA) with SYBR green fluorescent label. Samples (15ul final volume) contained: SYBR green master mix (Bio-Rad), 3–5 pmol of each primer, and equal concentration of cDNA. Cycling parameters were as follows: 95° C·3 min, then 40 cycles of the following 95° C·10 s, 60° C·1 min. A melting temperature-determining dissociation step was performed from 65° C to 95° C at increments of 0.5° C every 5 s at the end of the amplification phase.

Forward and reverse primers for target genes (Table 1) were obtained from Integrated DNA Technologies (Coralville, IA). The housekeeping gene S18 was used to normalize RNA

expression. Melt curves generated were analyzed to identify nonspecific products and primer-dimers. The data were analyzed by the $2^{-\Delta\Delta C_t}$ method^(24, 25). ΔC_t was measured by calculating the difference between the S18 and the corresponding gene of interest C_t values. For obtaining the $\Delta\Delta C_t$ value, this value was then subtracted from the difference between the average of control S18 and control gene of interest C_t values^(18, 26, 27).

PLASMA MEASUREMENTS

One to 2-ml of trunk blood was collected from each rat after decapitation and prepared for measuring plasma osmolality and hematocrit as previously described⁽¹⁸⁾. Plasma osmolality was measured on a vapor pressure osmometer (Wescor, Logan, UT). Two heparinized capillary tubes (Fisher Scientific, Hampton, NH) were filled for measuring hematocrit using Micro-Hematocrit capillary tube reader (Lancer, St. Louis, MO).

Another 5 - to 6 -ml blood was collected in Vacutainer tubes containing the anticoagulant, EDTA (12 mg). The proteinase inhibitor, aprotinin (0.6 TIU/ml of blood; Phoenix Pharmaceuticals, Inc, Burlingame, CA) was added and the sample was centrifuged at 1600 g for 15 minutes at 4° C. Two-three ml of plasma were removed from each sample and peptides were extracted from plasma by solid phase extraction using C-18 SEP-Column (Phenomenex, Torrance, CA). After the extraction, each sample was subjected to vacuum centrifugal concentration. Circulating AVP concentration was measured by using specific ELISA according to the manufacturer's instructions (EK-065-07, Phoenix Pharmaceuticals, Inc). Four parametric logistic analysis (4-PL) was performed to quantify the concentration of peptide.

WESTERN BLOT ANALYSIS

At the end of 7-day salt loading protocol, the rats were anesthetized with inactin (100 mg/kg ip) and decapitated. Punches containing the SON were collected from 1 mm coronal section from each brain as previously described^(18, 28). Protein was extracted from the SON punches using RIPA lysis buffer containing DTT, chelators, and protease phosphatase inhibitor cocktail. Protein concentration was determined by bicinchoninic acid assay (BCA assay) with varying concentrations of BSA as reference standards. Total lysate (20–25 ug) were loaded onto a 4-15% acrylamide sodium dodecyl sulphate (SDS) gel and separated by electrophoresis in Tris-glycine buffer with denaturing conditions. The protein was transferred to Polyvinylidene difluoride (PVDF) membrane (Immobilon-P; EMD-Millipore, Burlington, MA) in Tris-glycine buffer (25 mM Tris, 192 mM glycine, 0.1% SDS; pH 8.3) with 20% (v/v) methanol. Membranes were blocked with 5% BSA in Tris-buffered saline-Tween 20 (25 mM Tris base, 125 mM NaCl, 0.1% Tween 20) for 30 min at room temperature. The membranes were incubated with primary antibodies made in 5% BSA overnight at 4° C. The primary antibodies used were: Phosphorylated TrkB (Y515; rabbit polyclonal; 1:1000; ab109684, Abcam, Cambridge, MA), Total TrkB (goat;1:1000; GT15080, Neuromics), Phosphorylated KCC2 (Ser940; rabbit polyclonal; 1:500; 612-401-E15, Rockland), mCherry (rabbit polyclonal;1:500; ab167453, Abcam) and GAPDH (mouse monoclonal;1:2000; MAB374, Millipore).

Membranes were rinsed three times at 10 min intervals with TBS-Tween followed by a 2 h incubation at room temperature with a horseradish peroxidase-conjugated secondary antibody against the primary antibody host species (anti-rabbit, anti-goat, or anti-mouse; 1:1000; Sigma, St Louis, MO, USA). The membranes were washed three times at 5 min intervals with TBS-Tween. Proteins were visualized using an enhanced chemiluminescence substrate kit

(Supersignal West Femto Maximum Sensitivity kit; Thermo Scientific, Waltham, MA). Blots were developed, and the digital image was obtained by using Gbox (Genesnap program) and densitometry analysis of the bands was performed using ImageJ. Densitometry measurements of the immunoreactive bands were normalized using GAPDH as loading control.

MAP AND HR MEASUREMENTS USING RADIO TELEMETRY

After a week of recovery from stereotaxic injections, some rats from each group were instrumented with radio telemetry transmitters (TA11PA-C40 telemetry unit, Data Science International, St. Paul, MN) under isoflurane anesthesia (2-3%) as previously described ⁽²⁹⁾. The blood pressure catheter was advanced into the abdominal aorta and the radio transmitter device was placed in the peritoneal cavity for the duration of the experiment. Direct recording of mean arterial pressure, heart rate and activity was done using transmitters. After two weeks of recovery period, signals from the telemetry device were recorded for 7-day baseline followed by 7-day SL using a Dataquest IV radio telemetry system (Data Sciences International, St. Paul, MN). During the experiments, heart rate (HR), activity (ACT), and mean arterial pressure (MAP) were all measured for 10 seconds every 10 minutes for 24 h/day and averaged as previously described ⁽²⁹⁾.

EXPERIMENTAL GROUPS AND STATISTICAL ANALYSIS

In all the above experiments, the rats were divided into four groups based as follows: 1) Euhydrated rats injected with SCR virus (Eu SCR), 2) Euhydrated rats injected with shBDNF virus (Eu shBDNF), 3) Salt loaded rats injected with SCR virus (Salt SCR), and 4) Salt loaded rats injected with shBDNF virus (Salt shBDNF).

Data from the metabolic cage studies and electrolyte measurements were analyzed by separate two-way repeated measures ANOVA with time as first factor and treatment (drinking fluid with

stereotaxic injection) as second factor followed by Bonferroni post hoc tests. All other data were analyzed using one-way ANOVA with Bonferroni post hoc tests using Sigma Plot 12.0. Figures were assembled using the ‘magick’ package in RStudio. The group sizes were determined by power analysis and effect size calculated from our previously published work^(16, 18, 19) and preliminary data using Sigma plot 12.0. Power analysis calculation elements included considerations of $p < 0.05$, η^2 of 0.8, largest difference between means, and the largest standard deviation we had observed from our studies. η^2 (η^2 method was chosen to calculate the effect sizes and the sample sizes were balanced (equal) in all the groups and were independent of each other. Sum of squares (SS) of effect and total from our previous studies^(15, 16, 18, 19) were used for the effect size determination. The minimal n’s per group for each experiment was decided to have an appropriately powered study with the effect size (η^2) of approximately 0.7 (70%).

RESULTS

CHANGES IN AVP AND BDNF GENE EXPRESSION IN SON

Using LCM, we verified the accuracy of the stereotaxic injections by visualizing the mCherry reporter (Figure 1A) and collected the SONs to measure changes in the BDNF mRNA and AVP hnRNA expression using qRT PCR by $2^{-\Delta\Delta Ct}$ method. Rats that did not have successful virus injections in the SON were separately analyzed. One-way ANOVA revealed significant difference between the groups in BDNF ($F(3,23) = 5.78, P < 0.05$) and AVP ($F(3,23) = 8.83, P < 0.05$) gene expression. Bonferroni post hoc analysis showed that salt loading significantly increased BDNF and AVP gene expression in the SON of rats injected with SCR compared to the euhydrated rats (Bonferroni t tests, all $P < 0.05$, Figure 1). Post hoc multiple comparison of mRNA levels between Salt SCR and Salt shBDNF groups showed that SON injections of shBDNF significantly blocked the increases in BDNF mRNA (Bonferroni t = 3.310, $P < 0.05$)

and AVP hnRNA (Bonferroni $t = 4.09$, $P < 0.05$) in SON of salt loaded rats. In rats with injections of shBDNF outside of the SON, salt loading significantly increased BDNF mRNA in the SON ($F(3, 12) = 7.33$, $P < 0.05$; Figure 2) and the increase produced by salt loading was not different compared to the Salt SCR group (Bonferroni $t = 0.37$, $P > 0.05$; Figure 2).

CHANGES IN PHOSPHORYLATION OF TrkB AND KCC2 IN SON

We used mCherry expression to verify the specificity of stereotaxic injections (Figure 3). One-way ANOVA analysis revealed significant difference between the groups in TrkB phosphorylation ($F(3,23) = 6.778$, $P < 0.05$) and KCC2 phosphorylation ($F(3,24) = 4.546$, $P < 0.05$). Seven days of 2% salt loading significantly increased TrkB phosphorylation without affecting total TrkB expression and decreased phosphorylation of KCC2 (Bonferroni t tests, all $P < 0.05$, Figure 3) in the SON of rats injected with the control vector compared to the euhydrated rats. Virally mediated BDNF knockdown in the SON of salt loaded rats significantly prevented the increase in TrkB phosphorylation and decrease in KCC2 phosphorylation compared to euhydrated rats (Bonferroni t tests, all $P < 0.05$, Figure 3). One to two rats in each group did not have successful virus injections in the SON which were verified at the end of the experiment using either LCM/qRT PCR or western blot analysis and were excluded from the data analysis in all the following experiments.

CHANGES IN FLUID INTAKE, URINE EXCRETION, FOOD INTAKE AND BODY WEIGHT

Fluid intake was measured daily before and during 7 days of 2% salt loading. Two-way repeated measures ANOVA revealed a significant interaction indicating that fluid intake was affected by time and the treatment protocol (Time x Treatment $F(39,351) = 18.44$, $P < 0.001$; Figure 4A).

Post hoc multiple comparisons between the factors revealed that while there were not differences among the groups during baseline, salt loading significantly increased fluid intake and this increase was not affected by BDNF knockdown in the SON. Similar results were obtained for urine excretion (Time x Treatment $F(39,351) = 24.419$, $P < 0.001$; Figure 4B) and food intake (Time x Treatment $F(39,351) = 18.420$, $P < 0.001$; Figure 4C). The average daily urine volume during baseline was not different among the groups and salt loading increased urine output comparably in both Salt SCR and Salt shBDNF rats (Figure 4B). Food intake was significantly decreased in both groups of salt loaded rats compared to the euhydrated rats (Figure 4C). Concomitantly, the average body weight increase during salt loading was significantly decreased in both Salt SCR and Salt shBDNF rats compared to the euhydrated rats ($F(3, 36) = 27.48$, $P < 0.001$; Bonferroni t tests, $P < 0.05$; Figure 4D).

CHANGES IN ELECTROLYTE EXCRETION

Urine sodium excretion was measured before and during the 7-day salt loading protocol. Average daily changes in sodium excretion were significantly affected by time and the treatment protocol ($F(39,312) = 35.65$, $P < 0.001$; Figure 5A). There were no differences among the groups during baseline. During salt loading, daily average change in sodium excretion significantly increased in the Salt SCR rats as compared to the two euhydrated control groups (Bonferroni t tests, all $P < 0.05$; Figure 5A). The daily changes in sodium excretion following BDNF knockdown in the SON was significantly increased during the 7-day salt loading as compared to all the other groups (Bonferroni t tests, $P < 0.05$; Figure 5A). Knockdown of BDNF in the SON also significantly increased total average daily sodium concentration ($F(3, 32) = 43.55$, $P < 0.001$; Figure 5B). The average daily urine sodium concentrations of salt loaded rats were significantly higher than the euhydrated groups during salt treatment. In addition, the Salt

shBDNF group had significantly higher urine sodium excretion than the Salt SCR rats (Bonferroni t tests, all $P < 0.05$; Figure 5B).

CHANGES IN PLASMA AVP, OSMOLALITY AND VOLUME

One-way ANOVA revealed significant difference between the groups in plasma AVP concentration ($F(3,18) = 26.227, P < 0.05$). Bonferroni multiple comparisons show that rats with SCR injections and salt loading had significantly increased circulating AVP compared to all the other groups (Bonferroni t tests, all $P < 0.001$; Table 2). Knockdown of BDNF in the SON of salt loaded rats significantly decreased plasma AVP as compared to the Salt SCR group (Bonferroni t = 6.661, $P < 0.05$; Table 2). Plasma osmolality and hematocrit values were significantly different between the groups (Plasma osmolality $F(3,47) = 20.746, P < 0.001$; Hematocrit $F(3,47) = 18.478, P < 0.001$). The Salt SCR rats also had plasma osmolality and hematocrit values that were significantly higher than all other groups (Bonferroni t tests, all $P < 0.05$). The Salt shBDNF group had significantly lower plasma osmolality (Bonferroni t = 4.146, $P < 0.05$; Table 2) and hematocrit (Bonferroni t = 3.708, $P < 0.05$; Table 2) as compared to the Salt SCR group.

CHANGES IN MEAN ARTERIAL PRESSURE AND HEART RATE

Two-way repeated measures ANOVA revealed a significant interaction indicating that MAP was affected by time and the treatment protocol (Time x Treatment $F(39,312) = 21.169, P < 0.001$; Figure 6). Post hoc multiple comparisons between the factors revealed that there were not differences among the groups during baseline (Table 3). Salt loading was associated with significant increases in MAP in rats injected in the SON with either SCR or shBDNF. The mean arterial pressure increases in the two salt loaded groups were not different from each other (Figure 6A & B). Two-way repeated measures ANOVA followed by post hoc analysis show that

salt loading was associated with a significant decrease in heart rate (Time x Treatment F (39,312) = 3.221, P < 0.001; Figure 6C & D; Table 3) that was not different between the SCR and shBDNF injected rats.

DISCUSSION

It is known that AVP MNCs are regulated by negative feedback from arterial baroreceptors mediated by GABA_A inhibition^(6, 21). Previous studies have established that chronic salt loading can impair this baroreceptor inhibition by altering chloride homeostasis of MNCs through a BDNF –TrkB signaling mechanism⁽¹⁹⁻²¹⁾. It is important to identify the source of BDNF leading to changes in the regulatory mechanism to get a complete understanding of the pathophysiology of inappropriate AVP release. The results from this study show that the SON is the source of BDNF resulting in inappropriate release of AVP in salt loaded rats.

Circulating AVP is primarily determined by the activity of MNCs located in the PVN and SON of the hypothalamus^(3, 16). In addition, MNCs are reported to express both BDNF and TrkB⁽²⁰⁾. Because SON is less heterogeneous than PVN and we previously observed salt loading-mediated changes in GABA inhibition of SON MNCs, we injected an AAV vector constructed with shRNA against BDNF (AAV2- U6- shBDNF) bilaterally into the SON. This specific knockdown approach helped test whether increased expression of BDNF in the SON contributes to the elevated circulating AVP and MAP associated with salt loading. Previous studies using this shBDNF viral construct have shown that its effects are primarily neurotropic and that it produces stable knockdown of BDNF⁽¹⁹⁾.

Knocking down BDNF in the SON of salt loaded rats significantly attenuated the increases in AVP hnRNA in the SON and circulating AVP normally associated with salt loading. Chronic

salt intake increased the concentration of plasma sodium and proportionally increased plasma osmolality. Knockdown of BDNF in the SON was also associated with a significant decrease in plasma osmolality and a significant increase in sodium excretion. Blocking the increase in BDNF in the SON produced natriuresis in salt loaded rats that may have contributed to the observed decrease in plasma osmolality. It is likely the natriuresis is related to the decrease in circulating AVP⁽³⁰⁾ but this was not tested. It is also well established that elevation of plasma osmolality by salt loading can activate hypothalamic oxytocin neurons. An additional possibility is that oxytocin can facilitate the release of Atrial natriuretic peptide (ANP) which reduces an expanded extracellular fluid (ECF) volume by increasing urine and renal sodium excretion^(4, 31). Injections of shBDNF in the SON did not cause any changes in the volume of urine excretion or fluid and food intake behavior. Food intake and body weight in salt loaded groups were significantly decreased compared to the euhydrated groups. High salt intake caused the rats to decrease food intake and subsequently reduced body weight⁽³²⁾.

Although BDNF knockdown in the SON significantly attenuated AVP release in salt loaded rats, it did not similarly influence mean arterial pressure. In this study, MAP was significantly increased in the salt loaded groups compared to the euhydrated groups in accordance with the previous studies⁽¹⁹⁾. This data indicates that other mechanisms in addition to AVP from the SON could contribute to the observed increase in MAP during high salt loading. Moreover, studies have shown that recruitment of central osmoreceptor pathways enhance sympathetic tone through excitation of preautonomic neurons^(19, 33). Another factor that could have influenced these results is the experimental protocol. The AAV treatments were applied only to the SON. AVP that is dendritically released from magnocellular secretory neurons in the PVN has been shown to increase sympathetic outflow⁽³⁴⁾. This mechanism would not have been influenced by

the AAV injections in the SON and could still contribute to the increase in MAP associated with salt loading. Also, the BDNF knockdown was induced before the rats were exposed to salt loading. This was done because the time required to allow the AAV to transfect the cells in the SON is longer than the 7-day salt loading protocol. As mentioned above, this protocol significantly reduced AVP release, but it did not prevent the increase in MAP. It could be that mechanisms related to autonomic function, which do not depend on the SON, were able to compensate for the lack of AVP release. Inhibiting BDNF-TrkB signaling in the SON during the 7-day salt loading protocol could possibly prevent the increase in MAP.

Our results show that increased BDNF expression in the SON during chronic salt loading leads to TrkB receptor activation as indicated by increased tyrosine (Y⁵¹⁵) phosphorylation. In most neurons, the low [Cl]_i required for the GABA_A synaptic inhibition is due to relative activity of KCC2 and/or NKCC1 (Na⁺/K⁺/Cl⁻ co-transporter) membrane co-transporters. In the SON, salt loading was associated with decreased serine (S⁹⁴⁰) phosphorylation of KCC2. Decreased phosphorylation of KCC2 at this residue is associated with translocation of the protein from the membrane and functional loss of its chloride transport activity⁽³⁵⁻³⁷⁾. This could be the mechanism responsible for a change in the valence of the GABA_A in the SON produced by salt loading. However, the proposed changes in membrane expression of KCC2 in the SON and its effect on [Cl]_i are yet to be investigated.

Other studies have suggested that changes in the function of NKCC1 also modulates the valence of GABA_A on MNCs in the SON^(38, 39). There are several different signaling pathways that influence the function of both KCC2 and NKCC1 and can potentially impact GABAergic function^(40, 41). Although our study shows that salt loading induced activity-dependent mechanisms can affect KCC2 phosphorylation, the role of posttranslational mechanisms in

controlling KCC2 expression, specifically at the cell-surface are poorly understood. However, the cellular mechanisms through which changes in Cl⁻ homeostasis affect the GABA-mediated feedback inhibition in MNCs have not been resolved yet.

This study indicates that the SON neurons themselves are source of BDNF causing dysregulation of AVP neurons during salt loading. However, we cannot conclude whether the source is AVP or oxytocin or both the SON neurons. Therefore, BDNF could be having autocrine or paracrine effects in the SON that change the phosphorylation status of KCC2. This would change the valence of the GABA response of AVP neurons to baroreceptor stimulation as has been previously demonstrated ⁽¹⁹⁾. However, BDNF knockdown in the SON was not sufficient to prevent the salt loading induced increase in mean arterial pressure.

This study advances our understanding about the pathophysiology of AVP neuron regulation. Identifying the source of BDNF underlying the changes in postsynaptic inhibition of AVP neurons in response to salt loading may result in novel strategies for reducing AVP secretion in other pathological states such as heart and liver failure ^(9, 16, 42). This would provide a novel therapeutic target for the treatment of inappropriate AVP release and its associated morbidities.

ACKNOWLEDGEMENTS

The authors would like to thank M. Bachelor and Dr. L. A. Wang for their assistance.

GRANTS

This work was supported by R01 HL119458 to JTC.

DISCLOSURES

The authors have nothing to disclose.

REFERENCES

1. Cunningham JT, Penny ML, Murphy D. Cardiovascular regulation of supraoptic neurons in the rat: synaptic inputs and cellular signals. *Prog Biophys Mol Biol.* 2004; 84: 183-96.
2. Armstrong WE. Morphological and electrophysiological classification of hypothalamic supraoptic neurons. *Progress in Neurobiology.* 1995; 47: 291-339.
3. Di S, Tasker JG. Dehydration-induced synaptic plasticity in magnocellular neurons of the hypothalamic supraoptic nucleus. *Endocrinology.* 2004; 145: 5141-9.
4. Gizowski C, Bourque CW. The neural basis of homeostatic and anticipatory thirst. *Nature Reviews Nephrology.* 2017; 14: 11.
5. Bourque CW. Central mechanisms of osmosensation and systemic osmoregulation. *Nature reviews Neuroscience.* 2008; 9: 519-31.
6. Verbalis JG. Osmotic Inhibition of Neurohypophysial Secretion. *Annals of the New York Academy of Sciences.* 1993; 689: 146-60.
7. Leng G, Brown CH, Bull PM, Brown D, Scullion S, Currie J, Blackburn-Munro RE, Feng J, Onaka T, Verbalis JG, Russell JA, Ludwig M. Responses of magnocellular neurons to osmotic stimulation involves coactivation of excitatory and inhibitory input: an experimental and theoretical analysis. *The Journal of neuroscience : the official journal of the Society for Neuroscience.* 2001; 21: 6967-77.
8. Potapenko ES, Biancardi VC, Zhou Y, Stern JE. Astrocytes modulate a postsynaptic NMDA-GABAA-receptor crosstalk in hypothalamic neurosecretory neurons. *The Journal of neuroscience : the official journal of the Society for Neuroscience.* 2013; 33: 631-40.
9. Braun MM, Barstow CH, Pyzocha NJ. Diagnosis and management of sodium disorders: hyponatremia and hypernatremia. *American family physician.* 2015; 91: 299-307.

10. Iovino M, Iacoviello M, De Pergola G, Licchelli B, Iovino E, Guastamacchia E, Giagulli VA, Triggiani V. Vasopressin In Heart Failure. *Endocrine, metabolic & immune disorders drug targets*. 2018.
11. Verbalis JG. Disorders of body water homeostasis. *Best Pract Res Clin Endocrinol Metab*. 2003; 17: 471-503.
12. Boscoe A, Paramore C, Verbalis JG. Cost of illness of hyponatremia in the United States. *Cost Eff Resour Alloc*. 2006; 4: 10.
13. Corona G, Giuliani C, Parenti G, Norello D, Verbalis JG, Forti G, Maggi M, Peri A. Moderate Hyponatremia Is Associated with Increased Risk of Mortality: Evidence from a Meta-Analysis. *PLOS ONE*. 2013; 8: e80451.
14. Oren RM. Hyponatremia in congestive heart failure. *Am J Cardiol*. 2005; 95: 2-7.
15. Carreño FR, Ji LL, Cunningham JT. Altered central TRPV4 expression and lipid raft association related to inappropriate vasopressin secretion in cirrhotic rats. *American Journal of Physiology - Regulatory, Integrative and Comparative Physiology*. 2009; 296: R454-R66.
16. Cunningham JT, Nedungadi TP, Walch JD, Nestler EJ, Gottlieb HB. Δ FosB in the supraoptic nucleus contributes to hyponatremia in rats with cirrhosis. *American Journal of Physiology - Regulatory, Integrative and Comparative Physiology*. 2012; 303: R177-R85.
17. Cunningham JT, Nissen R, Renaud LP. Norepinephrine injections in diagonal band of Broca selectively reduced the activity of vasopressin supraoptic neurons in the rat. *Brain research*. 1993; 610: 152-5.
18. Nedungadi TP, Cunningham JT. Differential regulation of TRPC4 in the vasopressin magnocellular system by water deprivation and hepatic cirrhosis in the rat. *American Journal of Physiology - Regulatory, Integrative and Comparative Physiology*. 2014; 306: R304-R14.

19. Choe KY, Han SY, Gaub P, Shell B, Voisin DL, Knapp BA, Barker PA, Brown CH, Cunningham JT, Bourque CW. High salt intake increases blood pressure via BDNF-mediated downregulation of KCC2 and impaired baroreflex inhibition of vasopressin neurons. *Neuron*. 2015; 85: 549-60.
20. Carreno FR, Walch JD, Dutta M, Nedungadi TP, Cunningham JT. Brain-derived neurotrophic factor-tyrosine kinase B pathway mediates NMDA receptor NR2B subunit phosphorylation in the supraoptic nuclei following progressive dehydration. *Journal of neuroendocrinology*. 2011; 23: 894-905.
21. Choe KY, Trudel E, Bourque CW. Effects of Salt Loading on the Regulation of Rat Hypothalamic Magnocellular Neurosecretory Cells by Ionotropic GABA and Glycine Receptors. *Journal of neuroendocrinology*. 2016; 28.
22. Marosi K, Mattson MP. Hold the salt: vasopressor role for BDNF. *Cell metabolism*. 2015; 21: 509-10.
23. Paxinos G, Watson C. *The Rat Brain in Stereotaxic Coordinates* San Diego: Academic Press, 1997.
24. Livak KJ, Schmittgen TD. Analysis of relative gene expression data using real-time quantitative PCR and the 2^{(-Delta Delta C(T))} Method. *Methods (San Diego, Calif)*. 2001; 25: 402-8.
25. Schmittgen TD, Livak KJ. Analyzing real-time PCR data by the comparative C(T) method. *Nature protocols*. 2008; 3: 1101-8.
26. Walch JD, Carreño FR, Cunningham JT. Intracerebroventricular losartan infusion modulates angiotensin type 1 receptor expression in the subfornical organ and drinking behaviour in bile duct ligated rats. *Experimental physiology*. 2013; 98: 922-33.

27. Walch JD, Nedungadi TP, Cunningham JT. ANG II receptor subtype 1a gene knockdown in the subfornical organ prevents increased drinking behavior in bile duct-ligated rats. *American journal of physiology Regulatory, integrative and comparative physiology*. 2014; 307: R597-607.
28. Nedungadi TP, Carreno FR, Walch JD, Bathina CS, Cunningham JT. Region specific changes in TRPV channel expression in the vasopressin magnocellular system in hepatic cirrhosis induced hyponatremia. *Journal of neuroendocrinology*. 2011.
29. Cunningham JT, Knight WD, Mifflin SW, Nestler EJ. An Essential role for DeltaFosB in the median preoptic nucleus in the sustained hypertensive effects of chronic intermittent hypoxia. *Hypertension (Dallas, Tex : 1979)*. 2012; 60: 179-87.
30. Kortenoeven MLA, Pedersen NB, Rosenbaek LL, Fenton RA. Vasopressin regulation of sodium transport in the distal nephron and collecting duct. *American Journal of Physiology-Renal Physiology*. 2015; 309: F280-F99.
31. Neuroendocrine Regulation of Hydromineral Homeostasis. *Comprehensive Physiology*.
32. Watts AG, Boyle CN. The functional architecture of dehydration-anorexia. *Physiology & behavior*. 2010; 100: 472-7.
33. Toney GM, Stocker SD. Hyperosmotic activation of CNS sympathetic drive: implications for cardiovascular disease. *The Journal of Physiology*. 2010; 588: 3375-84.
34. Son SJ, Filosa JA, Potapenko ES, Biancardi VC, Zheng H, Patel KP, Tobin VA, Ludwig M, Stern JE. Dendritic Peptide Release Mediates Interpopulation Crosstalk between Neurosecretory and Preautonomic Networks. *Neuron*. 2013; 78: 10.1016/j.neuron.2013.04.025.
35. Zhao B, Wong AY, Murshid A, Bowie D, Presley JF, Bedford FK. Identification of a novel di-leucine motif mediating K(+)/Cl(-) cotransporter KCC2 constitutive endocytosis. *Cellular signalling*. 2008; 20: 1769-79.

36. Wright R, Newey SE, Ilie A, Wefelmeyer W, Raimondo JV, Ginham R, McLlhinney RAJ, Akerman CJ. Neuronal Chloride Regulation via KCC2 Is Modulated through a GABAB Receptor Protein Complex. *J Neurosci*. 2017; 37: 5447-62.
37. Hewitt SA, Wamsteeker JI, Kurz EU, Bains JS. Altered chloride homeostasis removes synaptic inhibitory constraint of the stress axis. *Nature neuroscience*. 2009; 12: 438-43.
38. Kim JS, Kim WB, Kim YB, Lee Y, Kim YS, Shen FY, Lee SW, Park D, Choi HJ, Hur J, Park JJ, Han HC, Colwell CS, Cho YW, Kim YI. Chronic hyperosmotic stress converts GABAergic inhibition into excitation in vasopressin and oxytocin neurons in the rat. *J Neurosci*. 2011; 31: 13312-22.
39. Kim YB, Kim YS, Kim WB, Shen FY, Lee SW, Chung HJ, Kim JS, Han HC, Colwell CS, Kim YI. GABAergic excitation of vasopressin neurons: possible mechanism underlying sodium-dependent hypertension. *Circulation research*. 2013; 113: 1296-307.
40. Kaila K, Price TJ, Payne JA, Puskarjov M, Voipio J. Cation-chloride cotransporters in neuronal development, plasticity and disease. *Nat Rev Neurosci*. 2014; 15: 637-54.
41. Kahle KT, Delpire E. Kinase-KCC2 coupling: Cl⁻ rheostasis, disease susceptibility, therapeutic target. *Journal of neurophysiology*. 2016; 115: 8-18.
42. Better OS, Aisenbrey GA, Berl T, Anderson RJ, Handelman WA, Linas SL, Guggenheim SJ, Schrier RW. Role of antidiuretic hormone in impaired urinary dilution associated with chronic bile-duct ligation. *Clinical science (London, England : 1979)*. 1980; 58: 493-500.

FIGURES & TABLES

CHAPTER II - Figure II-1 LCM and gene expression of hits

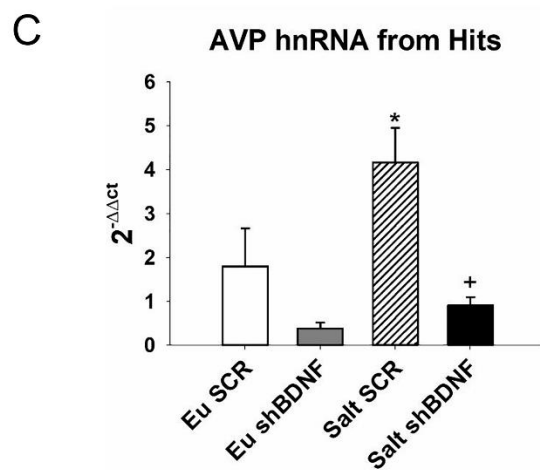
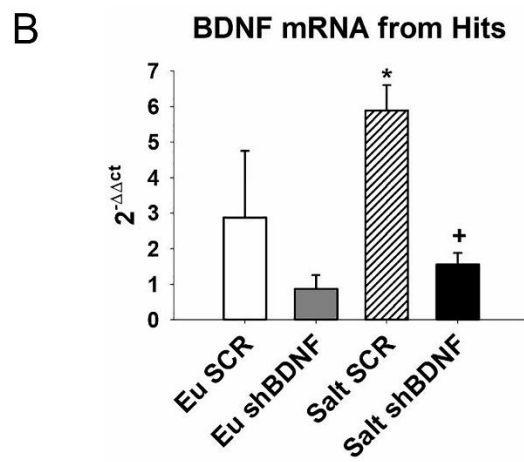
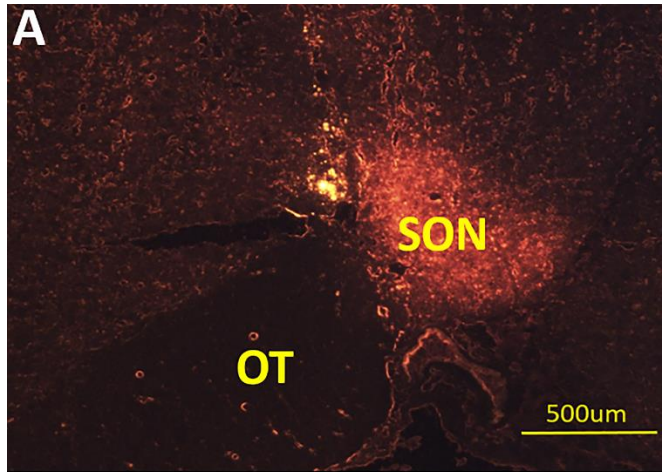


Figure 1: A: Representative digital image of mCherry fluorescence in the SON illustrating a successful injection. **B:** qRT-PCR data showing BDNF mRNA expression from the SON of rats with successful SON injections. **C:** AVP hnRNA expression from the SONs of rats with successful SON injections. Groups: Euhydrated rats injected with SCR virus, (Eu SCR, n = 6); Euhydrated rats injected with shBDNF virus (Eu shBDNF, n = 7); Salt loaded rats injected with SCR virus, (Salt SCR, n = 7) and Salt loaded rats injected with shBDNF virus (Salt shBDNF, n = 7). Data are mean \pm SEM. *P<0.05 vs. all other groups. [†]P<0.05 vs. Salt SCR.

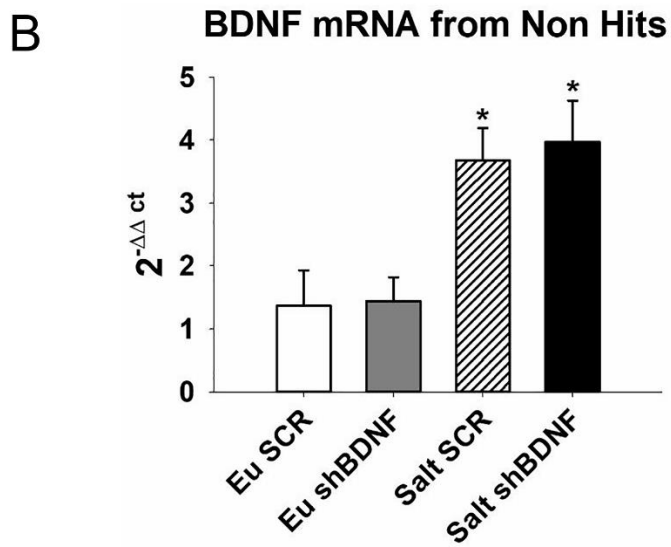
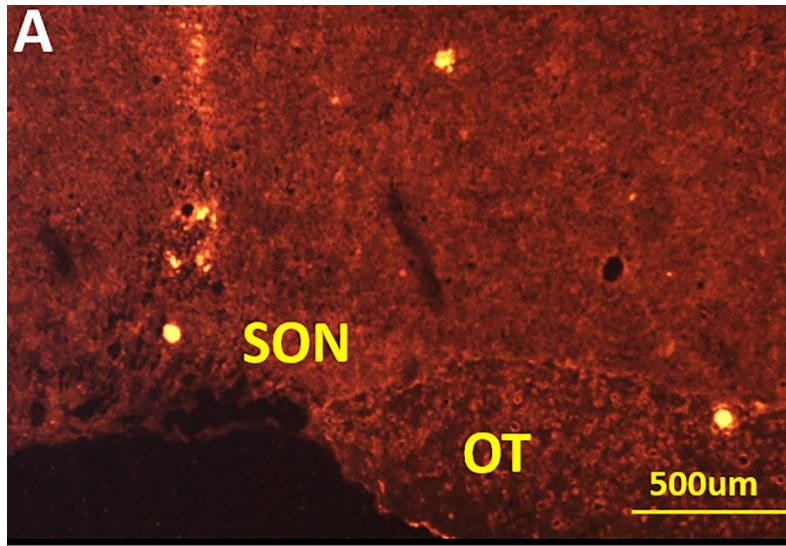
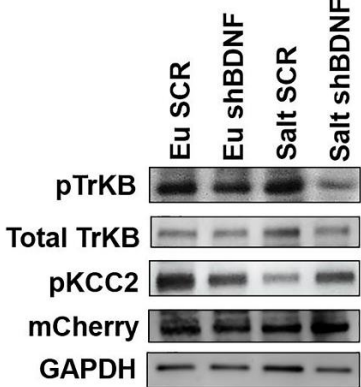
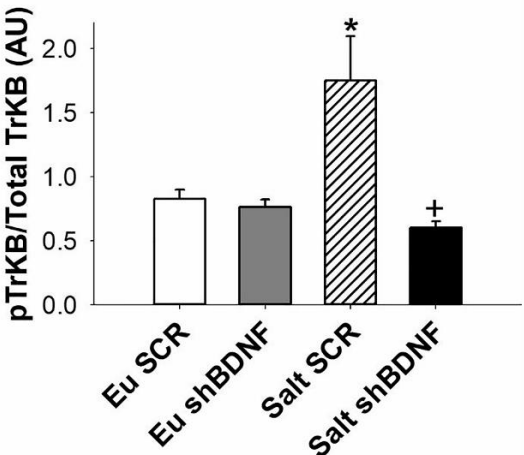


Figure 2: **A:** Example of missed injection. mCherry fluorescence is not seen in the SON as the viral injection did not include the SON. **B:** BDNF RNA from the SONs of rats with injections that did not include the SON. Groups: Eu SCR (n = 4); Eu shBDNF (n = 5); Salt SCR (n = 4); Salt shBDNF (n = 3). Data are mean \pm SEM. * is $P < 0.05$ vs. Eu groups.

A



B



C

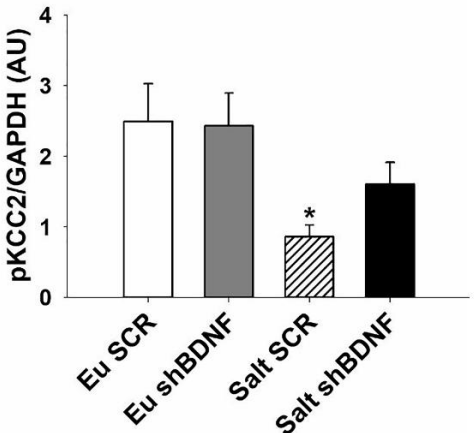


Figure 3: A: Sample Western blot images showing changes in protein expression of SON punches. mCherry protein expression images shows successful injections at SON **B:** Quantification of phosphorylated TrkB (normalized to total TrkB). Data are mean \pm SEM. * $P < 0.05$ vs. all other groups. [†] $P < 0.05$ vs. Salt SCR. **C:** Phosphorylated KCC2 normalized to GAPDH. * $P < 0.05$ vs. all other groups. Groups: Eu SCR (n = 6); Eu shBDNF (n = 6); Salt SCR (n = 8); Salt shBDNF (n = 8).

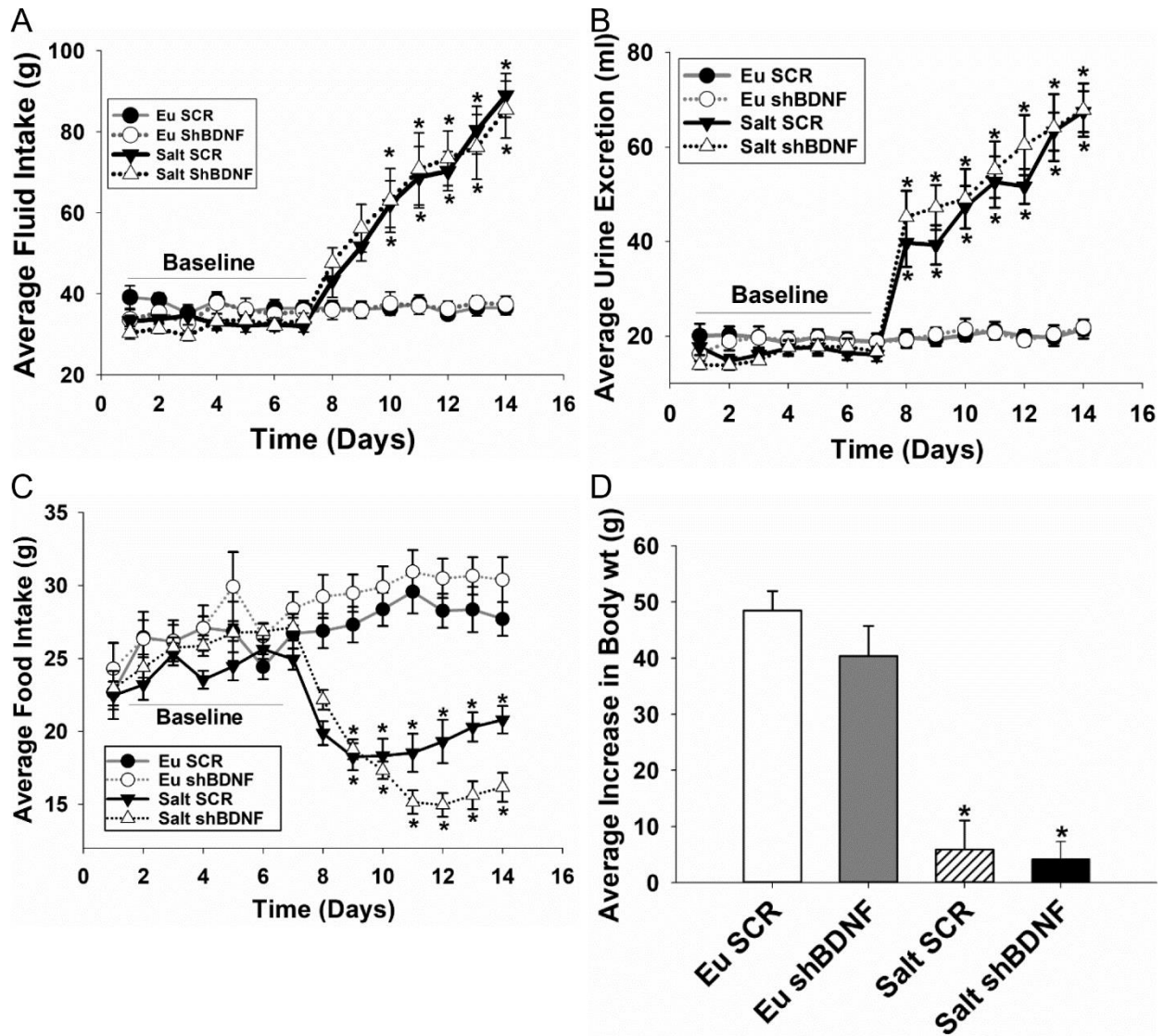


Figure 4: The effects of Salt loading and BDNF knockdown in the SON on **A:** Daily average fluid intake. **B:** Daily average urine excretion. **C:** Daily average food intake. In A-C, *P<0.05 vs. Eu groups and vs. Baseline. **D:** Average daily changes in body weight. Data are mean \pm SEM. *P<0.05 vs. Eu groups. Groups: Eu SCR (n = 8); Eu shBDNF (n = 8); Salt SCR (n = 8); Salt shBDNF (n = 8).

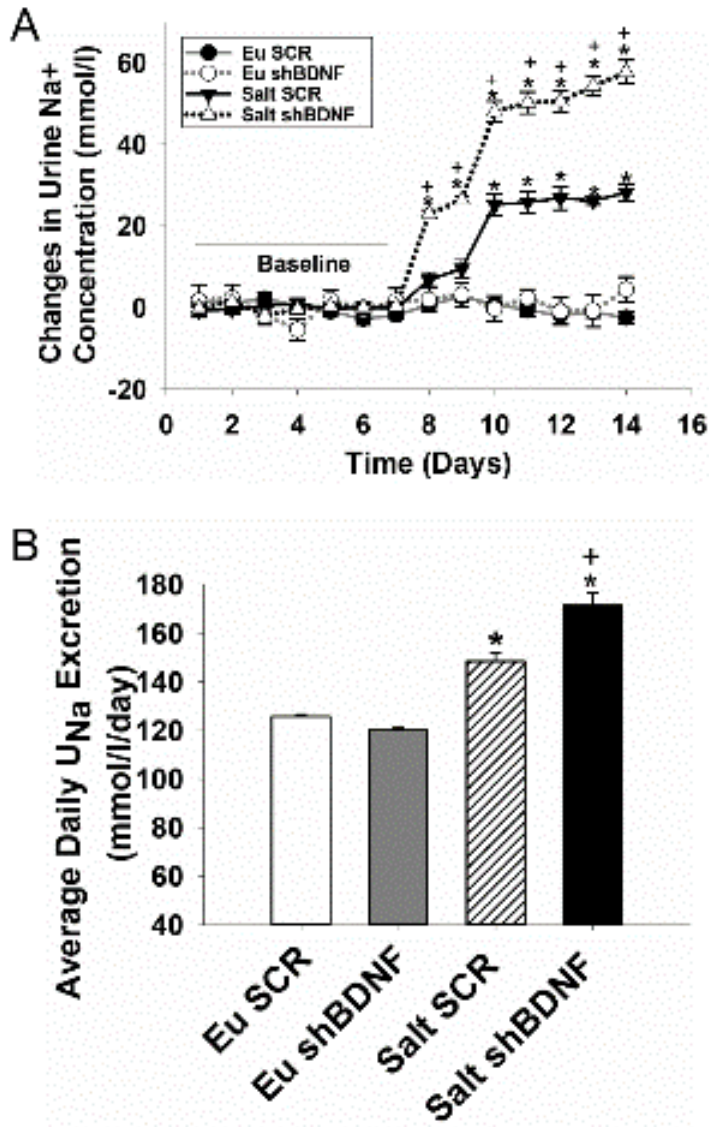


Figure 5: Urine sodium excretion **A:** Daily average changes in urine sodium concentration.

* $P < 0.05$ vs. Eu groups and baseline. † $P < 0.05$ vs. Salt SCR **B:** Average urine sodium excretion during 7 days of salt treatment. Data are mean \pm SEM. * $P < 0.05$ vs. Eu groups. † $P < 0.05$ vs. Salt SCR. Groups: Eu SCR (n = 8); Eu shBDNF (n = 8); Salt SCR (n = 8); Salt shBDNF (n = 8).

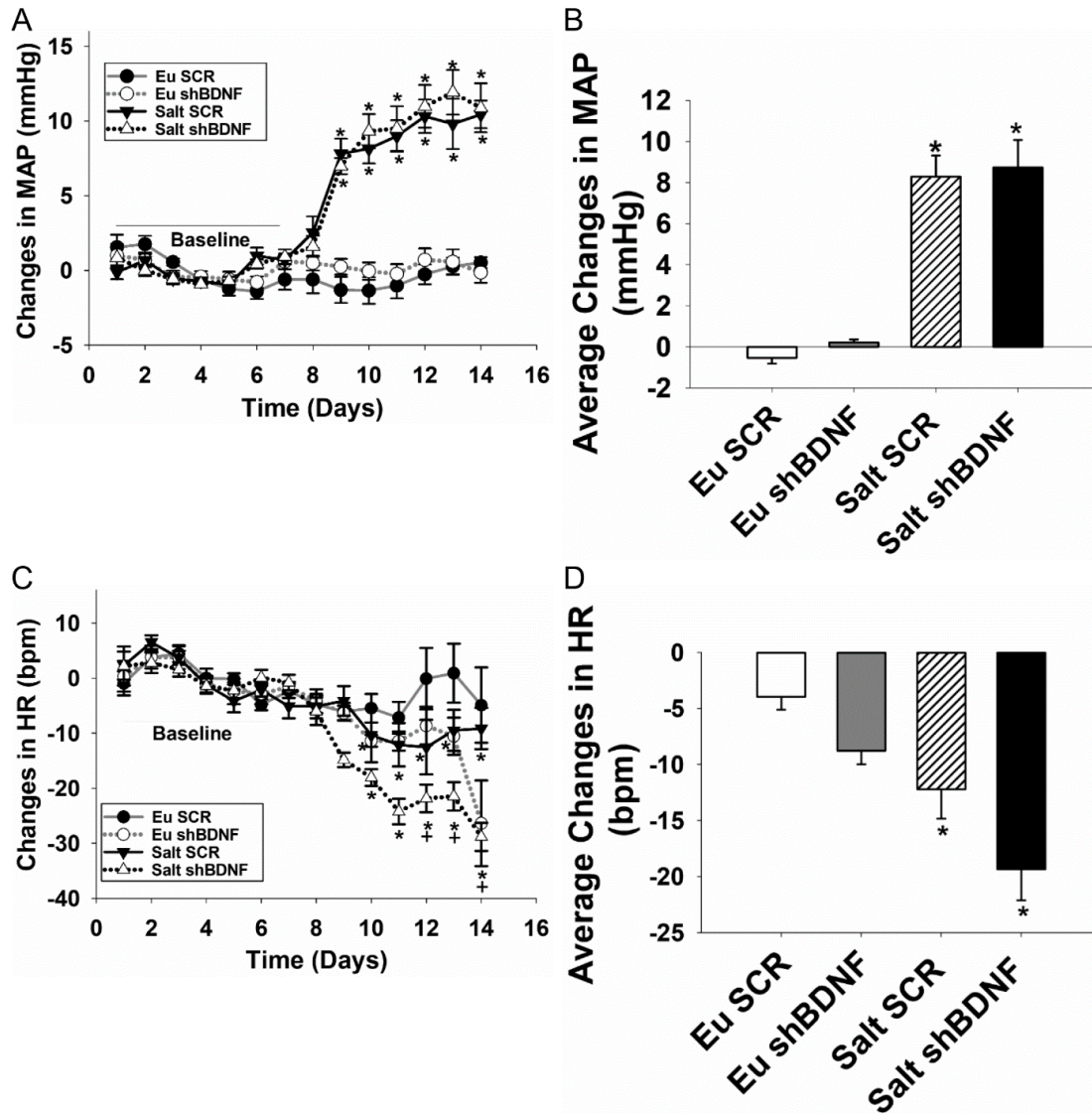


Figure 6: Effect of salt loading and BDNF knockdown in the SON on **A:** Daily average changes in Mean Arterial Pressure. * $P < 0.05$ vs. Baseline and Eu groups. **B:** Average changes in Mean Arterial Pressure. * $P < 0.05$ vs. Eu groups. **C:** Daily average changes in Heart Rate. * $P < 0.05$ vs. Baseline. $^+P < 0.05$ vs. Eu SCR. **D:** Average changes in Heart rate. Data are mean \pm SEM. * $P < 0.05$ vs. Eu groups. Groups: Eu SCR (n = 9); Eu shBDNF (n = 9); Salt SCR (n = 9); Salt shBDNF (n = 9).

CHAPTER II – TABLE II-I Primer sequences for qRT-PCR

Gene	Primer Sequences
BDNF Forward	5'-ATGACCATCCTTTTCCTTACTATGGT-3'
BDNF Reverse	5'-TCTTCCCCTTTTAATGGTCAGTGTAC-3'
hnAVP Forward	5'-GCCCTCACCTCTGCCTGCTA-3'
hnAVP Reverse	5'-CCTGAACGGACCACAGTGGT-3'
S18 Forward	5'-CAGAAGGACGTGAAGGATGG-3'
S18 Reverse	5'-CAGTGGTCTTGGTGTGCTGA-3'

Table 1: Primer sequences for qRT-PCR

CHAPTER II – TABLE II-2 Primer sequences for qRT-PCR

Table 2: Plasma osmolality, hematocrit and AVP concentration in euhydrated rats injected with the control vector (Eu SCR), euhydrated rats injected with shRNA against BDNF (Eu shBDNF), salt loaded rats injected with control vector (Salt SCR), and salt loaded rats injected with shRNA against BDNF (Salt shBDNF) groups.

	Eu SCR	Eu shBDNF	Salt SCR	Salt shBDNF
Osmolality (mOsm/kg)	301.3±1.45 (14)	299.8±1.05 (13)	313.3±1.75 (13)*	305.1±0.68 (11) ⁺
Hematocrit (%)	42.6±0.53 (14)	41.8±0.64 (13)	47.8±0.74 (13)*	44.4±0.60 (11) ⁺
Plasma AVP (pg/ml)	15.7±4.01 (6)	9.3±0.81 (6)	59.9±8.37 (5)*	16.2±1.30 (5) ⁺

Values are mean ±SEM; n, number of rats in each group, in parenthesis. *P<0.05 vs. Control groups, +P<0.05 vs. Salt SCR.

CHAPTER II – TABLE II-3 Telemetry values: MAP and HR

Table 3: Absolute mean arterial pressure and Heart rate in euhydrated rats injected with the control vector (Eu SCR), euhydrated rats injected with shRNA against BDNF (Eu shBDNF), salt loaded rats injected with control vector (Salt SCR), and salt loaded rats injected with shRNA against BDNF (Salt shBDNF) groups.

Absolute Values		Eu SCR	Eu shBDNF	Salt SCR	Salt shBDNF
MAP (mmHg)	Baseline	107.7±0.49 (9)	106.7±0.28 (9)	105.1±0.30 (9)	104.1±0.28 (9)
	Treatment	107.2±0.28 (9)	106.9±0.15 (9)	113.5±1.03 (9)*	112.8±1.33 (9)*
HR (bpm)	Baseline	387.6±1.23 (9)	385.4±1.05 (9)	378.7±1.86 (9)	379.0±0.73 (9)
	Treatment	383.7±1.17 (9)	374.1±2.72 (9)	366.5±1.62 (9) ⁺	359.6±2.74 (9) ⁺

Values are mean ±SEM; n, number of rats in each group, in parenthesis. *P<0.05 vs. Control groups. No significant difference between Salt SCR and Salt shBDNF groups. +P<0.05 vs. Eu SCR.

ORIGINAL RESEARCH ARTICLE – UNDER REVIEW

CHAPTER III

INTRACELLULAR CHLORIDE REGULATION OF SUPRAOPTIC VASOPRESSIN
NEURONS FROM SALT LOADED RATS

Kirthikaa Balapattabi, George E. Farmer, PhD, Blayne A. Knapp, Joel T. Little, Martha
Bachelor, Joseph P. Yuan, PhD and J. Thomas Cunningham, PhD

Submitted to J Neuroendocrinol. Under Review – ID: JNE-19-0039-OA

ABSTRACT

Salt loading (SL) impairs GABA_A inhibition of arginine vasopressin (AVP) neurons in the supraoptic nucleus (SON) of hypothalamus. Based on previous studies, we hypothesized that SL activates tyrosine receptor kinase B (TrkB) and downregulates the activity of K⁺/Cl⁻ co-transporter 2 (KCC2). Downregulation of KCC2 decreases the efflux of chloride ions causing increases in [Cl]_i in SON AVP neurons. In addition, the role of NKCC1 in chloride regulation during SL was tested. This study combined virally mediated chloride imaging with ClopHensorN with single cell Western blot analysis capillary based Simple Wes technology.

An adeno associated virus with ClopHensorN and a vasopressin promoter (AAV2-0VP1-ClopHensorN) was bilaterally injected in the SON of adult male Sprague Dawley rats that were either euhydrated (Eu) or salt loaded (SL) for 7 days. Acutely dissociated SON neurons expressing ClopHensorN were tested for decreases or increases in [Cl]_i in response to focal application of the GABA_A agonist muscimol (100uM). SON AVP neurons from Eu rats showed muscimol-induced chloride influx ($p < 0.05$; 23/35). SON AVP neurons from SL rats either significantly increased chloride efflux ($p < 0.05$; 27/39) or did not change chloride flux (12/39). The SON AVP neurons that responded to muscimol appeared viable and expressed KCC2 co-transporter and β -Actin. Neurons that did not respond during chloride imaging did not have KCC2 and β -Actin protein expression. The KCC2 antagonist (VU0240551, 10uM) significantly blocked the chloride influx in cells from Eu rats but did not affect cells from SL rats. A NKCC1 antagonist (Bumetanide, 10uM) significantly blocked the chloride efflux in cells from SL rats but had no effect on cells from Eu rats. The TrkB antagonist (AnA-12, 50uM) and protein kinase inhibitor (K252a, 100nM) each significantly blocked chloride efflux in SON AVP neurons from

SL rats. Salt loading increases $[Cl]_i$ in SON AVP neurons through TrkB-KCC2 dependent mechanism in rats.

INTRODUCTION

Magnocellular neurosecretory cells (MNCs) located in supraoptic nuclei (SON) and the paraventricular nuclei of the hypothalamus produce and release the hormone arginine vasopressin (AVP) into circulation⁽¹⁻³⁾. An important systemic effect of AVP is water reabsorption via V2 receptors in the kidney. Excess water retention associated with heart and liver failure negatively influences the morbidity and mortality associated with these disorders⁽⁴⁻⁶⁾. While it is known that AVP contributes to water retention in these disorders, the mechanisms responsible for the inappropriate secretion of AVP is not known^(7, 8).

Previous studies have shown that salt loading (SL; drinking water replaced by 2% NaCl solution for 7 days) can cause a sustained increase in AVP secretion due to changes in the excitability of AVP neurons^(1, 2, 9). One mechanism that has been shown to contribute to sustained AVP release in SL rats is a change in the valence of the neurons' response to GABA. Although controversial, GABA mediated neurotransmission is generally described as a primary inhibitory mechanism in SON AVP neurons⁽⁹⁻¹¹⁾. The inhibitory effect of GABA depends on a low intracellular chloride concentration ($[Cl^-]_i$). Increases in $[Cl^-]_i$ can change GABA-mediated inhibition to excitation by reversing the direction of chloride movement across the cell membrane. The balance between neural excitation and inhibition is crucial to maintain the concentration of circulating AVP within normal limits^(9, 12). In most neurons, $[Cl^-]_i$ is regulated by cation chloride cotransporters such as K^+/Cl^- co-transporter 2 (KCC2), which causes efflux of Cl^- ions, and $Na^+/K^+/Cl^-$ cotransporter 1 (NKCC1), which causes influx of Cl^- ions⁽¹³⁻¹⁵⁾. Changes in the expression or activity of these transporters has been shown to influence the strength and valence of the neuronal response to GABA in several systems⁽¹⁶⁻¹⁸⁾.

Previous studies demonstrate that SL, likely through the actions of Brain Derived Neurotrophic Factor (BDNF), decreases the activity of KCC2 in SON causing increased AVP secretion^(1, 2, 19). However, the mechanism leading to increases in $[Cl^-]_i$ is not completely understood. Based on previous studies^(1-3, 19), we hypothesize that SL activates the BDNF receptor, tyrosine receptor kinase B (TrkB) and downregulates the activity of KCC2 co-transporter. Downregulation of KCC2 decreases the efflux of chloride ions causing increases in $[Cl^-]_i$ in SON AVP neurons. Also, the expression of KCC2 in the SON AVP neurons is controversial, as few studies suggest AVP neurons lack KCC2 while others have shown the immunohistochemical expression of KCC2 in these neurons and the role of NKCC1 in chloride regulation during SL is not completely understood.

In this study, we used virally mediated ClopHensorN, a genetically encoded ratiometric fluorescent chloride imaging technique⁽²⁰⁾, to measure changes in $[Cl^-]_i$ in dissociated AVP neurons by combining it with an AVP specific promoter⁽²¹⁾. ClopHensorN is composed of a Cl^- -sensitive variant of green- fluorescent protein (E2GFP) and a Cl^- -insensitive red-fluorescent protein (TdTomato) acting as invariant reference for ratiometric imaging^(22, 23). The ratiometric analysis (E2GFP/TdTomato) of the emitted fluorescence provides the Cl^- measurement. Increased $[Cl^-]_i$ decreases E2GFP fluorescence relative to TdTomato and vice versa. ClopHensorN allows for measuring changes of neuronal $[Cl^-]_i$ at the single-cell level without disrupting the native cellular milieu. Furthermore, we combined single cell protein expression measurements with chloride imaging to determine KCC2 expression in SON AVP neurons and the modulation of neuronal $[Cl^-]_i$ in response to various antagonists.

SIGNIFICANCE

This study explores the mechanism contributing to dysregulation of Cl⁻ concentration leading to loss of synaptic GABA inhibition in AVP neurons of SON during SL. These experiments test the role of KCC2 and NKCC1 in chloride regulation of AVP neurons in response to SL using live cell chloride imaging and single cell western blot analyses.

MATERIALS AND METHODS

ANIMALS

The experiments were conducted in accordance with the National Institute of Health Guide for the Care and Use of Laboratory Animals. All the animal protocols used in this study were approved by the UNT Health Science Center Institutional Animal Care and Use Committee. The outbred adult male (250-300 g) Sprague-Dawley rats (Charles River, Wilmington, MA) used in this study were maintained on a 12/12h light dark cycle. The rats were individually housed due to the use of survival surgery and individual fluid intake measurements in the protocol. All animals were housed in a temperature (24-26 °C) and humidity (40-60%) controlled environment with *ad libitum* access to food (Teklad LM-485 Rat Sterilizable Diet with 0.3% Sodium, Envigo, Somerset, NJ) and water unless otherwise indicated. Aseptic techniques were used to conduct survival surgeries. All rats were subcutaneously administered with procaine penicillin G (30,000 U) to prevent postoperative infection. Carprofen (Rimadyl, 2 mg), non-steroidal anti-inflammatory drug was given orally before and after surgery for pain management.

STEREOTAXIC SURGERY

The AAV2-0VP1-ClopHensorN was bilaterally injected into the SON of each rat. Separate group of rats were injected in the SON with an AAV vector that contained only the AVP

promoter and GFP (also prepared by the UNC Vector Core). For each injection, the rats were anaesthetized with isoflurane (2-3%) and placed in stereotaxic frame (David Kopf Instruments, Tujunga, CA). Their skulls were exposed and leveled between two cranial suture landmarks - lambda and bregma⁽²⁴⁾. A micromanipulator was used to position the injector at the SONs (1.4 mm posterior, 9.1 mm ventral, and ± 1.4 mm lateral from bregma). The AAV2-0VP1-ClopHensorN, or the AAV2-0VP1-eGFP vectors were bilaterally injected in the SON (300 nl/side) at a titer of 1.0×10^{13} GC/ml (UNC Vector Core, Chapel Hill, NC). Each injection was made over a 10-min period. After the injection, the injector was left in place for 5 minutes then slowly removed. The incision was closed with absorbable antibiotic sutures.

IMMUNOHISTOCHEMISTRY

Four weeks after the injections with the AAV2-0VP1-eGFP, rats were deeply anesthetized with inactin (100mg/kg, ip.), perfused transcardially with phosphate-buffered saline (PBS) followed by 4% paraformaldehyde in PBS. After the perfusion, brains were extracted from the skull and placed in 30% sucrose until dehydrated. The brains were serial sectioned at 40um-thickness. Sections were processed for AVP using guinea pig polyclonal Anti-(Arg⁸)-VP (1:1000; Cat# T-5048 Peninsula Labs, San Carlos, CA), and oxytocin (OXT) using anti-OXT mouse monoclonal IgG (1:10000; Cat MAB5296, Millipore, Billerica, MA). Sections were incubated in primary antibodies for two days at 4°C. Following primary antibody incubation, sections were then rinsed with PBS, followed by sequential incubation in respective secondary antibodies against host species conjugated to Cy3 fluorophores (Cy3-conjugated anti-guinea pig IgG (1:10000; Cat 706-165-148, Jackson ImmunoResearch Laboratories, Inc. West Grove, PA) or Cy3-conj. Affinipure Anti-Mouse IgG (1:10000; Cat 715-165-151, Jackson ImmunoResearch Laboratories, Inc.). Sections were rinsed again in PBS, mounted on gelatin coated slides, and cover slipped with

Vectashield (Vecta Labs, Burlingame, CA) mounting media. Sections were examined for co-localization of the GFP reporter with AVP or OXT immunofluorescence to confirm vector transfection specificity.

SALT LOADING

After two weeks of recovery from surgery, daily fluid intake was measured by filling the water bottles up to a predetermined weight in grams and subtracting the remaining weight 24 h later. The rats were provided with *ad libitum* access to water for first 7 days to record baseline fluid intake and body weight. Following the baseline measurements, a subset of rats had their water replaced with 2% salt (NaCl) to drink for 7 days as previously described ⁽²⁾. The euhydrated (Eu) rats were used as controls and the salt loaded (SL) rats were used as treatment groups. At the end of the 7-day SL protocol, the rats were anesthetized with inactin (100 mg/kg ip, Millipore Sigma, Burlington, MA) and decapitated in order to isolate neurons from the SON.

PLASMA MEASUREMENTS

Trunk blood was collected from each rat after decapitation and it was centrifuged as previous described ⁽¹⁾. Plasma was collected from each sample for measuring plasma osmolality, hematocrit, circulating AVP and copeptin. Copeptin (CPP) is widely used as biomarker for AVP secretion ⁽²⁵⁾ and was measured in this study in addition to AVP.

Separate 5 to 6 ml of blood samples were collected in Vacutainer tubes containing the anticoagulant EDTA (12 mg). The proteinase inhibitor aprotinin (0.6 TIU/ml of blood; Phoenix Pharmaceuticals, Inc, Burlingame, CA) was added to the sample and centrifuged at 1600 g for 15 minutes at 4° C. Two-three ml of plasma was removed from each sample and an aliquot of plasma was used to extract peptides by solid phase extraction using C-18 SEP-Column

(Phenomenex, Torrance, CA). After the extraction, each sample was subjected to vacuum centrifugal concentration. The extracted peptide was used to measure circulating AVP with specific ELISA (EK-065-07, Phoenix Pharmaceuticals, Inc). CPP concentration was measured in plasma samples by using specific ELISA according to the manufacturer's instructions (MBS724037, MyBioSource, Inc, San Diego, CA). Four parametric logistic analysis (4-PL) was performed to quantify the concentration of AVP and CPP.

Another 1 to 2 ml of blood was collected in 2 ml microcentrifuge tube and prepared for measuring plasma osmolality and hematocrit as previously described ⁽²⁶⁾. Two heparinized capillary tubes (Fisher Scientific, Hampton, NH) were filled with blood for measuring hematocrit using Micro-Hematocrit capillary tube reader (Lancer, St. Louis, MO). The remaining blood sample was centrifuged at 1600 g for 5-10 minutes and plasma was collected to measure plasma osmolality using vapor pressure osmometer (Wescor, Logan, UT).

SON DISSOCIATION

The brains were rapidly removed and placed in ice-cold (0 to +4°C) artificial cerebrospinal fluid (aCSF), bubbled with carbogen gas (95% O₂, 5% CO₂). The composition of the standard aCSF was 120mM NaCl, 3mM KCl, 2mM MgCl₂, 2mM CaCl₂, 1.2mM NaH₂PO₄, 23mM NaHCO₃ and 11mM D-Glucose. The carbogen gas maintained the pH between 7.35 and 7.40. The osmolality was between 290 to 300mOsm. The SONs were dissected from surrounding tissue using a microscope and iris scissors. The extracted tissue containing the SONs was placed in calcium free Hibernate media that contained papain (0.2% w/v; Worthington Biochemical Corporation, Lakewood, NJ). The tissue was incubated at 32°C water bath for 30mins for enzymatic dissociation. The cells were dissociated mechanically by gentle trituration in Hibernate A media (Gibco Life Technologies, Gaithersburg, MD) with B27 supplement (2% v/v;

Gibco Life Technologies). The dissociated cells were then centrifuged and suspended in Neurobasal A medium (Gibco Life Technologies) with B27 supplement (2% v/v), L-Glutamine (200mM) and penicillin/streptomycin (100U/ml). Dissociated SON neurons were plated on coverslips coated with 0.1% poly-D-lysine (Sigma, St. Louis, MO) and incubated at 37°C in 5% CO₂ humidified incubator for 2 hours before recording⁽²⁷⁻³¹⁾. Images were collected after a 2-hour incubation period and recordings continued for up to 6 hours after the end of the incubation period.

ClophensorN CHLORIDE IMAGING

The coverslips with SON neurons were transferred to a recording chamber on the stage of an inverted microscope (Olympus Corporation, Center Valley, PA), which was equipped for epifluorescence imaging. The cells were continuously perfused with 95% O₂, 5% CO₂ oxygenated aCSF. The dissociated neurons were visualized using fluorescence as an estimate of neuronal viability. To determine if successful expression of ClophensorN resulted in corresponding expression of both green fluorophore (E2GFP) and the fused red fluorophore (TdTomato), cells were excited at 488nm (for E2GFP, “green channel”) and at 594nm (for the TdTomato, “red channel”). Emission was collected by switching filters (Prior Lumen 200 Pro, Prior Scientific, Inc., Rockland, MA): between 500 and 550nm for the green channel and between 650 and 700nm for the red channel^(22, 32). The reliability of cellular viability was confirmed by each cell’s ability to respond to antagonists during imaging and for some experiments by single cell measurements of β -Actin protein by Simple Wes analysis.

Individual SON neurons were visualized using a 40 \times water-immersion objective and selected for imaging. Putative healthy AVP neurons with uniform bright appearance indicative of an intact plasma membrane and expressing both E2GFP and TdTomato were chosen for imaging. Imaging

for ClopHensorN was performed by sequentially exciting the individual AVP neurons alternately using 458 and 594nm. The emission was collected between 500 and 550nm for the 458nm and between 650 and 700nm for the 594nm excitation. Images were captured with camera (Hamamatsu Camera Controller, C10600, San Jose, CA) using MetaFluor software (Molecular Devices, San Jose, CA). Each image was processed for background (measured from a non-fluorescent area) subtraction and fluorescence was measured every 3s within regions of interest selected from individual neurons using a F_{445}/F_{554} ratio.

In a subset of experiments, whole-cell micropipettes were used to induce changes in intracellular chloride concentrations that were measured using ClopHensorN fluorescence. The electrodes were prepared from borosilicate glass capillaries (World Precision Instruments, Sarasota, FL) using a horizontal pipette puller (Model P-2000, Sutter Instrument Co, Novato, CA). The diameter of the tip was approximately 1-2 μm for each micropipette. For these experiments, the micropipette solution consisted of either 130 mM CsCl, 10 mM KCl, 10 mM HEPES, 1.1 mM EGTA, 2 mM Mg_2ATP , 0.3 mM Na_3GTP to create a high $[\text{Cl}^-]$ solution or 140 mM K-gluconate, 10 mM HEPES, 1.1 mM EGTA, 2 mM Mg_2ATP , 0.3 mM Na_3GTP for a low $[\text{Cl}^-]$ solution. Baseline fluorescence F_{445}/F_{554} ratio was measured for 90 to 120 s prior to whole cell access. After whole cell access, the fluorescence was recorded for 10 minutes.

In other experiments, micropipettes were used for focal drug application by adding the GABA_A agonist muscimol to the aCSF solution. After recording the baseline fluorescence for one minute, muscimol (100 μM) was focally applied for 10s (10 psi) using a pneumatic Pico spritzer (WPI, Sarasota, FL) with a patch pipette placed 100-150 μm upstream of the AVP neuron. Following the initial 4-minute recording, bath solution (aCSF) was switched to aCSF containing antagonists and imaging resumed 5 minutes later. After 5 minutes of perfusion with the antagonist, the

muscimol injection was repeated to determine its effects on the muscimol response^(32, 33). The duration and experimental conditions utilized were first verified using control imaging to muscimol response with no bath application of antagonists.

At the end of some of the experiments, the cell was harvested with a patch pipette filled with aCSF. The cell was aspirated into the patch pipette by applying negative pressure while observing the process using the microscope.

DRUGS AND REAGENTS

Stock solutions of muscimol (100mM, Sigma-Aldrich, St. Louis, MO) were created by first dissolving the muscimol in 0.05M HCl and diluting it to the final concentration in aCSF (100µM). The other antagonists used in these studies (all obtained from Tocris, Bristol, UK) were first dissolved in DMSO (Sigma-Aldrich, St. Louis, MO; Stock Concentrations: K252a, 100µM; AnA-12, 10mM; VU0240511, 10mM and Bumetanide, 50mM) then diluted to their final concentrations in aCSF for bath application. The TrkB receptor was blocked by using either broad-spectrum protein kinase inhibitor K252a (100nM) or the TrKB receptor antagonist AnA-12 (50µM). KCC2 antagonist VU0240511 (10µM) and NKCC1 cotransporter antagonist bumetanide (10µM) were also used. The final concentration of DMSO used to solubilize the antagonists ranged from 0.5 to 0.02% when added to the bath solution.

AAV2-0VP1-ClopHensorN: An pAAV-bGH(+) shuttle vector containing poly(A) tail downstream of the multicloning site (Vector BioLabs, Malvern, PA) was used to prepare the plasmid for packaging as an AAV. The ClopHensorN plasmid (Addgene #25940 pcDNA3-PalmPalm-ClopHensorN) was cloned into the pAAV-bGH(+) vector along with an AVP specific promoter (p2.0VPI.EGFP; Addgene Plasmid #40868 from Harold Gainer⁽²¹⁾) using EcoRI/NotI restriction sites. The promoter and reading frame were sequenced to confirm the direction of

ClophensorN cDNA insertion and verify the entire sequence. The resulting plasmid-0VP1-ClophensorN was sent to the University of North Carolina Vector Core for packaging in an AAV2 vector.

SINGLE CELL WES ANALYSIS

Individual AVP neurons were used for Simple Wes analysis to measure KCC2 and β -Actin expression. Each cell that was collected as described above was released from the micropipette into a standard (volume) PCR tube using a syringe. Each PCR tube contained 5.0ul of RIPA lysis buffer containing DTT, chelators and protease phosphatase inhibitor cocktail. The samples were frozen on dry ice immediately for later protein analysis. As a control for contamination, an aCSF sample from the same preparation was collected in separate tube and it was analyzed in parallel with the single-cell samples. The cells were lysed by vortexing the tube for 1-2 mins followed by indirect sonication for 5 minutes in ice bath ^(34, 35).

The Simple Wes system (Protein Simple, San Jose, CA) was used to quantify total KCC2 and β -Actin protein expression in the individual neurons. In brief, the standard matrix (12–230 kDa) and Anti-Rabbit Detection Module were used. The undiluted protein samples were mixed with Fluorescent Master Mix and heat denatured at 95°C for 5 minutes. The samples, blocking reagent, primary antibodies: total KCC2 (rabbit; 1:50; 07-432, Millipore) and β -Actin (rabbit 1:500; NB600-532, Novus Biologicals), HRP-conjugated secondary antibodies, and chemiluminescent substrate were pipetted into the separation module plate. The assay plate and the capillary cartridge were loaded into the Simple Wes instrument. The samples were processed using default settings and according to the manufacturer's instructions: stacking and separation at 375 V for 30 min; blocking reagent for 5 min, primary and secondary antibody both for 30 min; Luminol/peroxide chemiluminescence detection for ~15 min (exposures of 1-2-4-8-16-32-64-

128-512s). The specific peaks for total KCC2 and β -Actin were obtained from resulting electropherograms using Compass software v2.7 (Protein Simple, San Jose, CA).

STATISTICAL ANALYSIS

Statistical analyses were performed using SigmaPlot 12.0 (Systat Software Inc., San Jose, CA). Data were reported as mean \pm SEM. For immunohistochemistry, the numbers of cells labeled with eGFP were manually counted using ImageJ software, and double labelling of AVP-GFP and OXT-GFP were calculated and expressed as a percentage of neurons containing double-labeling. Chloride imaging data were analyzed by Chi-squared test and two-way repeated measures ANOVA with treatment (SL vs. euhydrated) as first factor and bath applied antagonists as second factor along with Tukey comparisons. Fluid intake data were analyzed by separate two-way repeated measures ANOVA with treatment (SL vs. euhydrated) as first factor and time as second factor followed by Tukey post hoc tests. All other data were analyzed using Student's t-test. Composite figures were assembled using the 'magick' package in RStudio. For all tests, a p-value less than 0.05 was considered to be statistically significant. The group sizes were determined by power analysis and effect size calculated from our previously published work ^(2, 26, 36) and preliminary data using SigmaPlot software. The minimal n's per group for each experiment was decided to have an appropriately powered study with the effect size of approximately 0.7 (70%). The n's in the chloride imaging data indicates number of cells which are obtained from 4 to 6 rats in each group.

RESULTS

IMMUNOHISTOCHEMISTRY

In order to verify the specificity of the AVP promoter, we injected an AAV2 vector (p3.0VP1.EGFP) with an AVP promoter and an eGFP reporter targeted to the SON. Previous studies have shown the specific expression of eGFP in AVP neurons in the SON using this promoter⁽²¹⁾. Co-localization of GFP with either AVP or OXT neuron was determined by calculating percent double-labeling using fluorescent microscope. Our results indicate the co-localization of GFP and AVP MNCs in the SON (89% GFP-AVP double labeling, n=3) (Figures 1A-C) and GFP and OXT (0.08% GFP-OXT double labeling, n=3) (Figures 1D-F). Given this demonstration of successful vector transduction, we can conclude that vectors using this promoter are primarily selective to AVP expressing MNCs.

CHANGES IN FLUID INTAKE AND BODY WEIGHT

Fluid intake was measured daily for 7 days before and during the 7-day 2% SL protocol. The fluid intake increased steadily during the SL, these rats consumed larger volumes of fluid compared to the control Eu rats. In addition, the SL rats had less increase in body weight compared to the Eu rats. Two-way repeated measures ANOVA revealed a significant interaction indicating that fluid intake was affected by time and the treatment protocol (Time x Treatment $F(13,65) = 26.040, p < 0.001$; Figure 2). Post hoc multiple comparisons between the factors revealed that, while there were no differences between the groups during baseline, SL significantly increased fluid intake. Also, the average body weight increase during SL was significantly lower in SL group compared to the Eu group ($t = 2.956$; d.f. =10; $p < 0.05$; Figure 2).

CHANGES IN PLASMA AVP, CPP, OSMOLALITY AND VOLUME

At end of the study, plasma samples were collected to measure AVP and CPP concentrations along with osmolality and hematocrit measurements. Plasma samples from SL rats had higher AVP and CPP concentrations as compared to Eu rats. Seven days of SL significantly increased circulating AVP ($t = -4.682$; d.f. =10; $p < 0.001$) and CPP ($t = -4.831$; d.f. =10; $p < 0.001$) as compared to Eu rats (Table 1).

Plasma osmolality and hematocrit values were significantly different between the groups (Plasma osmolality $t = -6.799$; d.f. =16; $p < 0.001$; Hematocrit $t = -6.123$; d.f. =16; $p < 0.001$). Our data shows that SL significantly increased plasma osmolality and hematocrit values compared to the Eu group in accordance with the previous studies ^(1, 37).

CHLORIDE IMAGING

ClopHensorN CALIBRATION FOR CHLORIDE MEASUREMENT

The effectiveness of the cell dialysis established after whole-cell penetration were verified by patch capacitance and conductance. Images of AVP neurons expressing the ClopHensorN plasmid are shown in Figure 3. Note that an increase in intracellular chloride decreases the fluorescence F_{445}/F_{554} ratio (Figure 3A(i) & 3A(ii)) while a decrease in intracellular chloride increases the F_{445}/F_{554} ratio (Figure 3B(i) & 3B(ii)). When cesium chloride (CsCl, 130 mM) with high $[Cl^-]$ was used as patch pipette solution, ClopHensorN fluorescence decreased following whole-cell access indicating Cl^- influx due to a change in the concentration gradient (Figure 3A(iii)). Dialysis with potassium gluconate (KGlu, 140 mM) which should have decreased $[Cl^-]_i$ produced an increase in ClopHensorN fluorescence consistent with Cl^- efflux (Figure 3B(iii)). Calibration curves with CsCl and KGlu were obtained by averaging the responses of 5–7 cells.

PROTEIN EXPRESSION USING SIMPLE WES

We use an optimized Simple Wes protocol to measure KCC2 protein from single SON AVP neurons following imaging experiments. The β -Actin protein was used as control. The KCC2 and β -Actin antibodies used in this study could detect up to 4ng/ul of protein in Simple Wes. A sharply defined chemiluminescent signal was obtained for total KCC2 (Figures 4B & 5B) from both the SL and Eu neurons that responded to muscimol during chloride imaging (Figures 4C & 5C). The data are also displayed using KCC2 and β -Actin protein bands in Figures 4D & 5D. Cells that did not respond to muscimol typically displayed no KCC2 or β -Actin signals at the appropriate molecular weights (Figure 6). These results indicate that most AVP neurons from the SON express KCC2.

MUSCIMOL MEDIATED CHANGES IN INTRACELLULAR CHLORIDE

In our experiments, GABA_A receptors were activated by exogenous application of muscimol (100uM; 10s; 3 Cycles), a GABA_A agonist, in acutely dispersed SON AVP neurons from Eu or SL male rats. Majority of cells from Eu rats (23 out of 35) showed a decrease in the F₄₄₅/F₅₅₄ ratio consistent with chloride influx (Figure 7A). The decrease in fluorescence from baseline was significant in the responsive cells ($t = 3.195$; d.f = 3; $p < 0.05$) and a similar response could be evoked 10 minutes later (Figure 7A). In SON AVP neurons from SL rats, 27 out of 39 cells showed significant increases in the F₄₄₅/F₅₅₄ ratio indicative of chloride efflux ($t = -3.755$; d.f = 7; $p < 0.05$; Figure 7B) associated with muscimol application, while 12 out of 39 had no change in chloride flux ($\chi^2_{(2,74)} = 49.92$; $p < 0.001$).

The duration and experimental conditions utilized were first verified by recording the changes in chloride concentration to muscimol in the absence of antagonists. The response of the neuron to

muscimol applications was recorded at similar time interval used for following experimental conditions but with no bath application of antagonists (Figure 7). Two-way repeated measures ANOVA revealed no significant difference between the repeated muscimol applications ($F(1,8) = 0.0312, p = 0.864$). This data shows that cells were viable and responded uniformly for the entire duration of recording.

ROLE OF KCC2 IN CHLORIDE REGULATION

Since our data indicate Cl^- efflux in SON AVP neurons from SL rats, we tested the hypothesis that reduced activity of KCC2 and decreased chloride efflux contribute to this change in the valance of the muscimol response^(13, 14). To test for KCC2 in setting $[\text{Cl}^-]_i$ we used VU0240551, an antagonist that selectively targets the KCCs⁽¹²⁾. The muscimol induced increase in $[\text{Cl}^-]_i$ was inhibited by VU0240551 in neurons from Eu rats. In contrast, VU 0240551 did not have any effect on the SL rat neurons because KCC2 membrane expression is known to be downregulated in SL male rats^(1, 2) (Figure 8B & 8C). Two-way repeated measures ANOVA revealed a significant interaction indicating that chloride concentration was affected by treatment and bath antagonist protocol (Treatment x Antagonist $F(1,11) = 6.549, p < 0.05$). Post hoc multiple comparisons between the factors revealed that KCC2 antagonist (VU 0240551, 10 μM) significantly blocked the chloride influxes in SON AVP neurons from EU rats (Tukey $t = 4.906; p < 0.05$; Figure 8A & 8C).

ROLE OF NKCC1 IN CHLORIDE REGULATION

Previous studies have implicated NKCC1 in $[\text{Cl}^-]_i$ regulation in various neurons^(12, 38). To test for a contribution of NKCC1 to $[\text{Cl}^-]_i$ on SON AVP neurons during SL we used the NKCC1 antagonist bumetanide (10 μM) which selectively targets NKCC1 cotransporter⁽³⁸⁾. Bumetanide

inhibited the muscimol induced decrease in $[Cl]_i$ in AVP neurons from SL rats. In contrast, bumetanide did not alter the response of Eu rat neurons to muscimol. Two-way repeated measures ANOVA followed by post hoc multiple comparisons revealed that the bumetanide did not have any effect on the Cl^- influx of Eu rat neurons with muscimol application (Figure 9A & 9C). Bumetanide significantly blocked the chloride efflux in SON AVP neurons from SL male rats (Tukey $t = 3.629$; $p < 0.05$) as shown in (Figure 9B & 9C).

TrkB SIGNALING IN CHLORIDE REGULATION

Previous studies have shown the role of BDNF- TrkB-KCC2 signaling mechanism in the SON neurons in modulating AVP secretion during high SL in male rats^(2, 3, 19, 27). However, the role of this signaling mechanism in mediating changes in intracellular chloride concentration is not known. Here, we tested the role of TrkB receptor activation on $GABA_A$ -induced Cl^- flux associated with SL. Experiments were conducted using either a broad-spectrum protein kinase inhibitor, K252a, or a specific TrkB antagonist, AnA-12. Neurons from SL rats exhibited marked inhibition in muscimol induced decrease in $[Cl]_i$ with both K252a and AnA-12 application. But the antagonists did not alter the response of Eu rat neurons to muscimol. Two-way repeated measures ANOVA revealed a significant interaction indicating that chloride concentration was affected by treatment and K252a (Treatment x Antagonist $F(1,11) = 20.647$, $p < 0.05$). Post hoc multiple comparisons between the factors revealed that protein kinase inhibitor (K252a, 100nM) significantly blocked the blocked muscimol induced chloride efflux in SL male rats (Tukey $t = 8.358$; $p < 0.05$; Figure 10B & 10C). Similarly, specific TrkB antagonist (AnA-12, 50uM) significantly blocked the blocked muscimol induced chloride efflux in SL male rats (Tukey $t = 4.611$; $p < 0.05$; Figure 10E & 10F). The significant increase in $[Cl]_i$ in AVP neurons from Eu

rats in response to muscimol application was unaffected by both the kinase inhibitor and TrkB antagonist (Figure 10A & 10D).

DISCUSSION

In this study, ClopHensorN was expressed in AVP neurons using an AAV vector with a vasopressin specific promoter⁽²¹⁾. Our results confirmed the specificity of the promoter in a separate group of rats using immunohistochemistry for vasopressin and oxytocin as previously described^(21, 36). This approach allowed us to measure changes in $[Cl^-]_i$ associated with focal application of muscimol in acutely dissociated SON AVP neurons. This could offer several advantages compared to gramicidin perforated patch recording by leaving membrane voltage and intracellular chloride unperturbed^(12, 23).

Previous studies have shown that SL with 2% NaCl increases thirst and gradually causes hypernatremia and hyperosmolality^(1, 39, 40). Also, SL was associated with a decrease in body weight gain possibly due to anorexia that accompanies drinking of hypertonic saline⁽⁴¹⁾.

We measured plasma copeptin in addition to AVP in our experiments. Copeptin is a peptide derived from the C-terminus of pre-pro-hormone of AVP and is often used as surrogate marker for AVP. Previous studies have shown that plasma AVP and copeptin correlate strongly over a wide range of osmolalities⁽²⁵⁾. The reported AVP and copeptin plasma concentrations were in accordance with previous studies and both were significantly increased by SL^(1, 37).

In the adult nervous system, GABA primarily produces membrane hyperpolarization by opening $GABA_A$ receptors leading to Cl^- influx. However, there have been several reports that in some systems the valence of the GABA response can be altered so that it causes membrane depolarization due to Cl^- efflux^(2, 15-17, 42). Similar changes have been reported in the AVP

neurons^(2, 15). To assess how SL influences the valence of GABA transmission in SON AVP neurons, we performed focal applications of the GABA_A agonist muscimol in the presence of various antagonists applied individually to understand the specific role of various cotransporters and receptors. The time course and the concentrations for the drug treatments were chosen based on previous studies which have shown that this time course can cause transient shifts in [Cl⁻]_i that can affect GABA polarity^(32, 33).

The relative activity of NKCC and the KCC cotransporters can determine resting [Cl⁻]_i in most neurons^(2, 13). Normally, [Cl⁻]_i is kept low in neurons by the tonically active KCC2^(13, 15, 43). Membrane KCC2 expression is stabilized by post-translational modification, phosphorylation at Ser940 which is shown to correlate with its cellular activity⁽⁴⁴⁾. Our results demonstrate that individual SON AVP neurons express KCC2 and chloride imaging results support previous studies suggesting that SL effects this cotransporter to alter the inhibitory control of AVP release^(1, 2).

In addition to decreased KCC2 activity, increased activity of NKCC1 could also mediate the increase in [Cl⁻]_i⁽¹⁵⁾. To understand the role of NKCC1 in mediating the change in GABA mediated chloride flux followed by SL, we examined the functional contribution of this transporter in SON AVP neurons from EU and SL rats by using NKCC1 inhibitor bumetanide.

In SON AVP neurons from Eu rats, KCC2 inhibition significantly decreased the chloride influx associated with muscimol application which is consistent with increased [Cl⁻]_i caused by reduced chloride excretion. In contrast, KCC2 inhibition had no effect on the muscimol responses of SON AVP neurons from SL rats. This suggests that SL had already reduced KCC2 activity. However, NKCC1 inhibition with bumetanide significantly decreased in the amplitude of GABA-induced Cl⁻ efflux in SON AVP neurons from SL rats but did not affect the responses

of neurons from Eu rats. In the cells from Eu rats that presumably have low $[Cl^-]_i$, blocking chloride excretion had a greater impact on the muscimol response than inhibiting NKCC1 mediated influx. This is consistent with GABA having an inhibitory effect in SON AVP neurons from Eu rats due to a low $[Cl^-]_i$ that is dependent on KCC2. Inhibiting KCC2 had no effect on the muscimol responses of SON AVP neurons from SL rats presumably because its activity had already been reduced ⁽²⁾. In SON AVP neurons from SL rats, blocking NKCC1 did significantly reduce muscimol-mediated chloride efflux. The significant reduction in chloride efflux associated with NKCC1 inhibition might only be partially explained by reduced chloride transport into the cells from SL rats. Chloride extrusion mediated by KCC2 would be reduced in cells from SL rats. Another possible mechanism could be a leak chloride current. Additional experiments will be required for a complete understanding of the role of NKCC1 in the regulation of $[Cl^-]_i$ in SON AVP neurons during SL.

Capillary electrophoresis-based Protein Simple Wes was used in our study for its ability to analyze very low concentrations of protein and its automation ⁽⁴⁵⁾. This technology has allowed us to show that KCC2 and β -Actin expression is found in the neurons that responded to muscimol during chloride imaging. The subset of neurons that did not respond during chloride imaging, did not have KCC2 or β -Actin protein expression. The absence of β -Actin expression and its unresponsiveness to muscimol indicates these neurons might not have been viable.

Although previous immunohistochemical studies have shown colocalization of KCC2 with AVP in SON neurons ⁽²⁾, this is the first study to correlate the KCC2 protein expression in individual AVP neuron with chloride imaging. The KCC2 cotransporter expression in the AVP neuron have been controversial ^(2, 13, 15, 42). Differences in methodology are likely to underlie some of these inconsistencies. Although the response of the AVP neurons to bumetanide indicate the

expression of NKCC, the expression of NKCC and phosphorylation status of KCC2 in individual neurons will be addressed in future studies.

Previous studies have shown that TrkB mediated signaling contributes to the downregulation of KCC2 co-transporter in the SON neurons and increases AVP secretion in male rats during SL^(1, 2, 9). The effect of the TrkB inhibitor, AnA-12, and broad-spectrum protein kinase inhibitor, K252a, on muscimol evoked responses in SON AVP neurons was analyzed in this study. While they did not significantly influence the responses to muscimol in neurons from Eu rats, both inhibitors significantly blocked the effects of SL in SON AVP neurons responses to muscimol. This suggests that BDNF-TrkB signaling is a mechanism that contributes to the increase in $[Cl^-]_i$ associated with SL. However, the synaptic mechanisms leading to BDNF mediated activation of TrkB receptor is not known and could be the focus of future studies.

CONCLUSIONS

In this study, we used virally mediated expression of a chloride sensitive indicator and single cell based Western blot approach to examine the effects of SL on GABA signaling in SON neurons. Our data are consistent with earlier studies suggesting a TrkB-KCC2 dependent mechanism contributes to the increases in $[Cl^-]_i$ of SON AVP neurons from SL rats^(1, 2). The results also show that SON AVP neurons express KCC2 and a bumetanide-sensitive NKCC co-transporter. The relative contribution of these transporters to chloride homeostasis of vasopressin neurons is dependent on the physiological state of the animal. The regulation of intracellular chloride in AVP neurons may also involve a leak chloride conductance. Future studies will test whether or not other physiological challenges can influence the valence of the GABA response in SON AVP neurons.

ACKNOWLEDGEMENTS

The authors would like to thank Kathleen Borgmann PhD and Anuja Ghorpade PhD for the use of their Simple Wes instrument.

GRANTS

This work was supported by R01 HL119458 to JTC and AHA18PRE34060035 to KB.

DISCLOSURES

The authors have nothing to disclose.

REFERENCES

1. Balapattabi K, Little JT, Farmer GE, Cunningham JT. High salt loading increases brain derived neurotrophic factor in supraoptic vasopressin neurones. *Journal of neuroendocrinology*. 2018; 30: e12639.
2. Choe KY, Han SY, Gaub P, Shell B, Voisin DL, Knapp BA, Barker PA, Brown CH, Cunningham JT, Bourque CW. High salt intake increases blood pressure via BDNF-mediated downregulation of KCC2 and impaired baroreflex inhibition of vasopressin neurons. *Neuron*. 2015; 85: 549-60.
3. Carreno FR, Walch JD, Dutta M, Nedungadi TP, Cunningham JT. Brain-derived neurotrophic factor-tyrosine kinase B pathway mediates NMDA receptor NR2B subunit phosphorylation in the supraoptic nuclei following progressive dehydration. *Journal of neuroendocrinology*. 2011; 23: 894-905.
4. Carreño FR, Ji LL, Cunningham JT. Altered central TRPV4 expression and lipid raft association related to inappropriate vasopressin secretion in cirrhotic rats. *American Journal of Physiology - Regulatory, Integrative and Comparative Physiology*. 2009; 296: R454-R66.
5. John S, Thuluvath PJ. Hyponatremia in cirrhosis: Pathophysiology and management. *World Journal of Gastroenterology : WJG*. 2015; 21: 3197-205.
6. Martin PY, Schrier RW. Sodium and water retention in heart failure: pathogenesis and treatment. *Kidney Int Suppl*. 1997; 59: S57-61.
7. Better OS, Aisenbrey GA, Berl T, Anderson RJ, Handelman WA, Linas SL, Guggenheim SJ, Schrier RW. Role of antidiuretic hormone in impaired urinary dilution associated with chronic bile-duct ligation. *Clin Sci (Lond)*. 1980; 58: 493-500.

8. Boscoe A, Paramore C, Verbalis JG. Cost of illness of hyponatremia in the United States. *Cost Effectiveness and Resource Allocation*. 2006; 4: 10-.
9. Choe KY, Trudel E, Bourque CW. Effects of Salt Loading on the Regulation of Rat Hypothalamic Magnocellular Neurosecretory Cells by Ionotropic GABA and Glycine Receptors. *Journal of neuroendocrinology*. 2016; 28.
10. Share L. Role of vasopressin in cardiovascular regulation. *Physiological reviews*. 1988; 68: 1248-84.
11. Share L, Levy MN. Cardiovascular receptors and blood titer of antidiuretic hormone. *American Journal of Physiology-Legacy Content*. 1962; 203: 425-8.
12. Klett NJ, Allen CN. Intracellular Chloride Regulation in AVP+ and VIP+ Neurons of the Suprachiasmatic Nucleus. *Scientific Reports*. 2017; 7: 10226.
13. Chamma I, Chevy Q, Poncer JC, Levi S. Role of the neuronal K-Cl co-transporter KCC2 in inhibitory and excitatory neurotransmission. *Frontiers in cellular neuroscience*. 2012; 6: 5.
14. Farmer GE, Balapattabi K, Bachelor ME, Little JT, Cunningham JT. AT1a influences GABAa mediated inhibition through the regulation of KCC2 expression. *American journal of physiology Regulatory, integrative and comparative physiology*. 2018.
15. Kim YB, Kim YS, Kim WB, Shen FY, Lee SW, Chung HJ, Kim JS, Han HC, Colwell CS, Kim YI. GABAergic excitation of vasopressin neurons: possible mechanism underlying sodium-dependent hypertension. *Circulation research*. 2013; 113: 1296-307.
16. Hewitt SA, Wamsteeker JI, Kurz EU, Bains JS. Altered chloride homeostasis removes synaptic inhibitory constraint of the stress axis. *Nature neuroscience*. 2009; 12: 438-43.
17. Price TJ, Cervero F, Gold MS, Hammond DL, Prescott SA. Chloride regulation in the pain pathway. *Brain research reviews*. 2009; 60: 149-70.

18. Irwin RP, Allen CN. GABAergic signaling induces divergent neuronal Ca²⁺ responses in the suprachiasmatic nucleus network. *The European journal of neuroscience*. 2009; 30: 1462-75.
19. Marosi K, Mattson MP. Hold the salt: vasopressor role for BDNF. *Cell metabolism*. 2015; 21: 509-10.
20. Arosio D, Ricci F, Marchetti L, Galdani R, Albertazzi L, Beltram F. Simultaneous intracellular chloride and pH measurements using a GFP-based sensor. *Nature methods*. 2010; 7: 516-8.
21. Ponzio TA, Fields RL, Rashid OM, Salinas YD, Lubelski D, Gainer H. Cell-type specific expression of the vasopressin gene analyzed by AAV mediated gene delivery of promoter deletion constructs into the rat SON in vivo. *PLoS one*. 2012; 7: e48860.
22. Mukhtarov M, Liguori L, Waseem T, Rocca F, Buldakova S, Arosio D, Bregestovski P. Calibration and functional analysis of three genetically encoded Cl⁻/pH sensors. *Frontiers in molecular neuroscience*. 2013; 6: 9-.
23. Raimondo JV, Joyce B, Kay L, Schlagheck T, Newey SE, Srinivas S, Akerman CJ. A genetically-encoded chloride and pH sensor for dissociating ion dynamics in the nervous system. *Frontiers in cellular neuroscience*. 2013; 7: 202-.
24. Paxinos G, Watson C. *The Rat Brain in Stereotaxic Coordinates* San Diego: Academic Press, 1997.
25. Balanescu S, Kopp P, Gaskill MB, Morgenthaler NG, Schindler C, Rutishauser J. Correlation of Plasma Copeptin and Vasopressin Concentrations in Hypo-, Iso-, and Hyperosmolar States. *The Journal of Clinical Endocrinology & Metabolism*. 2011; 96: 1046-52.

26. Nedungadi TP, Cunningham JT. Differential regulation of TRPC4 in the vasopressin magnocellular system by water deprivation and hepatic cirrhosis in the rat. *American Journal of Physiology - Regulatory, Integrative and Comparative Physiology*. 2014; 306: R304-R14.
27. Black EAE, Smith PM, McIsaac W, Ferguson AV. Brain-derived neurotrophic factor acts at neurons of the subfornical organ to influence cardiovascular function. *Physiological reports*. 2018; 6: e13704-e.
28. Oliet SH, Bourque CW. Properties of supraoptic magnocellular neurones isolated from the adult rat. *J Physiol*. 1992; 455: 291-306.
29. Prager-Khoutorsky M, Khoutorsky A, Bourque CW. Unique interweaved microtubule scaffold mediates osmosensory transduction via physical interaction with TRPV1. *Neuron*. 2014; 83: 866-78.
30. Ferguson AV, Bicknell RJ, Carew MA, Mason WT. Dissociated adult rat subfornical organ neurons maintain membrane properties and angiotensin responsiveness for up to 6 days. *Neuroendocrinology*. 1997; 66: 409-15.
31. Kay AR, Wong RK. Isolation of neurons suitable for patch-clamping from adult mammalian central nervous systems. *Journal of neuroscience methods*. 1986; 16: 227-38.
32. Friedel P, Bregestovski P, Medina I. Improved method for efficient imaging of intracellular Cl(-) with Cl-Sensor using conventional fluorescence setup. *Frontiers in molecular neuroscience*. 2013; 6: 7-.
33. Sah R, Schwartz-Bloom RD. Optical Imaging Reveals Elevated Intracellular Chloride in Hippocampal Pyramidal Neurons after Oxidative Stress. *The Journal of Neuroscience*. 1999; 19: 9209-17.

34. Koob AO, Bruns L, Prassler C, Masliah E, Klopstock T, Bender A. Protein analysis through Western blot of cells excised individually from human brain and muscle tissue. *Analytical biochemistry*. 2012; 425: 120-4.
35. Maitre M, Roullot-Lacarriere V, Piazza PV, Revest JM. Western blot detection of brain phosphoproteins after performing Laser Microdissection and Pressure Catapulting (LMPC). *Journal of neuroscience methods*. 2011; 198: 204-12.
36. Cunningham JT, Nedungadi TP, Walch JD, Nestler EJ, Gottlieb HB. Δ FosB in the supraoptic nucleus contributes to hyponatremia in rats with cirrhosis. *American Journal of Physiology - Regulatory, Integrative and Comparative Physiology*. 2012; 303: R177-R85.
37. Carmichael CY, Carmichael ACT, Kuwabara JT, Cunningham JT, Wainford RD. Impaired sodium-evoked paraventricular nucleus neuronal activation and blood pressure regulation in conscious Sprague–Dawley rats lacking central Gai(2) proteins. *Acta Physiologica (Oxford, England)*. 2016; 216: 314-29.
38. Russell JM. Sodium-potassium-chloride cotransport. *Physiological reviews*. 2000; 80: 211-76.
39. Bourque CW. Central mechanisms of osmosensation and systemic osmoregulation. *Nature reviews Neuroscience*. 2008; 9: 519-31.
40. Gizowski C, Bourque CW. The neural basis of homeostatic and anticipatory thirst. *Nature Reviews Nephrology*. 2017; 14: 11.
41. Watts AG, Boyle CN. The functional architecture of dehydration-anorexia. *Physiology & behavior*. 2010; 100: 472-7.

42. Haam J, Popescu IR, Morton LA, Halmos KC, Teruyama R, Ueta Y, Tasker JG. GABA is excitatory in adult vasopressinergic neuroendocrine cells. *The Journal of neuroscience : the official journal of the Society for Neuroscience*. 2012; 32: 572-82.
43. Lu J, Karadsheh M, Delpire E. Developmental regulation of the neuronal-specific isoform of K-CL cotransporter KCC2 in postnatal rat brains. *Journal of Neurobiology*. 1999; 39: 558-68.
44. Lee HH, Walker JA, Williams JR, Goodier RJ, Payne JA, Moss SJ. Direct protein kinase C-dependent phosphorylation regulates the cell surface stability and activity of the potassium chloride cotransporter KCC2. *The Journal of biological chemistry*. 2007; 282: 29777-84.
45. Beekman C, Janson AA, Baghat A, van Deutekom JC, Datson NA. Use of capillary Western immunoassay (Wes) for quantification of dystrophin levels in skeletal muscle of healthy controls and individuals with Becker and Duchenne muscular dystrophy. *PloS one*. 2018; 13: e0195850-e.

FIGURES AND TABLES

CHAPTER III - Figure III-1 Immunofluorescence of AAV2-0VP1-GFP virus

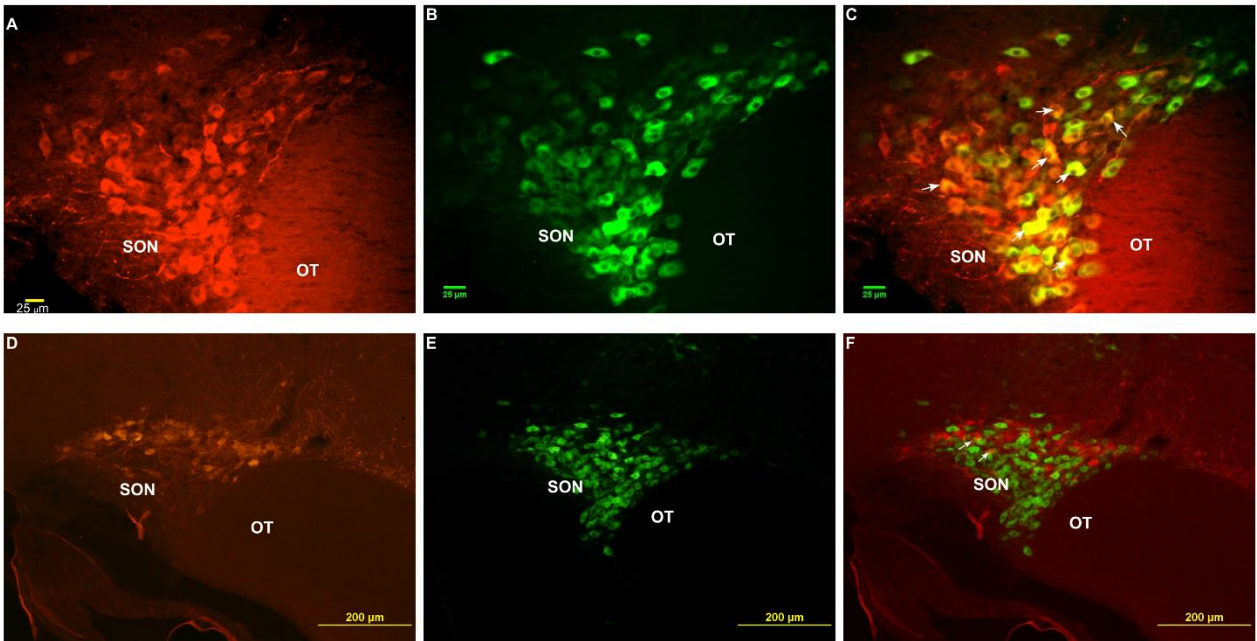


Figure 1: **A:** Immunofluorescence of AAV2-0VP1-GFP virus; **B:** AVP staining within the SON and **C:** merged digital image. Cells labeled with GFP and AVP are indicated with arrows. **D:** Immunofluorescence of AAV2-0VP1-GFP virus; **E:** OXT staining within the SON and **F:** merged digital image. Cells labeled with GFP and OXT are indicated with arrows.

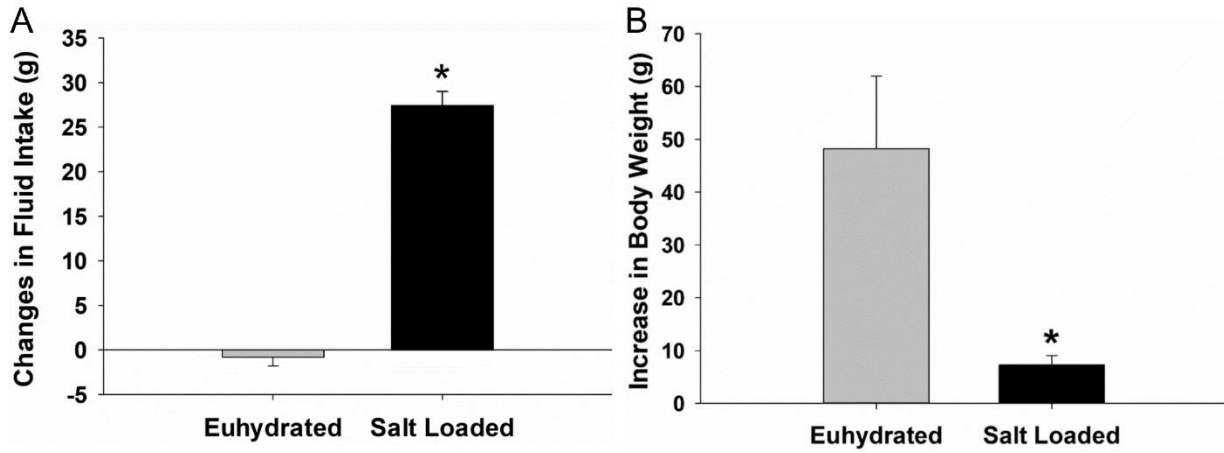


Figure 2: The effects of salt loading (SL) on **A:** Daily average fluid intake, * $p < 0.05$ vs. Eu rats and vs. Baseline. **B:** Average daily changes in body weight. Data are mean \pm SEM. * $p < 0.05$ vs. Eu rats. Groups: Eu (n = 6); SL (n= 6).

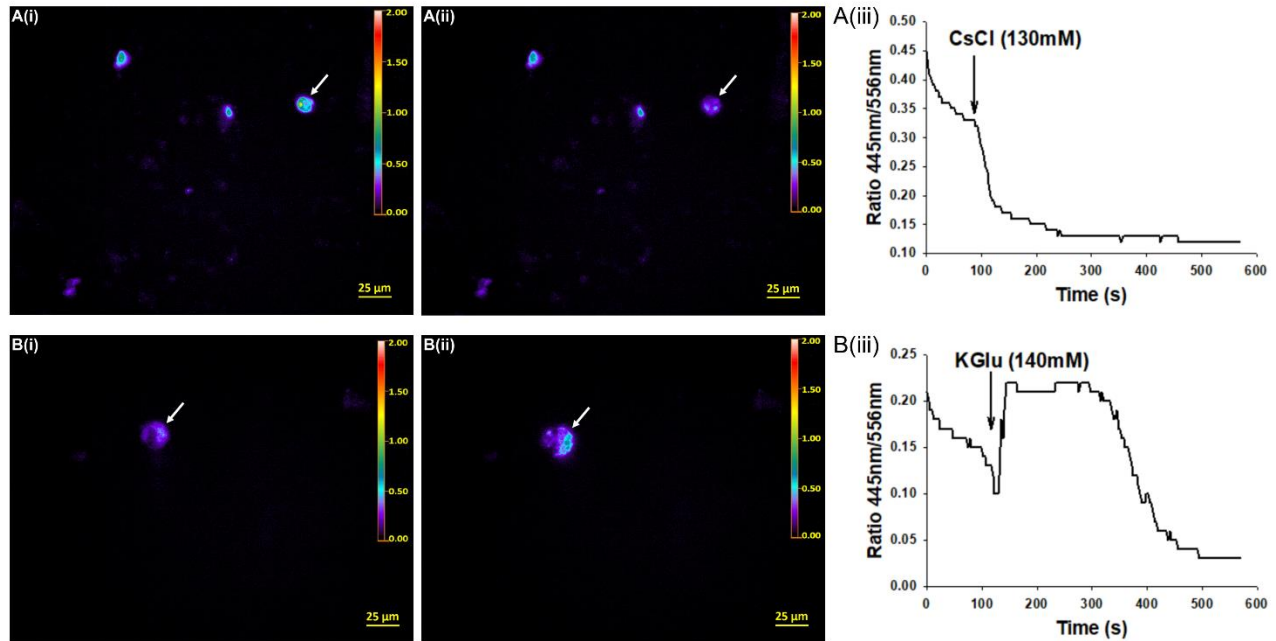


Figure 3: Representative digital image of SON AVP neuron expressing ClopHensorN plasmid showing F_{445}/F_{554} ratio. **A (i):** Image shows the fluorescence of the cell during baseline and **A(ii):** Representative image shows the decrease in fluorescence with increase in $[Cl]_i$ - cell during peak response. The inset table is color scale for changes in the F_{445}/F_{554} ratio (0.2– 0.5). **A(iii):** Ratiometric chloride imaging with ClopHensorN using whole cell patch with a CsCl filled electrode Arrow indicates the start of whole cell access. **B(i):** Image shows the fluorescence of the cell during baseline and **B(ii):** Representative image shows the increase in fluorescence with decrease in $[Cl]_i$ - cell during peak response and **B(iii):** Ratiometric chloride imaging with ClopHensorN using whole cell patch with a low chloride K Gluconate Electrode. Note that increasing intracellular chloride with CsCl decreases the F_{445}/F_{554} ratio while decreasing intracellular chloride with K gluconate increases the F_{445}/F_{554} ratio.

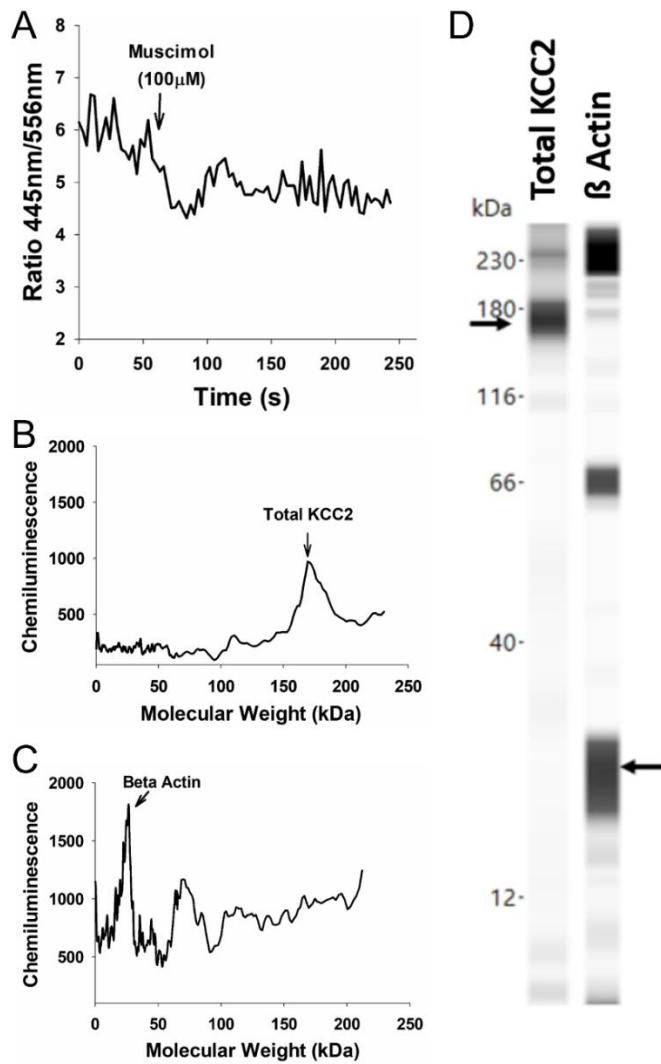


Figure 4: Representative protein expression of single SON AVP neuron from Eu rat. **A:** Chloride imaging of the neuron from which protein expression was analyzed. This neuron responded to the antagonists during imaging. **B:** Chemiluminescent signal showing sharp peak for total KCC2 protein expression at 174 kDa. (Electropherogram view). **C:** Electropherogram plot showing chemiluminescent signal for β -Actin protein expression at 24- 26 kDa. **D:** Total KCC2 and β -Actin expression of the same neuron in traditional densitometry view using Simple Wes.

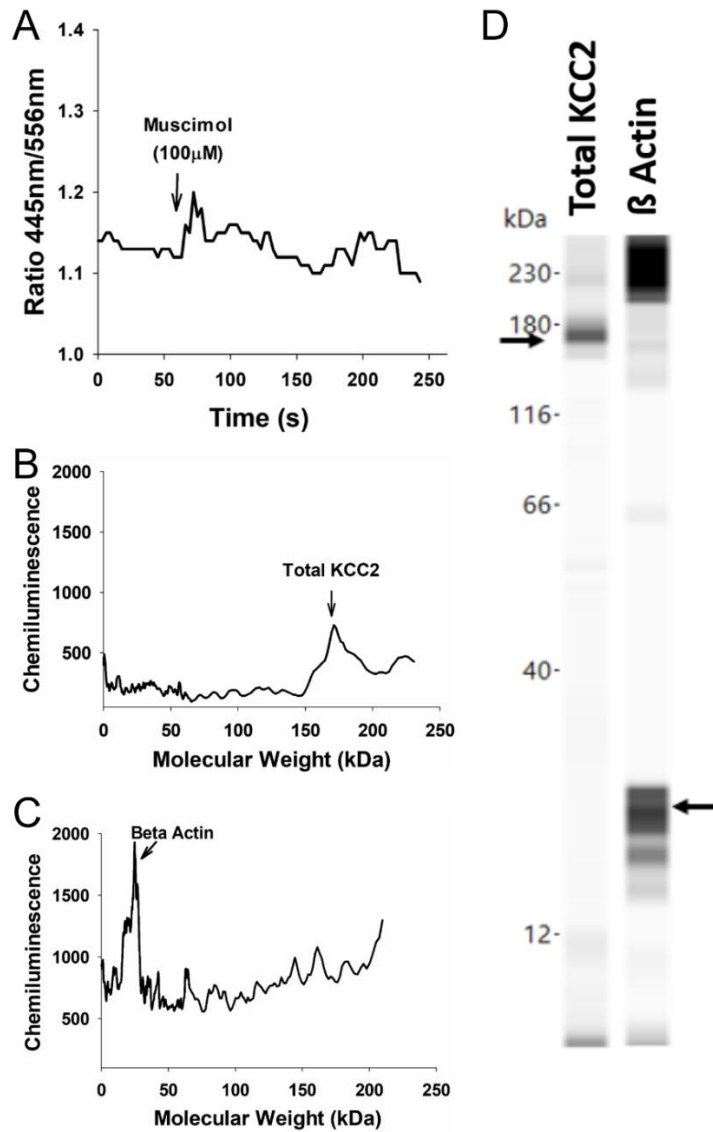


Figure 5: Representative protein expression of single SON AVP neuron from SL rat. **A:** Chloride imaging of the neuron from which protein expression was analyzed. This neuron responded to the antagonists during imaging. **B:** Chemiluminescent signal showing sharp peak for total KCC2 protein expression at 174 kDa. (Electropherogram view). **C:** Electropherogram plot showing chemiluminescent signal for β-Actin protein expression at 24- 26 kDa. **D:** Total KCC2 and β-Actin expression of the same neuron in traditional lane view.

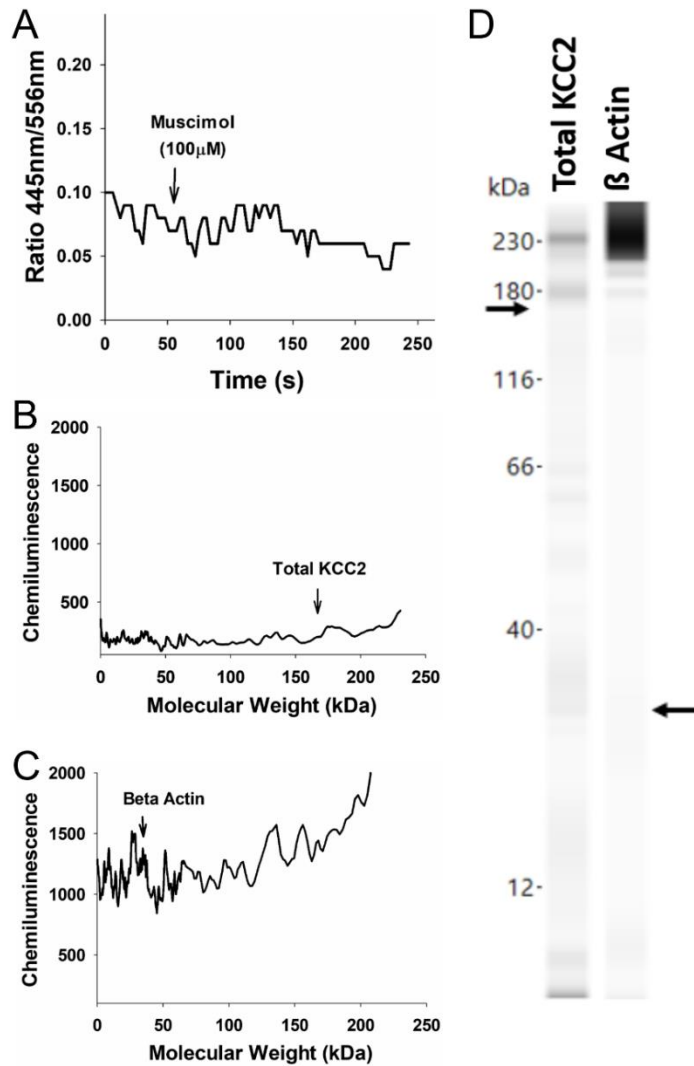


Figure 6: Representative protein expression of single SON AVP neuron from Eu rat that did not respond during chloride imaging. **A:** Chloride imaging of the neuron from which protein expression was analyzed. This neuron did not respond to the antagonists during imaging. **B:** Chemiluminescent signal for total KCC2 protein expression did not show a peak (Electropherogram view). **C.** Electropherogram plot had no chemiluminescent signal for β-Actin protein expression. **D:** Total KCC2 and β-Actin expression of the same neuron in traditional lane view.

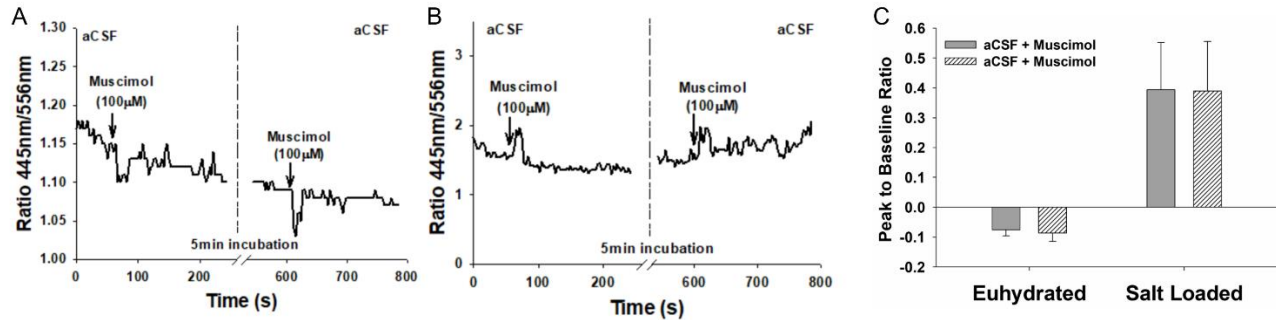


Figure 7: Control experiment to verify changes in $[Cl]_i$ in acutely dissociated SON AVP neurons with no bath application of antagonists. **A:** response of cell from an euhydrated (Eu) rat to focal application of muscimol (100 μ M; 10s; 3 Cycles). aCSF was bath applied without any antagonists for the second response of the same cell to muscimol focal application. **B:** response of cell from a salt loaded (SL) rat to focal application of muscimol (100 μ M; 10s; 3 Cycles) twice without bath application of antagonists. The duration and experimental conditions utilized in this control imaging were similar to the drug treatment recordings.

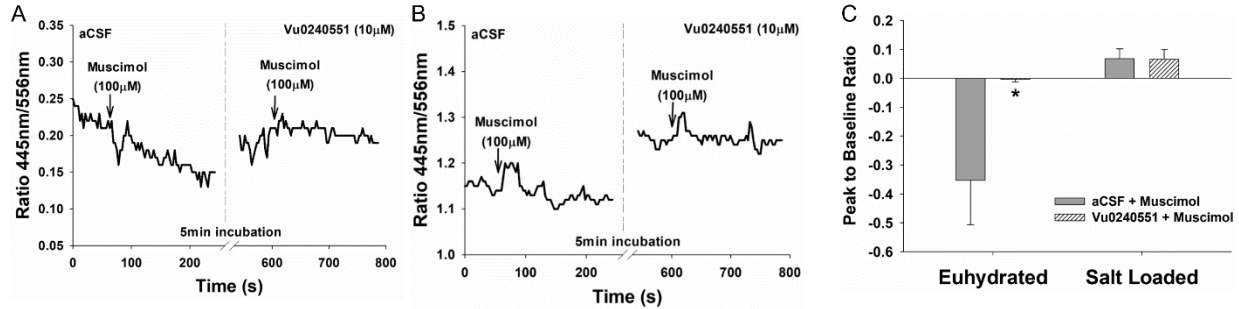


Figure 8: KCC2 mediated changes in $[Cl]_i$ measured by ClpHensorN in acutely dissociated SON AVP neurons. **A:** response of cell from an euhydrated (Eu) rat to focal application of muscimol (100µM; 10s; 3 Cycles) and KCC2 antagonist VU0240511, 10µM (incubated for 5 mins and continuously bath applied for second half recording). Cells from control rats showed muscimol induced Cl influx (7/9; $p < 0.05$). VU0240511 significantly blocked the Cl influxes. **B:** 2% salt loaded (SL) rat AVP neuron responses to muscimol and VU0240511 application. Muscimol application to SON AVPs from SL rats caused either significant increase in chloride efflux (7/10; $p < 0.05$) or no change in chloride flux (3/10). **C:** Quantification graph showing average changes in peak to Muscimol from baseline before and after VU0240511 application in both Eu and SL rats. Statistical difference is calculated using two-way repeated measures ANOVA, Chi-squared test and Bonferroni posthoc analysis. Data are mean \pm SEM. * $p < 0.05$ vs. aCSF with Muscimol.

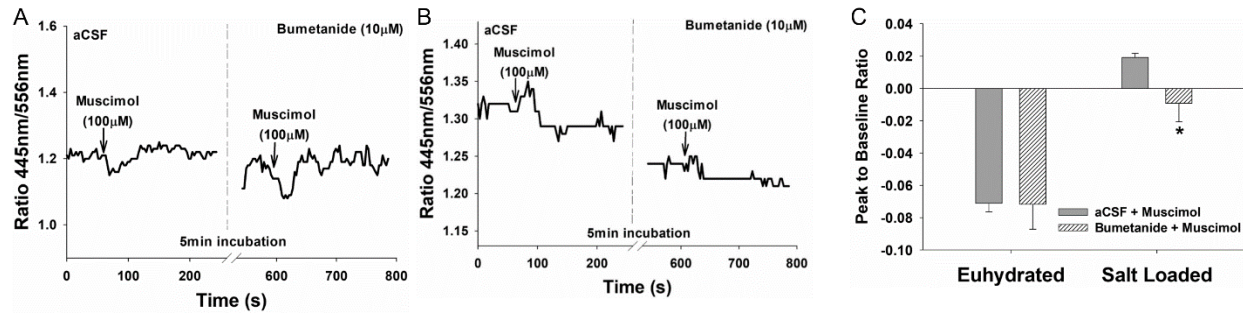


Figure 9: NKCC1 mediated changes in $[Cl]_i$ measured by ClopHensorN in acutely dissociated SON AVP neurons. **A:** response of cell from an Eu rat to focal application of muscimol (100 μ M; 10s; 3 Cycles) and NKCC1 antagonist bumetanide, 10 μ M (incubated for 5 mins and continuously bath applied for second half recording) (5/8). Bumetanide did not have any effect on Cl influxes in Eu rats. **B:** 2% SL rat AVP neuron responses to muscimol and bumetanide application (6/10). Bumetanide significantly blocked the Cl effluxes. **C:** Quantification graph showing average changes in peak to Muscimol from baseline before and after bumetanide application in both Eu and SL rats. Statistical difference is calculated using two-way repeated measures ANOVA, Chi-squared test and Bonferroni posthoc analysis. Data are mean \pm SEM. * $p < 0.05$ vs. aCSF with Muscimol.

CHAPTER III - Figure III-10 – Chloride imaging with TrkB antagonists

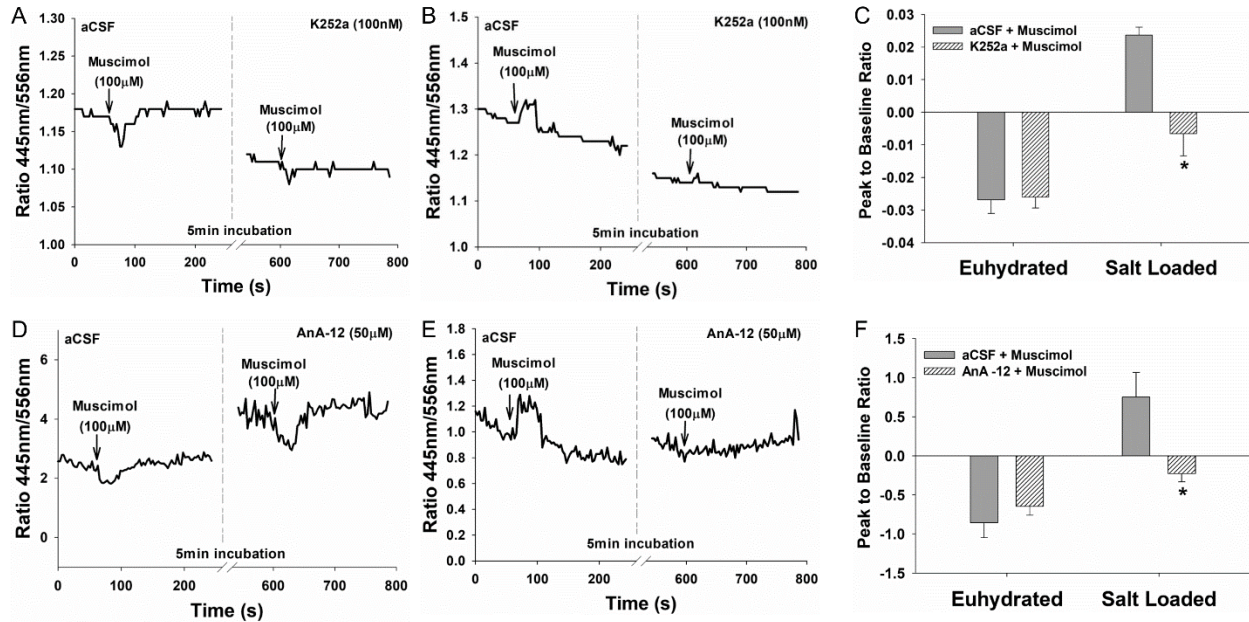


Figure 10: TrkB mediated changes in $[Cl]_i$ measured by ClopHensorN in acutely dissociated SON AVP neurons. **A:** response of an Eu rat to focal application of muscimol (100µM; 10s; 3 Cycles) and protein kinase inhibitor K252a,100nM (7/10). **B:** 2% SL rat AVP neuron responses to muscimol and K252a application. K252a significantly blocked the Cl effluxes (6/8). **C:** Quantification graph showing average changes in peak to Muscimol from baseline before and after K252a application in both Eu and SL rats. **D:** response of cell from an Eu rat to focal application of muscimol (100µM; 10s; 3 Cycles) and TrKB antagonist AnA-12,50µM (incubated for 5 mins and continuously bath applied for second half recording) (5/9). **E:** 2% SL rat AVP neuron responses to muscimol and AnA-12 application (6/10). AnA-12 significantly blocked the Cl effluxes. **F:** Quantification graph showing average changes in peak to Muscimol from baseline before and after AnA-12 application in both Eu and SL rats. Statistical difference is calculated using two-way repeated measures ANOVA, Chi-squared test and Bonferroni posthoc analysis. Data are mean \pm SEM. * $p < 0.05$ vs. aCSF with Muscimol.

CHAPTER III – TABLE 1-1 Plasma osmolality, hematocrit and CPP concentration

Table 1: Plasma osmolality, hematocrit, AVP and CPP concentration in euhydrated and salt loaded rats.

	Male Eu	Male SL
Osmolality (mOsm/kg)	298.8±1.12 (11)	308.6±0.55 (7)*
Hematocrit (%)	42.5±0.5 (11)	47±0.43 (7)*
Plasma AVP (pg/ml)	14.8±5.31 (6)	57.6±7.91 (6)*
Plasma CPP (pg/ml)	49.4±1.98 (6)	77.8±5.53 (6)*

Values are mean ±SEM; n, number of rats in each group, in parenthesis. *p<0.05 vs. Eu.

CHAPTER IV

To be submitted to J Neuroendo by end of April 2019

BRAIN DERIVED NEUROTROPHIC FACTOR IN THE REGULATION OF SUPRAOPTIC VASOPRESSIN NEURONS IN DEVELOPMENT OF HYPONATREMIA

Kirthikaa Balapattabi, Joel T. Little, and J. Thomas Cunningham

ABSTRACT

Dilutional hyponatremia due to elevated arginine vasopressin (AVP) secretion increases mortality in patients with liver failure. The neural mechanisms causing dysregulation of AVP secretion are not completely understood. Based on previous studies, we hypothesize that inappropriate AVP release associated with liver failure is due to increased brain derived neurotrophic factor (BDNF) in the supraoptic nucleus (SON). BDNF diminishes GABA_A inhibition in SON AVP neurons by increasing intracellular chloride ([Cl]_i) through tyrosine receptor kinase B (TrkB) activation and downregulation of K⁺/Cl⁻ co-transporter 2 (KCC2). This loss of inhibition could increase AVP secretion. To test this hypothesis, chronic bile duct ligated (BDL) rats, a model of dilutional hyponatremia associated with liver failure, were injected with shRNA to prevent increased BDNF in the SON.

The BDL rats had ascites and significant increases in liver to body weight ratio ($p < 0.05$; 6-9) compared to sham rats indicating liver failure due to bile duct ligation. BDL rats with scrambled injections (BDL SCR) developed hyponatremia indicated by significant decreases in plasma osmolality and hematocrit along with significant increases in plasma copeptin concentration (all $p < 0.05$; 6-9) compared to sham groups. Copeptin (CPP) was used as biomarker for plasma AVP. Phosphorylation of TrkB (pTrkB^{Y515}) was significantly increased and phosphorylation of KCC2 (pKCC2^{S940}) was significantly lower in the SON of BDL SCR rats compared to the sham rats ($p < 0.05$; 6-8).

Knockdown of BDNF in the SON of BDL rats (BDL shBDNF) prevented the rats from developing hyponatremia and blocked the decrease in plasma osmolality and hematocrit observed in BDL SCR rats ($p < 0.05$; 6-9). The BDL shBDNF rats had significant ($p < 0.05$; 6-9) decreases in plasma CPP concentration compared to BDL SCR rats. shBDNF injections in the

SON of BDL rats significantly blocked the increase in TrkB phosphorylation and decrease in KCC2 phosphorylation ($p < 0.05$; 6-8) associated with bile duct ligation. mCherry expression was used to verify the specificity of stereotaxic injections. Rats that did not have successful virus injections in the SON were analyzed separately. The results indicate that BDNF produced in the SON contributes to increased CPP secretion and hyponatremia associated with liver failure in male rats.

INTRODUCTION

Dilutional hyponatremia is the most frequent electrolyte abnormality and is characterized by serum sodium <135 mEq/L. The cost of its treatment in the US has been estimated to be \$1.6-\$3.6 billion per year⁽¹⁾. Hyponatremia often results from congestive heart failure or liver failure. Hyponatremia during liver failure is caused by inappropriate Arginine vasopressin (AVP) release which leads to ascites, seizures, pulmonary and cerebral edema⁽²⁻⁵⁾.

The secretion of AVP is regulated by magnocellular neurosecretory cells (MNCs) located in the supraoptic (SON) and paraventricular (PVN) nuclei of the hypothalamus⁽⁶⁻¹³⁾. Dilutional hyponatremia due to dysregulation of AVP release increases morbidity and mortality in patients with liver and heart failure⁽²⁻⁵⁾. The intervention of hyponatremia in the setting of liver failure is a challenge as conventional therapies are frequently inefficacious^(14, 15). Although treatments with AVP antagonists can improve hyponatremia, the cause of AVP dysregulation is unknown^(1, 5, 16, 17). The development of effective therapeutic approaches for dilutional hyponatremia may require understanding molecular mechanisms behind the abnormality.

Inappropriate AVP release is also reported in high salt loaded rats. MNCs continue to release AVP into the systemic circulation despite elevated blood pressure during salt loading⁽¹⁸⁻²⁰⁾. Previous studies have shown that during high salt loading and dehydration, MNCs upregulate brain derived neurotrophic factor (BDNF)⁽¹⁸⁻²¹⁾. BDNF can have profound effects on GABA neurotransmission through several mechanisms, including the regulation of chloride transporters through tyrosine receptor kinase B (TrkB) activation. Increases in intracellular chloride ($[Cl]_i$) can diminish or reverse the inhibitory effects of GABA on AVP neurons creating a feed forward loop that drives AVP release^(20, 22). This study explores the role of a BDNF-TrkB mechanism in increased AVP secretion using a liver failure rat model^(23, 24). Chronic bile duct ligation (BDL)

in male rats is a model of liver failure associated with increased AVP induced dilutional hyponatremia. The decrease in plasma volume and vasodilation in response to portal hypertension during liver failure are reported to increase AVP secretion as a compensatory mechanism^(2, 5, 14, 25, 26).

We hypothesize that BDNF in the SON contributes to the increased AVP release associated with liver failure. BDNF diminishes GABA_A inhibition in SON AVP neurons by increasing intracellular chloride ([Cl]_i) through TrkB receptor activation and downregulation of K⁺/Cl⁻ co-transporter 2 (KCC2). This loss of inhibition could increase AVP secretion. In this study, we used adeno-associated viral vectors with shRNA against BDNF to test our hypothesis by knocking down BDNF in the SON. This study reveals a new mechanism by which AVP release is increased during liver failure and that could contribute to other diseases such as heart failure and neurogenic hypertension⁽²⁷⁾.

MATERIALS AND METHODS

ANIMALS

All the experiments were conducted on outbred adult male Sprague-Dawley rats with initial body weights of 200-250 g (Charles River, Wilmington, MA). Experimental protocols involving animals were approved by the UNT Health Science Center IACUC and conducted in accordance to the National Institute of Health *Guide for the Care and Use of Laboratory Animals*. All animals were maintained in a temperature-controlled environment on a 12/12h light dark cycle with *ad libitum* access to food and water unless otherwise indicated. Rats were individually housed due to the use of survival surgery and individual fluid intake measurements in the protocol. Survival surgeries were conducted using aseptic techniques. All rats were given

procaine penicillin G (30,000 U, sc) and the non-steroidal anti-inflammatory drug, carprofen (Rimadyl, 2 mg po), was given before and after surgery for pain management.

AAV-MEDIATED KNOCKDOWN OF BDNF IN THE SUPRAOPTIC NUCLEUS

Each rat receiving stereotaxic surgery was anaesthetized with isoflurane (2-3%) and placed in stereotaxic frame equipped to deliver isoflurane throughout the procedure. Their skulls were exposed and leveled between lambda and bregma⁽²⁸⁾. A micromanipulator was oriented to lower the probe to the targeted coordinates of SONs (1.4 mm posterior, 9.1 mm ventral, and ± 1.4 mm lateral from bregma). Rats were bilaterally injected in the SON (300 nl/side) with an Adeno-associated virus (AAV) serotype 2 conjugated with a shRNA directed against BDNF, a mCherry reporter, and a U6 promoter (shBDNF) (Vector Biolabs, Malvern, PA). Another group of rats received bilateral SON injections of equal titer and amount of AAV2 conjugated with a scrambled sequence of shRNA, a mCherry reporter, and a U6 promoter (SCR) as controls. The vectors were injected at a titer of 1.0×10^{13} GC/ml (Vector Biolabs). Each construct was injected in both the SONs over a 10-min period. After 5 min, the injector was removed, and the incision was closed with sutures.

BILE DUCT LIGATION SURGERY

Two weeks following stereotaxic injections, the rats were anaesthetized with isoflurane (2-3%). The abdomen was shaved and cleaned. A midline abdominal incision was performed, and the common bile duct was isolated and cauterized between two ligatures as previously described^(23, 24). Visual inspection of ascetic fluid in the peritoneal cavity was performed daily after surgery. Any rat showing morbidity or ascites of greater than 10% of the body weight was euthanized (Inactin 100 mg/kg ip). Sham rats received the same surgical procedure except their bile duct

was not cauterized. Liver to body weight ratio was determined at the end of the study for verification of liver failure development.

METABOLIC CAGE STUDY

After two weeks of recovery from BDL surgery, the rats were moved into metabolic cages (Lab Products, Seaford, DE) for measurement of daily food intake, fluid intake, and urine excretion. The rats were provided with *ad libitum* access to food and water for 14 days to record various parameters as previously described^(18, 24, 29). Food and fluid intake were measured by filling the containers up to a predetermined weight in grams and subtracting the remaining weight 24 h later. Mineral oil was added to the urine collection vials to prevent evaporation of water from urine. Urine excretion volume was recorded, and urine samples were collected for measuring daily sodium excretion.

PLASMA MEASUREMENTS

Trunk blood was collected from each rat after decapitation and plasma was collected for measuring plasma osmolality, hematocrit, circulating copeptin concentration. Copeptin (CPP) is widely used as biomarker for AVP secretion⁽³⁰⁾ and was measured in this study in addition to AVP.

For CPP analysis, separate 5 to 6 ml samples of blood were collected in vacutainer tubes containing the anticoagulant, EDTA (12 mg). The proteinase inhibitor, aprotinin (0.6 TIU/ml of blood; Phoenix Pharmaceuticals, Inc, Burlingame, CA) was added and the sample was centrifuged at 1600 g for 15 minutes at 4° C. CPP concentration was measured in plasma samples by using specific ELISA according to the manufacturer's instructions (MBS724037,

MyBioSource, Inc, San Diego, CA). Four parametric logistic analysis (4-PL) was performed to quantify the concentration of AVP and CPP.

Another 1 to 2 ml of blood were collected in a 2 ml microcentrifuge tube and prepared for measuring plasma osmolality and hematocrit as previously described⁽³¹⁾. Two heparinized capillary tubes (Fisher Scientific, Hampton, NH) were filled with blood for measuring hematocrit using Micro-Hematocrit capillary tube reader (Lancer, St. Louis, MO). The remaining blood sample was centrifuged at 1600 g for 5-10 minutes and plasma was collected to measure plasma osmolality using vapor pressure osmometer (Wescor, Logan, UT).

WESTERN BLOT ANALYSIS

Four weeks after bile duct ligation, the rats were anesthetized with inactin (100 mg/kg ip) and decapitated. Punches containing the SON were collected from 1 mm coronal section from each brain as previously described^(31, 32). Protein was extracted from the SON punches using RIPA lysis buffer containing DTT, chelators, and protease phosphatase inhibitor cocktail. Protein concentration was determined by Bio-Rad DC assay (detergent compatible) with varying concentrations of BSA as reference standards. Total lysate (20–25 ug) were loaded onto a 4-15% acrylamide sodium dodecyl sulphate (SDS) gel and separated by electrophoresis in Tris-glycine buffer with denaturing conditions. The protein was transferred to Polyvinylidene difluoride (PVDF) membrane (Immobilon-P; EMD-Millipore, Burlington, MA) in Tris-glycine buffer (25 mM Tris, 192 mM glycine, 0.1% SDS; pH 8.3) with 20% (v/v) methanol. Membranes were blocked with 5% BSA in Tris-buffered saline-Tween 20 (25 mM Tris base, 125 mM NaCl, 0.1% Tween 20) for 30 minutes at room temperature. The membranes were incubated with primary antibodies made in 5% BSA overnight at 4° C. The primary antibodies used were: Phosphorylated TrkB (Y515; rabbit polyclonal; 1:1000; ab109684, Abcam, Cambridge, MA),

Total TrkB (goat;1:1000; GT15080, Neuromics), Phosphorylated KCC2 (Ser940; rabbit polyclonal; 1:500; 612-401-E15, Rockland), mCherry (rabbit polyclonal;1:500; ab167453, Abcam) and GAPDH (mouse monoclonal;1:2000; MAB374, Millipore).

Membranes were rinsed three times at 10 min intervals with TBS-Tween followed by a 2 h incubation at room temperature with a horseradish peroxidase-conjugated secondary antibody against the primary antibody host species (anti-rabbit, anti-goat, or anti-mouse; 1:1000; Sigma, St Louis, MO, USA). The membranes were washed three times at 5 min intervals with TBS-Tween. Proteins were visualized using an enhanced chemiluminescence substrate kit (Supersignal West Femto Maximum Sensitivity kit; Thermo Scientific, Waltham, MA). Blots were developed, and the digital image was obtained by using Gbox (Genesnap program) and densitometry analysis of the bands was performed using ImageJ. Densitometry measurements of the immunoreactive bands were normalized using GAPDH as loading control.

EXPERIMENTAL GROUPS AND STATISTICAL ANALYSIS

The plasma measurements and posttranslational modifications of the proteins were first determined in rats that did not receive stereotaxic injections. The animals were divided into two groups in these experiments: 1) Male sham and 2) Male BDL. Based on the data from the initial experiments, the shRNA was stereotaxically injected in the further experiments. In these experiments, the rats were divided into four groups as follows: 1) Sham rats injected with SCR virus (Sham SCR), 2) Sham rats injected with shBDNF virus (Sham shBDNF), 3) BDL rats injected with SCR virus (BDL SCR), and 4) BDL rats injected with shBDNF virus (BDL shBDNF).

The data from BDL and sham rats without any stereotaxic injections were analyzed using Student's t-test using Sigma plot 12.0. Data from the metabolic cage studies were analyzed by separate two-way repeated measures ANOVA with time as first factor and treatment (BDL/sham with stereotaxic injection) as second factor followed by Bonferroni post hoc tests. All other data were analyzed using one-way ANOVA with Bonferroni post hoc tests using Sigma Plot 12.0. Figures were assembled using the 'magick' package in RStudio. The group sizes were determined by power analysis and effect size calculated from our previously published work^(19, 24, 31) and preliminary data using Sigma plot 12.0. Power analysis calculation elements included considerations of $p < 0.05$, α of 0.8, largest difference between means, and the largest standard deviation we had observed from our studies. η^2 (η^2 method was chosen to calculate the effect sizes and the sample sizes were balanced (equal) in all the groups and were independent of each other. Sum of squares (SS) of effect and total from our previous studies^(19, 23, 24, 31) were used for the effect size determination. The minimal n's per group for each experiment was determined to have an appropriately powered study with the effect size (η^2) of approximately 0.7 (70%).

RESULTS

EFFECT OF BDL IN MALE RATS

CHANGES IN LIVER WEIGHT AND PLASMA PARAMETERS

The liver weight and plasma parameters were measured 4 weeks after BDL/ sham ligation surgery. The liver to body weight ratio was very high in BDL rats compared to the sham rats. The increase in liver to body weight ratio indicates the BDL rats develop liver failure. The Student's t test indicates that the liver weight was significantly increased in BDL rats compared to the sham rats ($t = -5.936$, d.f. =23; $p < 0.001$; Figure 1A). Plasma osmolality and hematocrit

values were significantly decreased in BDL rats compared to the sham rats indicating the development of hyponatremia with bile duct ligation (Osmolality: $t = 24.982$; d.f. = 10; $p < 0.001$; Hematocrit: $t = 4.089$; d.f. = 9; $p < 0.05$; Figure 1B & 1C). Plasma CPP values were used as biomarker for circulating AVP concentration. The concentration of CPP in BDL sham rats was higher compared to the sham rats. Student's t test indicates significant increase in plasma CPP concentration in male BDL rats compared to the sham rats ($t = -8.030$; d.f. = 10; $p < 0.05$; Figure 1D).

POST TRANSLATIONAL MODIFICATIONS OF TrkB AND KCC2

The phosphorylation status of TrkB and KCC2 co-transporter were first determined in male BDL and sham rats without stereotaxic injections (Figure 2A). Bile duct ligation for 4 weeks increased TrkB phosphorylation without affecting total TrkB expression and decreased phosphorylation of KCC2 in the SON. The phosphorylation of TrkB receptor was significantly increased in BDL rats compared to the sham rats which was determined using student's test ($t = -2.486$; d.f = 14; Figure 2B). The phosphorylation of KCC2 was significantly decreased in BDL rats compared to the sham rats ($t = 3.578$; d.f = 14; Figure 2C).

EFFECT OF BDL AND BDNF KNOCKDOWN IN MALE RATS

CHANGES IN FLUID INTAKE, URINE EXCRETION, FOOD INTAKE AND BODY WEIGHT

Fluid intake, urine excretion and food intake were measured daily for 14 days after two weeks from BDL or sham surgery^(18, 24, 29). Both the fluid intake and urine excretion were increased in BDL rats with SCR injections compared to the sham rats. But this increase in both fluid intake and urine excretion was not observed in the BDL rats injected with shBDNF. Two-way repeated

measures ANOVA revealed significant difference indicating that fluid intake was affected by time and the treatment protocol (Time: $F(13,156) = 5.734$, $p < 0.001$; Treatment: $F(3,156) = 11.818$, $p < 0.001$; Figure 3A). Post hoc multiple comparisons between the factors revealed that bile duct ligation significantly increased fluid intake (vs Sham SCR: Bonferroni $t = 4.942$; $p < 0.05$; vs. Sham shBDNF: Bonferroni $t = 5.271$; $p < 0.05$). The BDNF knockdown significantly decreased the fluid intake in BDL rats compared to the sham ligated rats (Bonferroni $t = 4.027$; $p < 0.05$). The significant interaction between the factors are observed in the volume of urine excreted (Time x Treatment $F(39,156) = 1.984$, $p < 0.05$; Figure 3B). The average daily urine volume significantly increased in BDL SCR compared to the sham rats (Bonferroni t tests, $p < 0.05$). Post hoc multiple comparisons show that the urine excretion was not significantly increased in BDL shBDNF rats compared to the sham rats. The food intake was not significantly different in all the four groups ($F(3, 19) = 0.595$, $p = 0.626$; Figure 3C). Concomitantly, the average body weight increase was not significantly different between the four groups. (Figure 3D).

CHANGES IN LIVER TO BODY WEIGHT RATIO

The liver weight was measured four weeks after BDL/ sham ligation surgery. The increase in liver weight is widely used as a biomarker to verify the liver failure animal model (24, 29). The liver to body weight ratio was higher in both BDL SCR and BDL shBDNF rats compared to the sham rats. One-way ANOVA followed by Bonferroni multiple comparisons show that both SCR and shBDNF rats with bile duct ligation had significantly increased liver to body weight ratio compared to the sham groups ($F(3,25) = 59.304$, $p < 0.001$; Figure 4A). The BDNF knockdown in BDL rats did not have any effect on the liver to body weight ratio compared to BDL SCR rats.

CHANGES IN PLASMA, OSMOLALITY, HEMATOCRIT AND COPEPTIN

The plasma parameters osmolality, hematocrit and CPP concentration were measured 4 weeks after BDL/ sham ligation surgery. The development of hyponatremia with bile duct ligation caused decrease in plasma osmolality and hematocrit values in BDL rats with SCR injections compared to the sham rats. The BDL induced hyponatremia is not observed with BDNF knockdown. The concentration of CPP in BDL sham rats was higher compared to the sham rats. This increase in plasma CPP values was not seen in the BDL rats injected with shBDNF.

One- way ANOVA followed by post hoc multiple comparisons show that plasma osmolality and hematocrit values were significantly different between the groups (Plasma osmolality $F(3,23) = 32.115$, $p < 0.001$; Hematocrit $F(3,22) = 20.771$, $p < 0.001$). The BDL SCR rats also had plasma osmolality and hematocrit values that were significantly lower than all other groups (Bonferroni t tests, all $p < 0.05$). The BDL shBDNF group had significantly higher plasma osmolality (Bonferroni $t = 4.269$, $p < 0.05$; Figure 4B) and hematocrit (Bonferroni $t = 5.945$, $p < 0.05$; Figure 4C) as compared to the BDL SCR group. One-way ANOVA revealed significant difference between the groups in plasma CPP concentration ($F(3,18) = 48.260$, $p < 0.05$). Bonferroni multiple comparisons show that rats with SCR injections and bile duct ligation had significantly increased circulating CPP compared to all the other groups (Bonferroni t tests, all $p < 0.001$; Figure 4D). Knockdown of BDNF in the SON of bile duct ligated rats significantly decreased plasma CPP as compared to the BDL SCR group (Bonferroni $t = 6.498$, $p < 0.05$; Figure 4D).

CHANGES IN PHOSPHORYLATION OF TrkB AND KCC2 IN SON

The SONs from the BDL rats with SCR injections had increased phosphorylation of TrkB receptor and decreased phosphorylation of KCC2. The phosphorylation of TrkB receptor was decreased in the BDL rats with BDNF knockdown in the SON. In addition, the downregulation of KCC2 phosphorylation was inhibited by BDNF knockdown in the BDL rats. The mCherry expression was used to verify the specificity of stereotaxic injections (Figure 5A). One-way ANOVA analysis revealed a significant difference between the groups in TrkB phosphorylation ($F(3,20) = 14.931, p < 0.05$; Figure 5B) and KCC2 phosphorylation ($F(3,20) = 5.973, p < 0.05$; Figure 5C). Bile duct ligation for four weeks significantly increased TrkB phosphorylation without affecting total TrkB expression and decreased phosphorylation of KCC2 (Bonferroni t tests, all $p < 0.05$, Figure 5) in the SON of rats injected with the control vector compared to the sham ligated rats. Virally mediated BDNF knockdown in the SON of BDL rats significantly prevented the increase in TrkB phosphorylation and the decrease in KCC2 phosphorylation compared to sham rats (Bonferroni t tests, all $p < 0.05$, Figure 5). One to two rats in each group did not have successful virus injections in the SON which were verified at the end of the experiment and were excluded from the data analysis in all the experiments.

DISCUSSION

It is well established that the liver failure causes portal hypertension due to obstruction of portal blood flow because of massive structural changes associated with fibrosis and intrahepatic vasoconstriction⁽³³⁾. The increase in hepatic vascular resistance to blood flow during liver failure is coupled with hypovolemia and vasodilation. These systemic responses to portal hypertension disturb circulatory physiology^(3, 5, 14, 34, 35). The compensatory neurohumoral mechanisms are activated and AVP secretion is increased to restore blood volume. But, the secretion of AVP is not suppressed relative to plasma osmolality leading to hyponatremia which increases morbidity and mortality of patients with liver failure. Dilutional hyponatremia is common in end stage liver disease due to fluid accumulation by decreased free water clearance which leads to life threatening complications such as cerebral and pulmonary edema^(15, 36).

Hyponatremia is characterized by relative excess of body water relative to body sodium content. The management of hyponatremia in liver failure is challenging as conventional treatment for hyponatremia including fluid restriction and loop diuretics to enhance the renal solute-free water excretion are frequently inefficacious. Diuretic therapy often leads to a worsening of the plasma sodium status and is shown to have very little effect on improving free water clearance^(5, 34). The majority of patients find it difficult to adhere to fluid restriction, and discontinuation of diuretics may further worsen ascites⁽¹⁵⁾. However, the rapid correction of serum sodium may lead to serious neurological complications such as central pontine myelinolysis or seizures^(15, 36). The AVP antagonists, vaptans, that selectively antagonizes the effects of AVP on the V2 receptors in the kidney tubules represents the logical step in the treatment of hyponatremia. However, most of currently available vaptans increase risk for hepatic failure and mortality^(1, 5, 36).

During liver failure, AVP secretion is increased due to non- osmotic mechanisms. However, the mechanisms involved in the increase in AVP secretion during liver failure are not known. In this study, we show a mechanism that contributes to the increased AVP secretion in an animal model of liver failure. This model is shown to induce hyponatremia due to increased AVP secretion caused by liver failure. This model is widely used as it is reproducible and the survival rate associated with this model is higher compared to other animal models of liver failure ^(37, 38). The cauterization of bile duct in BDL rats causes obstruction of bile duct resulting in cholestasis. Cholestasis is a condition where bile cannot flow from the liver to the duodenum and it leads to jaundice. The accumulation of bile in the liver causes necrosis of hepatocytes leading to liver failure. The yellowish pigmentation of skin, plasma and increase in liver to body weight ratio are used as biomarkers to verify the disease model in this study ^(23, 29, 31, 39).

We measured copeptin as biomarker for plasma AVP in our experiments. Copeptin is secreted at equal molar concentration (1:1) to AVP with longer half-life compared to AVP. Previous studies from our lab and several others have shown a correlation between plasma copeptin and AVP measurements at various osmolalities ^(30, 40).

The fluid intake and urine excretion in BDL rats are higher compared to the sham rats despite their lower plasma osmolalities which suggests the role of non-osmotic mechanisms in fluid intake of BDL rats. The fluid intake and urine excretion were decreased with BDNF knockdown in BDL rats. Previous studies from our laboratory reported the association between BDL, increased drinking behavior, increased angiotensin II type 1 receptor (AT1R) expression in the subfornical organ (SFO) and elevated peripheral renin angiotensin system ^(24, 29, 39). The renin angiotensin system is activated in response to systemic hypotension in BDL rats. The current study shows the similar decrease in drinking behavior and urine excretion in BDL rats. The

BDNF knockdown in the BDL rats might have compensated the decrease in mean arterial pressure thereby preventing the angiotensin mediated thirst response, although this was not directly tested in the current study. Also, the osmoreceptors in the SON are known to control both thirst and osmolality ^(7, 35, 41-43). It is possible BDNF plays a role in the transduction pathways of the osmoreceptors.

Body fluid and electrolyte homeostasis are maintained by the integration of physiological and behavioral systems ^(5, 41, 44). In the physiological context of decreasing copeptin secretion, behavioral decrease in fluid intake could contribute to progressively increasing plasma osmolality associated with BDNF knockdown in BDL rats. The role of BDNF in thirst and urine excretion is not understood and will be the focus of future studies.

KCC2 is the major co-transporter for the efflux of chloride ions, as KCC2 is downregulated Cl concentration within the neuron is increased which reverses the flux of ions through GABA_A receptor. This impairs GABA_A mediated inhibition of SON neurons ^(19, 20, 45). The loss of synaptic inhibition in SON neurons creates a feed forward loop in the secretion of AVP ^(18, 19, 46).

This is the first study to demonstrate increased activation of TrkB receptor and decreased phosphorylation of KCC2 co-transporter in BDL rats compared to sham ligated rats. The knockdown of BDNF, the primary ligand of TrkB receptor in the SON of BDL rats, prevented both the activation of TrkB receptor and downregulation of KCC2 cotransporter. The decrease in copeptin concentration in plasma samples correlate with the western blot data of BDNF knockdown rats. The mCherry protein expression is used to verify the specificity of viral injections.

The AAV- U6 - shBDNF used in this study to knockdown BDNF, specifically in the SON, is based on previous studies which show stable knockdown of BDNF and high transduction efficiency with this viral construct ^(18, 19). The studies from our lab previously demonstrated increased FosB staining and AVP hnRNA expression in the SON neurons of bile duct ligated male rats ^(24, 29). In addition, the increase in AVP secretion in SL rats was prevented by inhibiting the increase in BDNF in the SON ⁽¹⁸⁾. Based on these previous results, the bilateral SON was chosen in the current study to inject shRNA against BDNF.

Although the post translational modification of KCC2 implies the changes in intracellular chloride concentration ^(47, 48), the effect of BDL and BDNF knockdown on the chloride homeostasis and GABA mediated inhibition is not directly tested in this study and will be the focus of future studies. The synaptic mechanisms contributing to the increase in BDNF in SON are yet to be understood.

CONCLUSIONS

This study advances our understanding on the mechanisms involved in inappropriate AVP secretion leading to hyponatremia during liver failure. Our results are the first showing that BDNF from SON causes activation of TrkB receptor and downregulation of KCC2 in BDL male rats. This BDNF-TrkB- KCC2 regulatory mechanism contributes to the increase in AVP secretion resulting in hyponatremia. In addition, the knockdown of BDNF in the SON reduced the thirst and urine excretion associated with liver failure.

ACKNOWLEDGEMENT

The authors would like to thank M. Bachelor for her technical assistance.

GRANTS

This work was supported by R01 HL119458 to JTC and AHA18PRE34060035 to KB.

DISCLOSURES

The authors have nothing to disclose.

REFERENCES

1. Boscoe A, Paramore C, Verbalis JG. Cost of illness of hyponatremia in the United States. *Cost Effectiveness and Resource Allocation*. 2006; 4: 10-.
2. Martin PY, Schrier RW. Sodium and water retention in heart failure: pathogenesis and treatment. *Kidney international Supplement*. 1997; 59: S57-61.
3. Chatterjee K. Neurohormonal activation in congestive heart failure and the role of vasopressin. *The American journal of cardiology*. 2005; 95: 8b-13b.
4. Goldsmith SR. Current treatments and novel pharmacologic treatments for hyponatremia in congestive heart failure. *The American journal of cardiology*. 2005; 95: 14b-23b.
5. Verbalis JG. Disorders of body water homeostasis. *Best Pract Res Clin Endocrinol Metab*. 2003; 17: 471-503.
6. Armstrong WE. Morphological and electrophysiological classification of hypothalamic supraoptic neurons. *Progress in Neurobiology*. 1995; 47: 291-339.
7. Bourque CW. Central mechanisms of osmosensation and systemic osmoregulation. *Nat Rev Neurosci*. 2008; 9: 519-31.
8. Ferguson AV, Latchford KJ. Local circuitry regulates the excitability of rat neurohypophysial neurones. *Exp Physiol*. 2000; 85 Spec No: 153s-61s.
9. Hatton GI. Oxytocin and vasopressin neurones: vive la difference! *J Physiol*. 1997; 500 (Pt 2): 284.
10. Kombian SB, Hirasawa M, Mougnot D, Pittman QJ. Modulation of synaptic transmission by oxytocin and vasopressin in the supraoptic nucleus. *Progress in brain research*. 2002; 139: 235-46.

11. Ludwig M, Leng G. Dendritic peptide release and peptide-dependent behaviours. *Nat Rev Neurosci.* 2006; 7: 126-36.
12. McKinley MJ, Mathai ML, McAllen RM, McClear RC, Miselis RR, Pennington GL, Vivas L, Wade JD, Oldfield BJ. Vasopressin secretion: osmotic and hormonal regulation by the lamina terminalis. *J Neuroendocrinol.* 2004; 16: 340-7.
13. Renaud LP. CNS pathways mediating cardiovascular regulation of vasopressin. *Clinical and Experimental Pharmacology and Physiology.* 1996; 23: 157-60.
14. Cardenas A, Arroyo V. Mechanisms of water and sodium retention in cirrhosis and the pathogenesis of ascites. *Best Pract Res Clin Endocrinol Metab.* 2003; 17: 607-22.
15. John S, Thuluvath PJ. Hyponatremia in cirrhosis: Pathophysiology and management. *World Journal of Gastroenterology : WJG.* 2015; 21: 3197-205.
16. Schrier RW, Gross P, Gheorghide M, Berl T, Verbalis JG, Czerwiec FS, Orlandi C. Tolvaptan, a selective oral vasopressin V2-receptor antagonist, for hyponatremia. *The New England journal of medicine.* 2006; 355: 2099-112.
17. Corona G, Giuliani C, Parenti G, Norello D, Verbalis JG, Forti G, Maggi M, Peri A. Moderate hyponatremia is associated with increased risk of mortality: evidence from a meta-analysis. *PloS one.* 2013; 8: e80451.
18. Balapattabi K, Little JT, Farmer GE, Cunningham JT. High salt loading increases brain derived neurotrophic factor in supraoptic vasopressin neurones. *J Neuroendocrinol.* 2018; 30: e12639.
19. Choe KY, Han SY, Gaub P, Shell B, Voisin DL, Knapp BA, Barker PA, Brown CH, Cunningham JT, Bourque CW. High salt intake increases blood pressure via BDNF-mediated

- downregulation of KCC2 and impaired baroreflex inhibition of vasopressin neurons. *Neuron*. 2015; 85: 549-60.
20. Choe KY, Trudel E, Bourque CW. Effects of Salt Loading on the Regulation of Rat Hypothalamic Magnocellular Neurosecretory Cells by Ionotropic GABA and Glycine Receptors. *J Neuroendocrinol*. 2016; 28.
21. Marosi K, Mattson MP. Hold the salt: vasopressor role for BDNF. *Cell metabolism*. 2015; 21: 509-10.
22. Chamma I, Chevy Q, Poncer JC, Levi S. Role of the neuronal K-Cl co-transporter KCC2 in inhibitory and excitatory neurotransmission. *Frontiers in cellular neuroscience*. 2012; 6: 5.
23. Carreño FR, Ji LL, Cunningham JT. Altered central TRPV4 expression and lipid raft association related to inappropriate vasopressin secretion in cirrhotic rats. *American Journal of Physiology - Regulatory, Integrative and Comparative Physiology*. 2009; 296: R454-R66.
24. Cunningham JT, Nedungadi TP, Walch JD, Nestler EJ, Gottlieb HB. Δ FosB in the supraoptic nucleus contributes to hyponatremia in rats with cirrhosis. *American Journal of Physiology - Regulatory, Integrative and Comparative Physiology*. 2012; 303: R177-R85.
25. Cárdenas A, Ginès P. Pathogenesis and Treatment of Fluid and Electrolyte Imbalance. *Seminars in nephrology*. 2001; 21: 308-16.
26. Schrier RW. Water and sodium retention in edematous disorders: role of vasopressin and aldosterone. *The American journal of medicine*. 2006; 119: S47-53.
27. Kim YB, Kim YS, Kim WB, Shen FY, Lee SW, Chung HJ, Kim JS, Han HC, Colwell CS, Kim YI. GABAergic excitation of vasopressin neurons: possible mechanism underlying sodium-dependent hypertension. *Circulation research*. 2013; 113: 1296-307.

28. Paxinos G, Watson C. *The Rat Brain in Stereotaxic Coordinates* San Diego: Academic Press, 1997.
29. Walch JD, Carreño FR, Cunningham JT. Intracerebroventricular losartan infusion modulates angiotensin type 1 receptor expression in the subfornical organ and drinking behaviour in bile duct ligated rats. *Experimental physiology*. 2013; 98: 922-33.
30. Balanescu S, Kopp P, Gaskill MB, Morgenthaler NG, Schindler C, Rutishauser J. Correlation of Plasma Copeptin and Vasopressin Concentrations in Hypo-, Iso-, and Hyperosmolar States. *The Journal of Clinical Endocrinology & Metabolism*. 2011; 96: 1046-52.
31. Nedungadi TP, Cunningham JT. Differential regulation of TRPC4 in the vasopressin magnocellular system by water deprivation and hepatic cirrhosis in the rat. *American Journal of Physiology - Regulatory, Integrative and Comparative Physiology*. 2014; 306: R304-R14.
32. Nedungadi TP, Carreno FR, Walch JD, Bathina CS, Cunningham JT. Region specific changes in TRPV channel expression in the vasopressin magnocellular system in hepatic cirrhosis induced hyponatremia. *Journal of neuroendocrinology*. 2011.
33. Iwakiri Y. Pathophysiology of portal hypertension. *Clinics in liver disease*. 2014; 18: 281-91.
34. Lo R, Austin A, Freeman J. Vasopressin in liver disease--should we turn on or off? *Current clinical pharmacology*. 2008; 3: 156-65.
35. Gizowski C, Bourque CW. The neural basis of homeostatic and anticipatory thirst. *Nature Reviews Nephrology*. 2017; 14: 11.
36. D'Auria D, Marinosci GZ, De Benedictis G, Piazza O. Vaptans and hyponatremia in critical patients. *Translational medicine @ UniSa*. 2012; 3: 1-14.

37. Liu Y, Meyer C, Xu C, Weng H, Hellerbrand C, ten Dijke P, Dooley S. Animal models of chronic liver diseases. *American journal of physiology Gastrointestinal and liver physiology*. 2013; 304: G449-68.
38. Rahman TM, Hodgson HJ. Animal models of acute hepatic failure. *International journal of experimental pathology*. 2000; 81: 145-57.
39. Saxena A, Bachelor M, Park YH, Carreno FR, Nedungadi TP, Cunningham JT. Angiotensin II induces membrane trafficking of natively expressed transient receptor potential vanilloid type 4 channels in hypothalamic 4B cells. *American journal of physiology Regulatory, integrative and comparative physiology*. 2014; 307: R945-55.
40. Santillan MK, Santillan DA, Scroggins SM, Min JY, Sandgren JA, Pearson NA, Leslie KK, Hunter SK, Zamba GK, Gibson-Corley KN, Grobe JL. Vasopressin in preeclampsia: a novel very early human pregnancy biomarker and clinically relevant mouse model. *Hypertension (Dallas, Tex : 1979)*. 2014; 64: 852-9.
41. Johnson AK. The periventricular anteroventral third ventricle (AV3V): Its relationship with the subfornical organ and neural systems involved in maintaining body fluid homeostasis. *Brain research bulletin*. 1985; 15: 595-601.
42. Bourque CW. Osmoregulation of vasopressin neurons: a synergy of intrinsic and synaptic processes. *Progress in brain research*. 1998; 119: 59-76.
43. Prager-Khoutorsky M, Bourque CW. Mechanical basis of osmosensory transduction in magnocellular neurosecretory neurones of the rat supraoptic nucleus. *J Neuroendocrinol*. 2015; 27: 507-15.
44. Verbalis JG. Osmotic Inhibition of Neurohypophysial Secretion. *Annals of the New York Academy of Sciences*. 1993; 689: 146-60.

45. Chudotvorova I, Ivanov A, Rama S, Hübner CA, Pellegrino C, Ben-Ari Y, Medina I. Early expression of KCC2 in rat hippocampal cultures augments expression of functional GABA synapses. *The Journal of physiology*. 2005; 566: 671-9.
46. Choe KY, Prager-Khoutorsky M, Farmer WT, Murai KK, Bourque CW. Effects of Salt Loading on the Morphology of Astrocytes in the Ventral Glia Limitans of the Rat Supraoptic Nucleus. *Journal of Neuroendocrinology*. 2016; 28.
47. Rivera C, Li H, Thomas-Crusells J, Lahtinen H, Viitanen T, Nanobashvili A, Kokaia Z, Airaksinen MS, Voipio J, Kaila K, Saarma M. BDNF-induced TrkB activation down-regulates the K⁺-Cl⁻ cotransporter KCC2 and impairs neuronal Cl⁻ extrusion. *J Cell Biol*. 2002; 159: 747-52.
48. Rivera C, Voipio J, Payne JA, Ruusuvuori E, Lahtinen H, Lamsa K, Pirvola U, Saarma M, Kaila K. The K⁺/Cl⁻ co-transporter KCC2 renders GABA hyperpolarizing during neuronal maturation. *Nature*. 1999; 397: 251-5.

FIGURES

CHAPTER IV - Figure IV-1 – Parameters of male BDL rats without stereotaxic injections

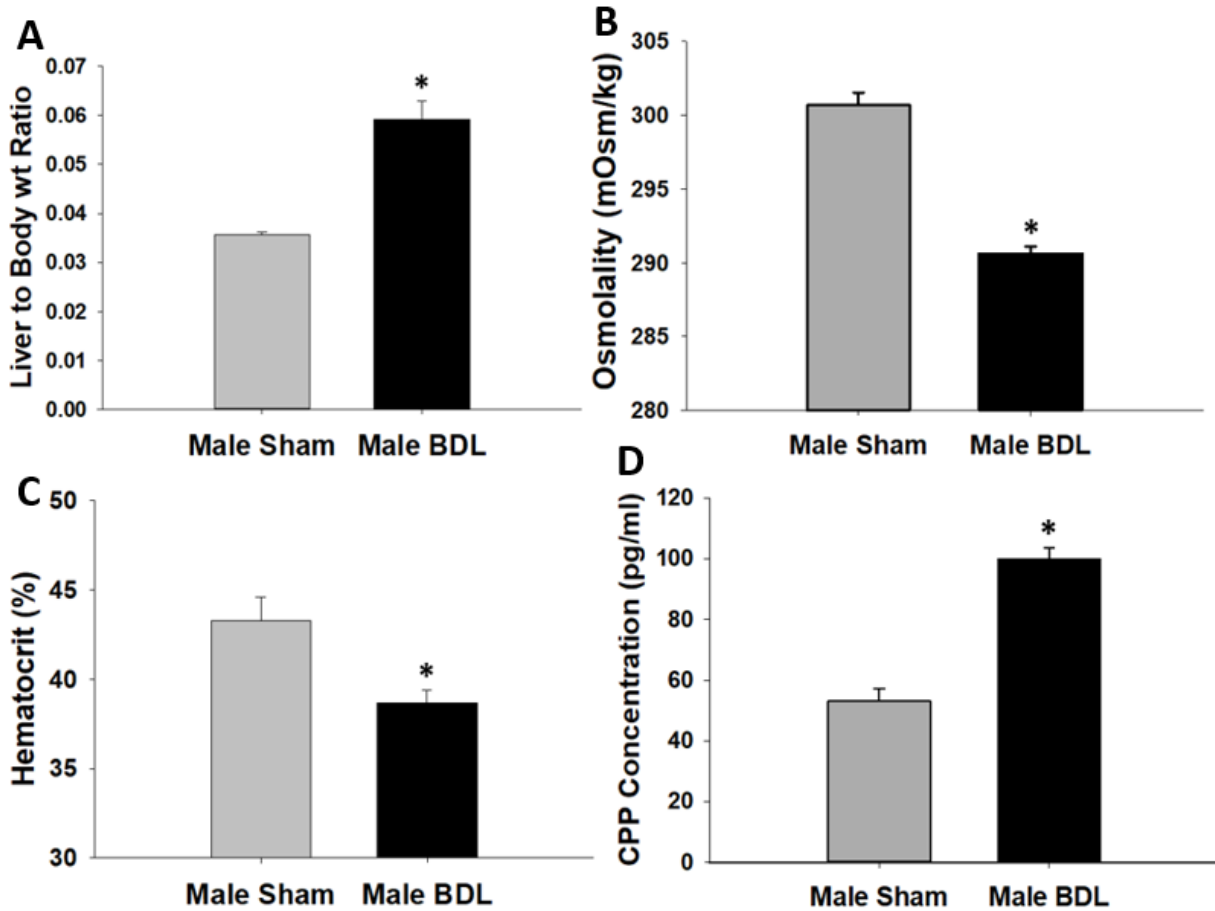


Figure 1: Effect of BDL in male rats without stereotaxic injections on **A:** Liver to body weight ratio of male sham and male BDL rats **B:** Plasma osmolality. **C:** Hematocrit values. **D:** Plasma CPP concentration. Data are mean \pm SEM. * $p < 0.05$ vs. sham. Groups: Male Sham (n = 7); Male BDL (n = 5).

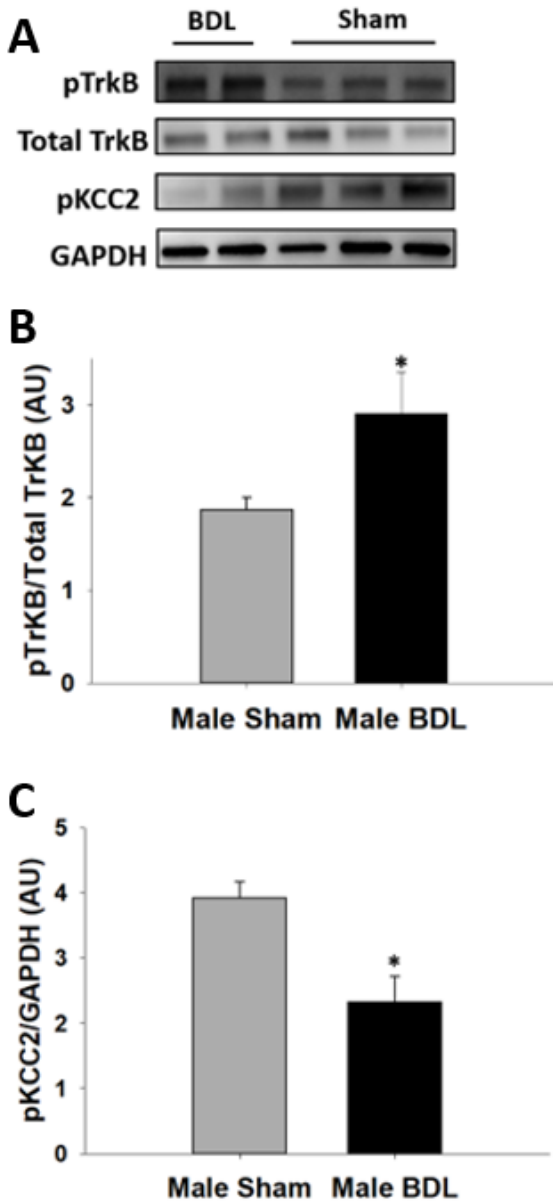


Figure 2: Effect of BDL in protein expression in SON of male rats. **A:** Sample Western blot images showing changes in protein expression of SON punches in male sham and BDL rats without stereotaxic injections. **B:** Quantification of phosphorylated TrkB (normalized to total TrkB). **C:** Phosphorylated KCC2 normalized to GAPDH. Data are mean \pm SEM. * $p < 0.05$ vs. male sham. Groups: Male sham (n = 7); Male BDL (n = 9).

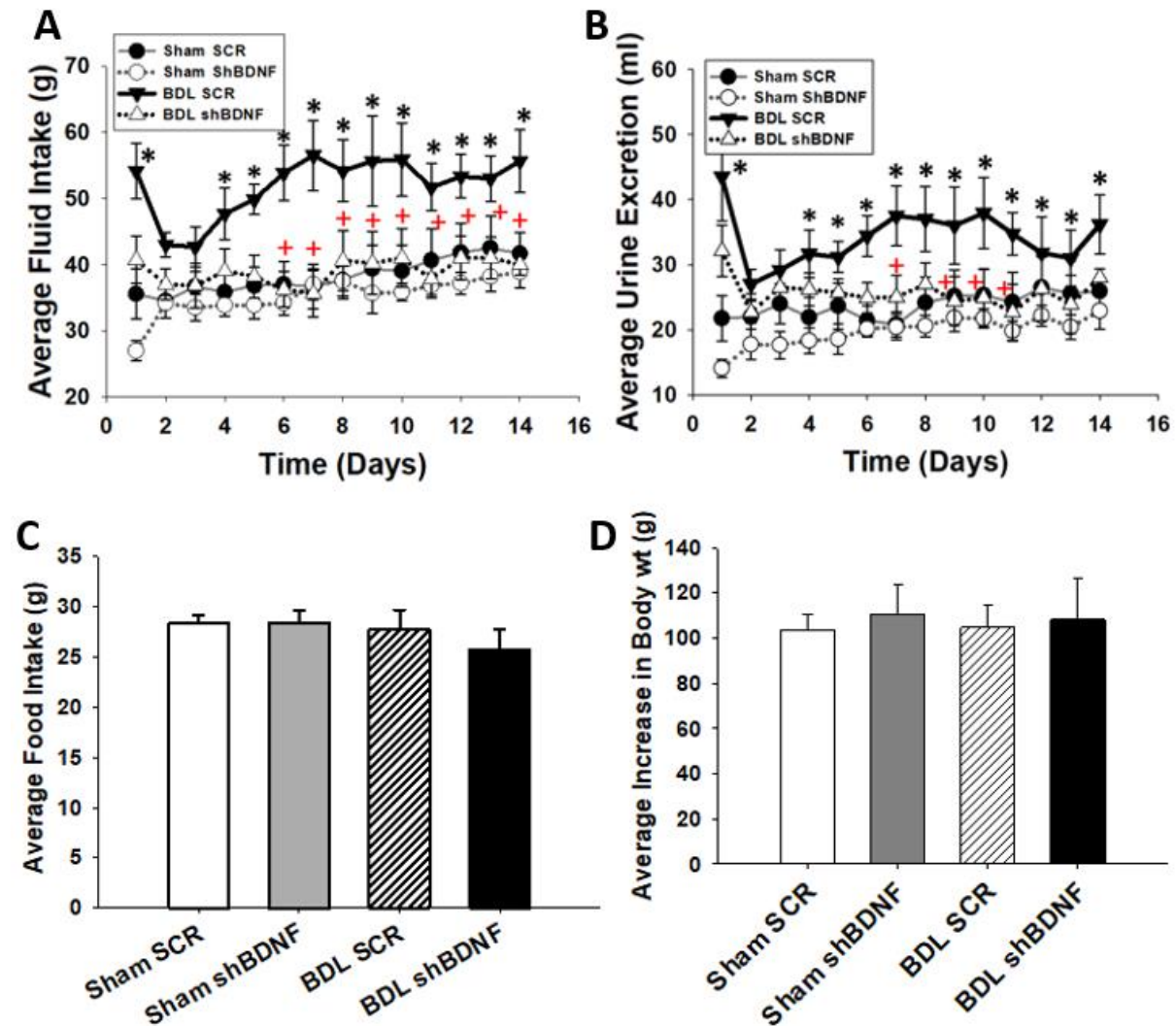


Figure 3: The effects of bile duct ligation and BDNF knockdown in the SON on **A:** Daily average fluid intake. **B:** Daily average urine excretion. **C:** Average daily changes in food intake. **D:** Average increase in body weight. Data are mean \pm SEM. * $p < 0.05$ vs. sham groups. + $p < 0.05$ BDL shBDNF vs. BDL SCR. Groups: Sham SCR (n = 6); Sham shBDNF (n = 6); BDL SCR (n = 6); BDL shBDNF (n = 5).

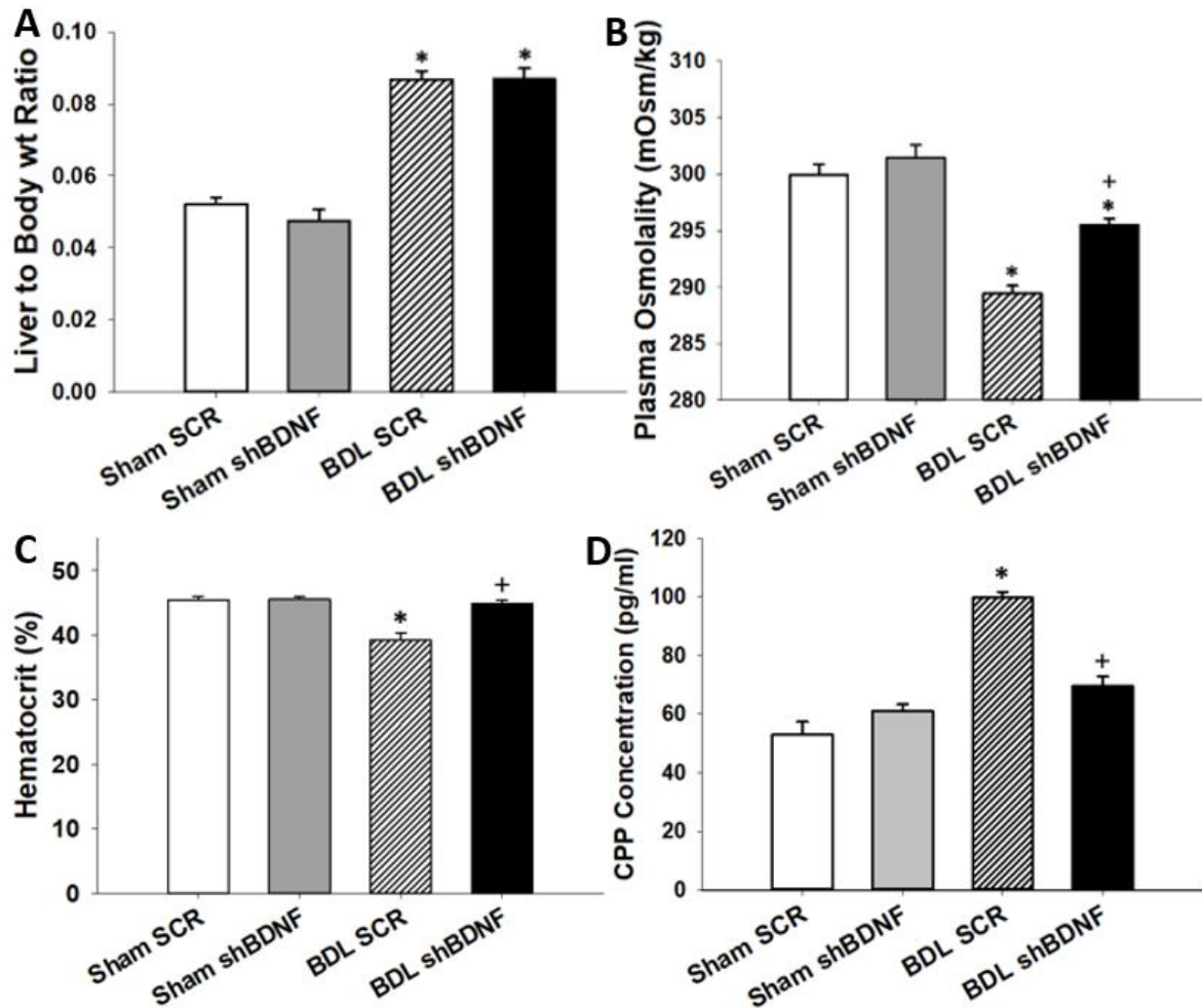


Figure 4: The effects of bile duct ligation and BDNF knockdown in the SON on **A:** Liver to body weight ratio **B:** Plasma osmolality **C:** Hematocrit values. **D:** Plasma CPP concentration.

Data are mean \pm SEM. *p < 0.05 vs. all other groups. Groups: Sham SCR (n = 6); Sham shBDNF (n = 6-9); BDL SCR (n = 6); BDL shBDNF (n = 6 - 8).

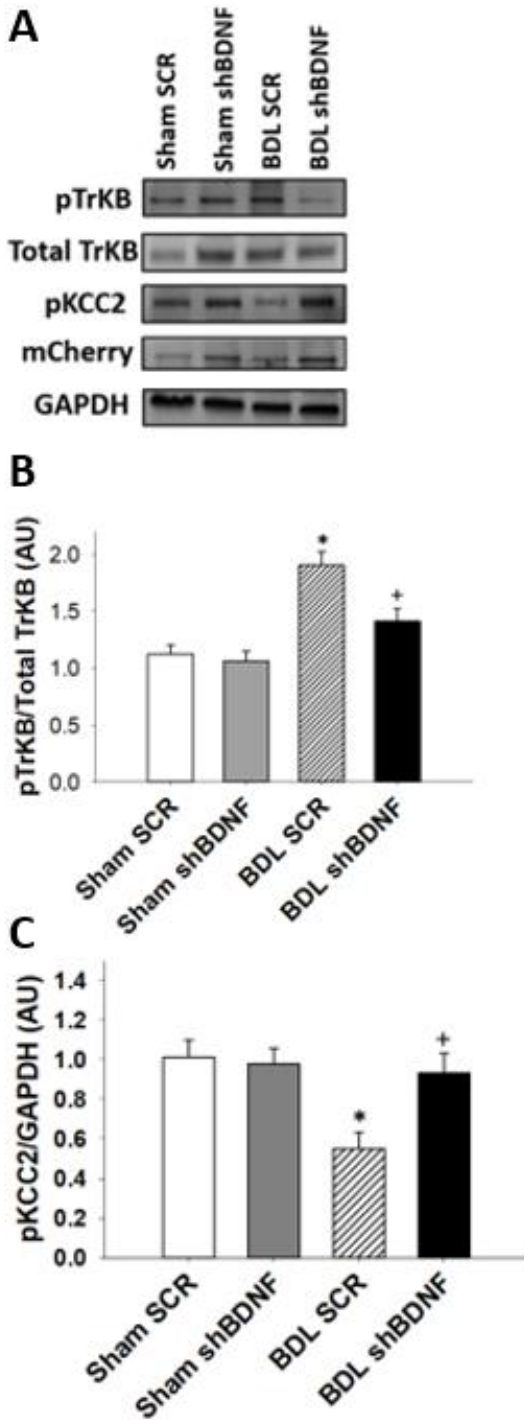


Figure 5: The effects of bile duct ligation and BDNF knockdown in the SON on protein expression. **A:** Sample Western blot images showing changes in protein expression of SON

punches. mCherry protein expression images shows successful injections at SON **B:**

Quantification of phosphorylated TrkB (normalized to total TrkB). **C:** Phosphorylated KCC2

normalized to GAPDH. Data are mean \pm SEM. * $p < 0.05$ vs. all other groups. $^{\dagger}p < 0.05$ vs. BDL

SCR. Groups: Sham SCR (n = 6); Sham shBDNF (n = 6); BDL SCR (n = 6); BDL shBDNF (n =

6).

CHAPTER V

FINAL DISCUSSION, PERSPECTIVES & SIGNIFICANCE AND

FUTURE DIRECTIONS

OVERALL DISCUSSION

The focus of this section is to discuss the comparable outcomes between the hypernatremia and hyponatremia animal models used in this dissertation. The detailed experimental discussions were addressed in the individual chapters. The first part of the dissertation focused on regulation of AVP secretion during salt loading (SL). It was reasonable to begin by interpreting the role of BDNF produced from SON in the SL model where preliminary studies on regulatory pathways have been reported⁽¹⁻³⁾. The results and techniques from the SL study set the stage for investigating AVP release associated with liver failure using bile duct ligated (BDL) rats, as there are not many previous studies on AVP neuron regulation during liver failure.

The salt loading and liver failure models were primarily chosen and studied in this dissertation as they both involve inappropriate AVP secretion⁽¹⁻⁶⁾. The results from this dissertation and several previous studies have shown that GABA_A mediated inhibition of SON AVP neurons is impaired in both the models^(1-3, 7-13). However, the neural mechanisms leading to the activation of PNZ GABAergic neurons that project to the neurosecretory cells in the SONs are different in both the models⁽¹⁴⁻²²⁾. The baroreceptor mediated inhibition of SON AVP neurons occurs during SL while the osmoreceptor mediated inhibition occurs during liver failure^(14, 15, 17, 23-25). Also, the osmotic mechanisms initiate AVP secretion during SL while non-osmotic mechanisms contribute to AVP secretion during BDL^(9, 26-31).

The metabolic cage data from SL and BDL experiments shows that BDNF knockdown in the SON decreased water intake in BDL rats but not in SL rats. This influence of BDNF on fluid intake is not completely understood. It is well established that BDL causes systemic hypotension that activates renin angiotensin system and angiotensin can increase water intake^(1, 2, 6, 32, 33). It is possible the BDNF knockdown in the BDL rats and the resulting changes in AVP release and

plasma osmolality might have systemic effects that mitigated the hypotension and angiotensin release mediated water intake, although this was not evaluated in the current study. However, in SL rats, renin angiotensin system remains inactivated as the mean arterial pressure was not decreased with BDNF knockdown in the SON ⁽⁷⁾. The decrease in angiotensin and increase in MAP indicates the possibility of inhibition of thirst. This inhibition might have been overruled by vicious cycle created between angiotensin mediated thirst inhibition and sustained high salt intake induced thirst as 2% salt is the only drinking fluid available for SL rats.

Also, the osmoreceptors in the SON are known to control both thirst and osmolality ^(14, 15, 31, 34, 35). It is possible that BDNF differentially regulate the osmoreceptors which might have influenced thirst response during hyponatremia but not during hypernatremia ^(25, 31, 33, 35, 36). The results of these studies show that behavioral response induced by BDNF in the SON might depend on the physiological state of the animal.

In addition to decreasing AVP secretion, the BDNF knockdown induced increased urine sodium excretion in SL rats ⁽⁷⁾ and decreased water retention by decreasing fluid intake in BDL rats. These responses induced by BDNF knockdown might contribute to the progressively normalized plasma osmolality in the SL and BDL models and might be independent of BDNF effects on AVP secretion. The increase in oxytocin during SL can cause natriuresis at high concentrations ^(37, 38) in addition to inducing atrial natriuretic peptide (ANP) mediated renal sodium excretion. However, the effect of BDNF knockdown on oxytocin and its subsequent role in urine sodium excretion during SL were not tested.

The results from this dissertation shows that the BDNF-TrkB-KCC2 mechanism in the SON impairs the GABAA inhibition of SON AVP neurons contributing to the increase in AVP secretion in both SL and BDL rats. Provided the difference in neural pathways for GABAergic

inputs to the SON AVP neurons in both the models, the presynaptic mechanisms that contribute to the increase in BDNF in the SON neurons might be different.

REFERENCES

1. Choe KY, Han SY, Gaub P, Shell B, Voisin DL, Knapp BA, Barker PA, Brown CH, Cunningham JT, Bourque CW. High salt intake increases blood pressure via BDNF-mediated downregulation of KCC2 and impaired baroreflex inhibition of vasopressin neurons. *Neuron*. 2015; 85: 549-60.
2. Choe KY, Trudel E, Bourque CW. Effects of Salt Loading on the Regulation of Rat Hypothalamic Magnocellular Neurosecretory Cells by Ionotropic GABA and Glycine Receptors. *J Neuroendocrinol*. 2016; 28.
3. Marosi K, Mattson MP. Hold the salt: vasopressor role for BDNF. *Cell metabolism*. 2015; 21: 509-10.
4. Cunningham JT, Nedungadi TP, Walch JD, Nestler EJ, Gottlieb HB. Δ FosB in the supraoptic nucleus contributes to hyponatremia in rats with cirrhosis. *American Journal of Physiology - Regulatory, Integrative and Comparative Physiology*. 2012; 303: R177-R85.
5. Nedungadi TP, Cunningham JT. Differential regulation of TRPC4 in the vasopressin magnocellular system by water deprivation and hepatic cirrhosis in the rat. *American Journal of Physiology - Regulatory, Integrative and Comparative Physiology*. 2014; 306: R304-R14.
6. Walch JD, Carreño FR, Cunningham JT. Intracerebroventricular losartan infusion modulates angiotensin type 1 receptor expression in the subfornical organ and drinking behaviour in bile duct ligated rats. *Experimental physiology*. 2013; 98: 922-33.
7. Balapattabi K, Little JT, Farmer GE, Cunningham JT. High salt loading increases brain derived neurotrophic factor in supraoptic vasopressin neurones. *J Neuroendocrinol*. 2018; 30: e12639.

8. Choe KY, Prager-Khoutorsky M, Farmer WT, Murai KK, Bourque CW. Effects of Salt Loading on the Morphology of Astrocytes in the Ventral Glia Limitans of the Rat Supraoptic Nucleus. *Journal of Neuroendocrinology*. 2016; 28.
9. Di S, Tasker JG. Dehydration-induced synaptic plasticity in magnocellular neurons of the hypothalamic supraoptic nucleus. *Endocrinology*. 2004; 145: 5141-9.
10. Rinehart J, Maksimova YD, Tanis JE, Stone KL, Hodson CA, Zhang J, Risinger M, Pan W, Wu D, Colangelo CM, Forbush B, Joiner CH, Gulcicek EE, Gallagher PG, Lifton RP. Sites of regulated phosphorylation that control K-Cl cotransporter activity. *Cell*. 2009; 138: 525-36.
11. Rivera C, Li H, Thomas-Crusells J, Lahtinen H, Viitanen T, Nanobashvili A, Kokaia Z, Airaksinen MS, Voipio J, Kaila K, Saarma M. BDNF-induced TrkB activation down-regulates the K⁺-Cl⁻ cotransporter KCC2 and impairs neuronal Cl⁻ extrusion. *J Cell Biol*. 2002; 159: 747-52.
12. Rivera C, Voipio J, Payne JA, Ruusuvuori E, Lahtinen H, Lamsa K, Pirvola U, Saarma M, Kaila K. The K⁺/Cl⁻ co-transporter KCC2 renders GABA hyperpolarizing during neuronal maturation. *Nature*. 1999; 397: 251-5.
13. Rivera C, Voipio J, Thomas-Crusells J, Li H, Emri Z, Sipila S, Payne JA, Minichiello L, Saarma M, Kaila K. Mechanism of activity-dependent downregulation of the neuron-specific K-Cl cotransporter KCC2. *J Neurosci*. 2004; 24: 4683-91.
14. Bourque CW. Osmoregulation of vasopressin neurons: a synergy of intrinsic and synaptic processes. *Progress in brain research*. 1998; 119: 59-76.
15. Bourque CW. Central mechanisms of osmosensation and systemic osmoregulation. *Nat Rev Neurosci*. 2008; 9: 519-31.

16. Cunningham JT, Nissen R, Renaud LP. Norepinephrine injections in diagonal band of Broca selectively reduced the activity of vasopressin supraoptic neurons in the rat. *Brain research*. 1993; 610: 152-5.
17. Cunningham JT, Penny ML, Murphy D. Cardiovascular regulation of supraoptic neurons in the rat: synaptic inputs and cellular signals. *Prog Biophys Mol Biol*. 2004; 84: 183-96.
18. Renaud LP, Jhamandas JH, Buijs R, Raby W, Randle JC. Cardiovascular input to hypothalamic neurosecretory neurons. *Brain research bulletin*. 1988; 20: 771-7.
19. Robertson GL, Shelton RL, Athar S. The osmoregulation of vasopressin. *Kidney Int*. 1976; 10: 25-37.
20. Verbalis JG. Osmotic Inhibition of Neurohypophysial Secretion. *Annals of the New York Academy of Sciences*. 1993; 689: 146-60.
21. Verbalis JG. Disorders of body water homeostasis. *Best Pract Res Clin Endocrinol Metab*. 2003; 17: 471-503.
22. Verney EB. The antidiuretic hormone and the factors which determine its release. *Proceedings of the Royal Society of London Series B, Biological sciences*. 1947; 135: 25-106.
23. Brown CH. Rhythmogenesis in Vasopressin Cells. *Journal of Neuroendocrinology*. 2004; 16: 727-39.
24. Brown CH, Bains JS, Ludwig M, Stern JE. Physiological regulation of magnocellular neurosecretory cell activity: integration of intrinsic, local and afferent mechanisms. *J Neuroendocrinol*. 2013; 25: 678-710.
25. Carreño FR, Ji LL, Cunningham JT. Altered central TRPV4 expression and lipid raft association related to inappropriate vasopressin secretion in cirrhotic rats. *American Journal of Physiology - Regulatory, Integrative and Comparative Physiology*. 2009; 296: R454-R66.

26. Baylis PH. Osmoregulation and control of vasopressin secretion in healthy humans. *The American journal of physiology*. 1987; 253: R671-8.
27. Cárdenas A, Ginès P. Pathogenesis and Treatment of Fluid and Electrolyte Imbalance. *Seminars in nephrology*. 2001; 21: 308-16.
28. Dreifuss JJ, Kalnins I, Kelly JS, Ruf KB. Action potentials and release of neurohypophysial hormones in vitro. *The Journal of physiology*. 1971; 215: 805-17.
29. Dunn FL, Brennan TJ, Nelson AE, Robertson GL. The role of blood osmolality and volume in regulating vasopressin secretion in the rat. *The Journal of clinical investigation*. 1973; 52: 3212-9.
30. Ferguson AV, Latchford KJ. Local circuitry regulates the excitability of rat neurohypophysial neurones. *Exp Physiol*. 2000; 85 Spec No: 153s-61s.
31. Gizowski C, Bourque CW. The neural basis of homeostatic and anticipatory thirst. *Nature Reviews Nephrology*. 2017; 14: 11.
32. Cardenas A, Arroyo V. Mechanisms of water and sodium retention in cirrhosis and the pathogenesis of ascites. *Best Pract Res Clin Endocrinol Metab*. 2003; 17: 607-22.
33. Saxena A, Bachelor M, Park YH, Carreno FR, Nedungadi TP, Cunningham JT. Angiotensin II induces membrane trafficking of natively expressed transient receptor potential vanilloid type 4 channels in hypothalamic 4B cells. *American journal of physiology Regulatory, integrative and comparative physiology*. 2014; 307: R945-55.
34. Johnson AK. The periventricular anteroventral third ventricle (AV3V): Its relationship with the subfornical organ and neural systems involved in maintaining body fluid homeostasis. *Brain research bulletin*. 1985; 15: 595-601.

35. Prager-Khoutorsky M, Bourque CW. Mechanical basis of osmosensory transduction in magnocellular neurosecretory neurones of the rat supraoptic nucleus. *J Neuroendocrinol.* 2015; 27: 507-15.
36. Prager-Khoutorsky M, Khoutorsky A, Bourque CW. Unique interweaved microtubule scaffold mediates osmosensory transduction via physical interaction with TRPV1. *Neuron.* 2014; 83: 866-78.
37. Verbalis JG, Mangione MP, Stricker EM. Oxytocin produces natriuresis in rats at physiological plasma concentrations. *Endocrinology.* 1991; 128: 1317-22.
38. Soares TJ, Coimbra TM, Martins AR, Pereira AG, Carnio EC, Branco LG, Albuquerque-Araujo WI, de Nucci G, Favaretto AL, Gutkowska J, McCann SM, Antunes-Rodrigues J. Atrial natriuretic peptide and oxytocin induce natriuresis by release of cGMP. *Proceedings of the National Academy of Sciences of the United States of America.* 1999; 96: 278-83.

DISSERTATION PERSPECTIVES AND SIGNIFICANCE

Arginine Vasopressin (AVP) plays a major role in regulating body fluid and electrolyte homeostasis. In spite of vast existing knowledge on the regulation of AVP secretion, mechanisms contributing to inappropriate increase in AVP secretion during osmotic stress are not completely understood. These studies explored a possible mechanism in the context of salt loading and liver failure in male rats. During salt loading, AVP is released into systemic circulation although mean arterial pressure is elevated. Similarly, AVP secretion is high despite lower plasma osmolality during liver failure. The major results from these projects are outlined below.

SALT LOADING INDUCED AVP SECRETION

Salt loading (SL) male rats with 2% salt for 7 days causes hypernatremia and a sustained increase in AVP secretion. The first part of the specific aim 1 is intended to determine if the supraoptic nucleus (SON) is the source of brain derived neurotrophic factor (BDNF) that leads to increases in AVP secretion and mean arterial pressure during SL. The major findings of this study are that shRNA against BDNF successfully prevents the increase in BDNF and AVP gene expression induced by SL. Virally mediated BDNF knockdown in the SON of SL rats prevents the increase in tyrosine receptor kinase B (TrkB) phosphorylation and decrease in K^+/Cl^- Co-transporter 2 (KCC2) phosphorylation. Plasma osmolality, hematocrit and AVP concentration are decreased in SL rats with the BDNF knockdown. Also, blocking the increase in BDNF in the SON produced natriuresis in salt loaded rats. However, BDNF knockdown in the SON was not sufficient to prevent the salt loading induced increase in mean arterial pressure (Figure 1).

SALT LOADING INDUCED INCREASE IN INTRACELLULAR CHLORIDE CONCENTRATION

Salt loading impairs GABA_A mediated inhibition of AVP neurons in the SON of hypothalamus through increase in intracellular chloride concentration ([Cl]_i). The second part of specific aim 1 is to determine if a TrkB-KCC2 mediated mechanism contributes to an increase in intracellular chloride concentration in SON AVP neurons of SL rats. Pharmacological antagonists were used to understand the role of TrkB receptor and chloride co-transporters in increasing [Cl]_i in SL rat AVP neurons. The effect of these antagonists on [Cl]_i during GABA_A inhibition was studied using focal application of the GABA_A agonist muscimol.

The important outcomes from this study are muscimol application causes an increase in [Cl]_i indicating influx of chloride ion in Eu rat neurons whereas in SL rat neurons the muscimol application causes decrease in [Cl]_i indicating efflux of chloride ion. This shows the GABA_A mediated inhibition is impaired during SL. The reversal of chloride flux progressively switches GABA_A mediated hyperpolarization to depolarization. The TrkB antagonist blocked the muscimol induced chloride efflux in SL rats (Figure 1). The KCC2 antagonist did not have any effect on the SL rats as KCC2 was already downregulated during SL. As the KCC2 cotransporter expression in the AVP neuron has been controversial, the KCC2 protein expression was correlated with the chloride imaging data. The results show that KCC2 and β-Actin expression is found in the neurons that responded to muscimol during chloride imaging.

LIVER FAILURE INDUCED AVP SECRETION

Specific aim 2 of the dissertation focused on understanding clinically relevant increase in AVP secretion. In this study, we used chronic bile duct ligated (BDL) rats as animal model of

dilutional hyponatremia associated with liver failure. The results and approaches from specific aim 1 were used to determine the role of a BDNF-TrkB- KCC2 mechanism in the development of hyponatremia and increased AVP secretion during liver failure. The major findings from this study are that bile duct ligation causes increased phosphorylation of TrkB receptor and decreased phosphorylation of KCC2 co-transporter. The BDNF knockdown in the SON inhibits the TrkB receptor activation and KCC2 downregulation (Figure 1). The plasma measurements mirror the protein expression data. Blocking the BDNF in SON of BDL rats causes increased plasma osmolality and hematocrit values and prevents the rats from developing hyponatremia. Also, the copeptin secretion decreases in BDL rats with shRNA against BDNF in the SON. In addition, knockdown of BDNF in the SON is associated with reduced thirst and urine excretion associated with liver failure.

SIGNIFICANCE

Taken together, these results demonstrate that loss of GABA_A inhibition through a BDNF-TrkB-KCC2 pathway in the SON contributes to increased AVP secretion during salt loading and liver failure in male rats. It is interesting to note that while the BDNF from the SON is essential for increased AVP secretion during SL, it is not necessary for the increase in mean arterial pressure. This indicates the involvement of other mechanisms, in addition to SON-dependent AVP release, that could contribute to the observed increase in MAP during high salt loading. A subset of neurons that responded during chloride imaging had KCC2 expression. The TrkB-KCC2 dependent mechanism contributes to the increases in [Cl]_i and impairment of GABA_A mediated inhibition of SON AVP neurons from SL rats. The BDNF from the SON contributes to the increase in AVP secretion and fluid retention resulting in hyponatremia during liver failure. This

could eventually lead to the discovery of biomarkers or new treatments for hyponatremia in liver failure patients.

CHAPTER V - Figure V-1 – Schematic representation of specific aims with results

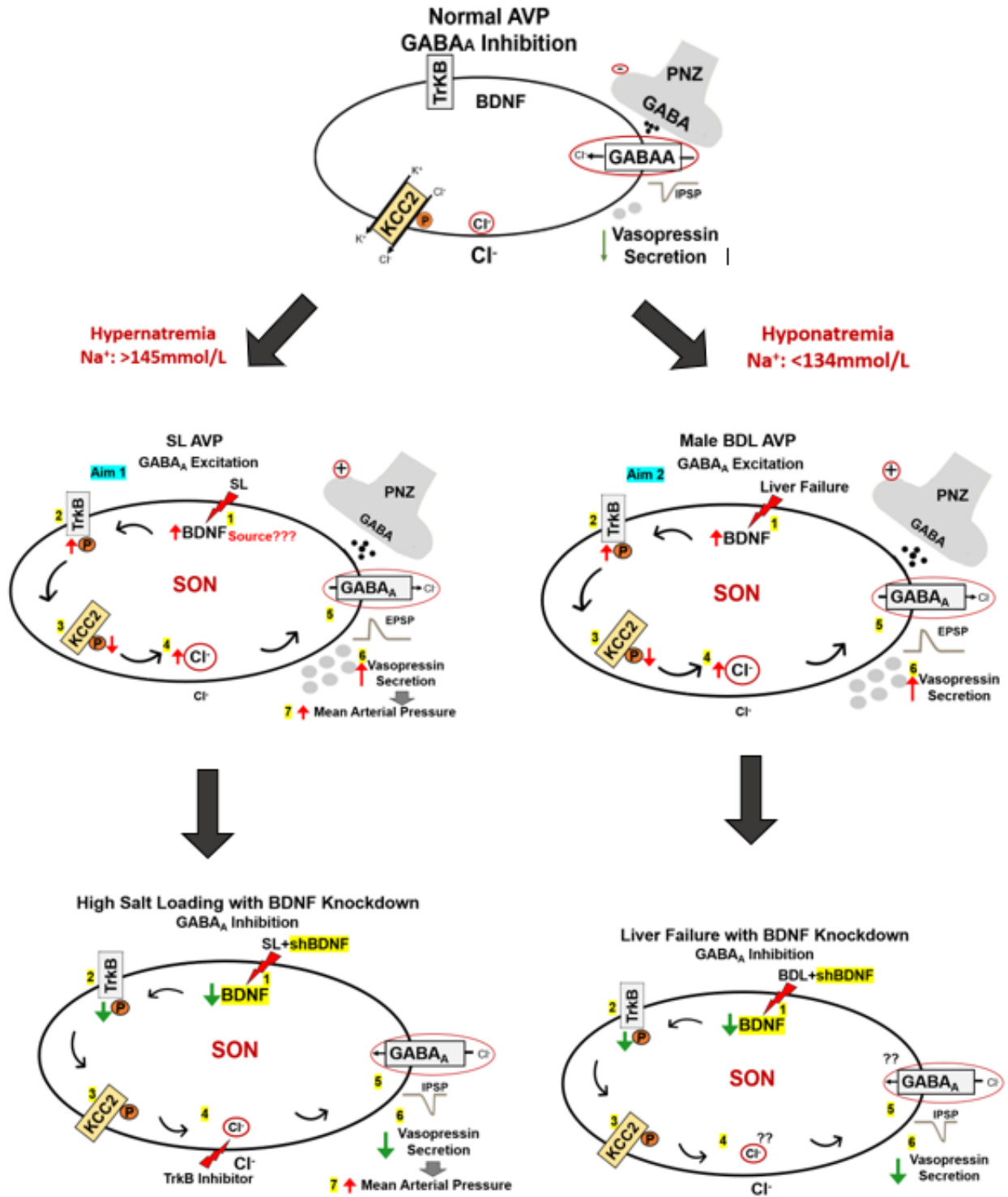


Figure 1: Schematic representation of specific aims with important results from the dissertation. Regulatory mechanism in normal vasopressin neuron (top); Regulatory mechanism in salt loaded male rats (middle, left; specific aim 1a and 1b); the results of BDNF knockdown in the SON in salt loaded male rats (bottom, left; specific aim 1a and 1b); bile duct ligation (BDL) in male rats leading to dilutional hyponatremia (middle, right; specific aim 2); the results of BDNF knockdown in the SON in male bile duct ligated rats (bottom, right; specific aim 2).

FUTURE DIRECTIONS

ROLE OF OXYTOCIN IN SALT LOADING

The results from this dissertation indicate that the SON neurons are the source of BDNF causing dysregulation of AVP neurons during salt loading (SL). However, the results cannot conclude whether the source is AVP or oxytocin or both neuronal types in the SON. Previous studies have shown that hypertonic saline can activate hypothalamic oxytocin neurons in addition to arginine vasopressin (AVP) neurons ^(1,2). Oxytocin at high concentrations can induce natriuresis ^(3,4) which could potentially be involved in the observed increase in urine sodium excretion in salt loaded rats with BDNF knockdown. It would be interesting to note in future studies whether oxytocin expression within the SON is similarly affected by shBDNF.

INCREASED BLOOD PRESSURE IN SALT LOADED RATS

Although BDNF knockdown in the SON inhibited the increase in AVP secretion, it was not sufficient to prevent the SL induced increase in mean arterial pressure (MAP). It is known that activation of osmoreceptors excites preautonomic neurons and enhance sympathetic tone ^(5,6). More studies will be required to assess the contribution of the sympathetic nervous system by determining the effects of ganglionic blockers in the sustained MAP response. Additionally, AVP that is dendritically released from magnocellular secretory neurons in the PVN has been shown to increase sympathetic outflow ⁽⁷⁾. This mechanism would not have been influenced by the AAV injections in the SON and could still contribute to the increase in MAP associated with salt loading. The role of AVP from PVN neurons in increase in MAP during SL will be addressed in future studies by injecting shRNA against BDNF in both SON and PVN.

POTENTIAL SYNAPTIC MECHANISM

This dissertation did not address synaptic mechanisms that could potentially influence BDNF mediated activation of TrkB receptors in the SON during SL and liver failure. As the noradrenergic projections from the brainstem are involved in both osmotic and non-osmotic activation of AVP neurons⁽⁸⁻¹⁶⁾, these projections could stimulate BDNF release in the SON. This could be tested by using the catecholamine specific toxins to disrupt the norepinephrine inputs to SON in bile duct ligated (BDL) rats and will be the focus of future studies.

MEMBRANE EXPRESSION OF KCC2

It is understood from the previous studies that phosphorylation of KCC2 at Ser940 stabilizes the co-transporter in cell membrane⁽¹⁷⁻²⁰⁾. Our results show the decrease in phosphorylation of KCC2 during SL and liver failure is inhibited by injecting shBDNF in the SON. Though this posttranslational modification correlates with the intracellular [Cl]_i measured in our experiments, the membrane expression was not directly tested. This will be verified in verified in future studies using cell fractionation methods.

ROLE OF BDNF IN THIRST

The studies from this dissertation shows that BDNF knockdown decreased fluid intake in BDL rats but not in SL rats⁽²¹⁾. The difference in this behavioral response between the two animal models of osmotic stress is not clear and several possibilities for this variation are discussed in earlier sections. The most important of which is the effect of BDNF knockdown on the transduction mechanisms in the osmoreceptors located in the SON as the transduction mechanisms during hypernatremia and hyponatremia are known to involve different TRPV

channels ⁽²²⁻²⁶⁾. Additional experiments are required to understand the role of BDNF in thirst at varying osmolalities.

REFERENCES

1. Fisher DA, Weitzman RE, Glatz TH. The Effect of Hemorrhage and Hypertonic Saline upon Plasma Oxytocin and Arginine Vasopressin in Conscious Dogs*. *Endocrinology*. 1978; 103: 2154-60.
2. Haanwinckel MA, Elias LK, Favaretto AL, Gutkowska J, McCann SM, Antunes-Rodrigues J. Oxytocin mediates atrial natriuretic peptide release and natriuresis after volume expansion in the rat. *Proceedings of the National Academy of Sciences*. 1995; 92: 7902-6.
3. Verbalis JG, Mangione MP, Stricker EM. Oxytocin produces natriuresis in rats at physiological plasma concentrations. *Endocrinology*. 1991; 128: 1317-22.
4. Soares TJ, Coimbra TM, Martins AR, Pereira AG, Carnio EC, Branco LG, Albuquerque-Araujo WI, de Nucci G, Favaretto AL, Gutkowska J, McCann SM, Antunes-Rodrigues J. Atrial natriuretic peptide and oxytocin induce natriuresis by release of cGMP. *Proceedings of the National Academy of Sciences of the United States of America*. 1999; 96: 278-83.
5. Choe KY, Han SY, Gaub P, Shell B, Voisin DL, Knapp BA, Barker PA, Brown CH, Cunningham JT, Bourque CW. High salt intake increases blood pressure via BDNF-mediated downregulation of KCC2 and impaired baroreflex inhibition of vasopressin neurons. *Neuron*. 2015; 85: 549-60.
6. Toney GM, Stocker SD. Hyperosmotic activation of CNS sympathetic drive: implications for cardiovascular disease. *The Journal of Physiology*. 2010; 588: 3375-84.
7. Son SJ, Filosa JA, Potapenko ES, Biancardi VC, Zheng H, Patel KP, Tobin VA, Ludwig M, Stern JE. Dendritic Peptide Release Mediates Interpopulation Crosstalk between Neurosecretory and Preautonomic Networks. *Neuron*. 2013; 78: 10.1016/j.neuron.2013.04.025.

8. Bourque CW. Central mechanisms of osmosensation and systemic osmoregulation. *Nat Rev Neurosci.* 2008; 9: 519-31.
9. Cunningham JT, Penny ML, Murphy D. Cardiovascular regulation of supraoptic neurons in the rat: synaptic inputs and cellular signals. *Prog Biophys Mol Biol.* 2004; 84: 183-96.
10. Leng G, Brown CH, Bull PM, Brown D, Scullion S, Currie J, Blackburn-Munro RE, Feng J, Onaka T, Verbalis JG, Russell JA, Ludwig M. Responses of magnocellular neurons to osmotic stimulation involves coactivation of excitatory and inhibitory input: an experimental and theoretical analysis. *J Neurosci.* 2001; 21: 6967-77.
11. Verbalis JG. Osmotic Inhibition of Neurohypophysial Secretion. *Annals of the New York Academy of Sciences.* 1993; 689: 146-60.
12. Choe KY, Trudel E, Bourque CW. Effects of Salt Loading on the Regulation of Rat Hypothalamic Magnocellular Neurosecretory Cells by Ionotropic GABA and Glycine Receptors. *J Neuroendocrinol.* 2016; 28.
13. Brown CH, Bains JS, Ludwig M, Stern JE. Physiological regulation of magnocellular neurosecretory cell activity: integration of intrinsic, local and afferent mechanisms. *J Neuroendocrinol.* 2013; 25: 678-710.
14. Grindstaff RJ, Grindstaff RR, Cunningham JT. Baroreceptor sensitivity of rat supraoptic vasopressin neurons involves noncholinergic neurons in the DBB. *American journal of physiology Regulatory, integrative and comparative physiology.* 2000; 279: R1934-43.
15. Grindstaff RR, Cunningham JT. Cardiovascular regulation of vasopressin neurons in the supraoptic nucleus. *Exp Neurol.* 2001; 171: 219-26.
16. Renaud LP, Jhamandas JH, Buijs R, Raby W, Randle JC. Cardiovascular input to hypothalamic neurosecretory neurons. *Brain research bulletin.* 1988; 20: 771-7.

17. Toda T, Ishida K, Kiyama H, Yamashita T, Lee S. Down-Regulation of KCC2 Expression and Phosphorylation in Motoneurons, and Increases the Number of in Primary Afferent Projections to Motoneurons in Mice with Post-Stroke Spasticity. *PloS one*. 2015; 9: e114328.
18. Roussa E, Speer JM, Chudotvorova I, Khakipoor S, Smirnov S, Rivera C, Krieglstein K. The membrane trafficking and functionality of the K⁺-Cl⁻ co-transporter KCC2 is regulated by TGF-β₂. *Journal of cell science*. 2016; 129: 3485-98.
19. Watanabe M, Wake H, Moorhouse AJ, Nabekura J. Clustering of neuronal K⁺-Cl⁻ cotransporters in lipid rafts by tyrosine phosphorylation. *The Journal of biological chemistry*. 2009; 284: 27980-8.
20. Wright R, Newey SE, Ilie A, Wefelmeyer W, Raimondo JV, Ginham R, McLlhinney RAJ, Akerman CJ. Neuronal Chloride Regulation via KCC2 Is Modulated through a GABA(B) Receptor Protein Complex. *The Journal of neuroscience : the official journal of the Society for Neuroscience*. 2017; 37: 5447-62.
21. Balapattabi K, Little JT, Farmer GE, Cunningham JT. High salt loading increases brain derived neurotrophic factor in supraoptic vasopressin neurones. *J Neuroendocrinol*. 2018; 30: e12639.
22. Carreño FR, Ji LL, Cunningham JT. Altered central TRPV4 expression and lipid raft association related to inappropriate vasopressin secretion in cirrhotic rats. *American Journal of Physiology - Regulatory, Integrative and Comparative Physiology*. 2009; 296: R454-R66.
23. Gizowski C, Bourque CW. The neural basis of homeostatic and anticipatory thirst. *Nature Reviews Nephrology*. 2017; 14: 11.

24. Prager-Khoutorsky M, Bourque CW. Mechanical basis of osmosensory transduction in magnocellular neurosecretory neurones of the rat supraoptic nucleus. *J Neuroendocrinol.* 2015; 27: 507-15.
25. Prager-Khoutorsky M, Khoutorsky A, Bourque CW. Unique interweaved microtubule scaffold mediates osmosensory transduction via physical interaction with TRPV1. *Neuron.* 2014; 83: 866-78.
26. Saxena A, Bachelor M, Park YH, Carreno FR, Nedungadi TP, Cunningham JT. Angiotensin II induces membrane trafficking of natively expressed transient receptor potential vanilloid type 4 channels in hypothalamic 4B cells. *American journal of physiology Regulatory, integrative and comparative physiology.* 2014; 307: R945-55.

APPENDIX I

To be submitted to Endocrinology in June 2019

SEX DIFFERENCE AND HORMONES IN THE REGULATION OF VASOPRESSIN
SECRETION DURING DILUTIONAL HYPONATREMIA

Kirthikaa Balapattabi, Joel T Little, Martha Bachelor, Rebecca L. Cunningham, PhD and J.

Thomas Cunningham, PhD

ABSTRACT

Dilutional hyponatremia due to elevated arginine vasopressin (AVP) secretion increases mortality in patients with liver failure. No previous studies have addressed sex difference in dilutional hyponatremia in animal models of liver failure. The aim of this study is to investigate potential sex differences in dilutional hyponatremia and the effect of ovarian hormones on AVP secretion. We used chronic bile duct ligated (BDL) rats, a model of dilutional hyponatremia associated with liver failure.

Adult male, female and ovariectomized (OVX) female Sprague Dawley rats were used. After two weeks, the rats had BDL or sham ligation surgery. Four weeks later, the brains were processed for immunohistochemistry analysis of FosB and AVP expression. Blood samples were collected to measure plasma osmolality, hematocrit, circulating estradiol and copeptin concentration. Copeptin was used as biomarker for plasma AVP. Liver weight, body weight, and fluid accumulation were recorded to verify if the rats developed liver failure and ascites. Data were analyzed by two-way ANOVA with Bonferroni post hoc comparisons.

All the BDL rats had ascites and significantly increased liver to body weight ratios compared to sham rats indicative of liver failure. Male BDL rats had hyponatremia along with significant increases in plasma copeptin and FosB expression in Supraoptic AVP neurons compared to male shams (all $p < 0.05$; 5-7). Unlike male BDL rats, the female BDL rats did not become hyponatremic and did not demonstrate increased Supraoptic AVP neuron activation or copeptin secretion compared to female shams.

Ovariectomy significantly decreased plasma estradiol concentration in sham rats compared to intact female sham ($p < 0.05$; 6-10). However, circulating estradiol concentration was

significantly elevated in ovariectomized BDL (OVX BDL) rats compared to the ovariectomized sham (OVX sham) and female sham rats ($p < 0.05$; 6-10). To identify a possible source of estradiol contributing to the observed increase in OVX BDL rats, adrenal glands were collected at the end of protocol. Adrenal gland steroids were extracted to measure estradiol and its precursors, testosterone and DHEA concentration.

The OVX BDL rats had significantly increased adrenal estradiol along with significantly decreased adrenal testosterone and DHEA compared to OVX sham rats (all $p < 0.05$; 6-7). Plasma osmolality, hematocrit and copeptin concentration were not different between OVX BDL and OVX sham rats. Our results show that unlike male BDL rats, female BDL rats did not develop hyponatremia, supraoptic AVP neuron activation, or increased copeptin secretion compared to sham ligated females. Female OVX BDL rats did not become hyponatremia or increased copeptin secretion compared to female OVX sham rats. It is possible that the increase in adrenal estradiol compensated for the lack of ovarian estrogens in OVX BDL rats. Additional experiments will be required to determine the effects of estrogen in this model.

Supported by R01 HL119458 and 18PRE34060035

MATERIALS AND METHODS

ANIMALS

Adult male and female Sprague-Dawley rats (Charles River, Wilmington, MA) were used in the experiments for this study. Experimental protocols involving animals were approved by the UNT Health Science Center IACUC and conducted in accordance to the National Institute of Health *Guide for the Care and Use of Laboratory Animals*. All animals were housed in a temperature (24-26 °C) and humidity (40-60%) controlled environment with *ad libitum* access to food (Teklad LM-485 Rat Sterilizable Diet with 0.3% Sodium, Envigo, Somerset, NJ) and water unless otherwise indicated. Rats were individually housed due to the use of survival surgery and individual fluid intake measurements in the protocol. Survival surgeries were conducted using aseptic techniques. All rats were given procaine penicillin G (30,000 U, sc) and non-steroidal anti-inflammatory drug, carprofen (Rimadyl, 2 mg po), was given before and after surgery for pain management.

BILATERAL OVARIECTOMY

Prior to ovariectomy, female rats were anaesthetized with isoflurane (2-3%). The left side of the abdomen was shaved, cleaned and incision was created. Ovary and uterine horn were identified and exposed. The ovary was cut by gently pulling it out by grabbing the surrounding adipose tissue to prevent detachment of a small piece of ovary, which may fall into the abdominal cavity where it may be replanted to carry on its normal function ⁽¹⁾. The fallopian tube was cauterized, and the remaining tissue was put back into the abdominal cavity. The incision was closed with absorbable antibiotic sutures. The procedure was repeated on the right side to remove the other ovary ⁽²⁾. Two weeks later, the rats received either bile duct ligation or sham ligation surgery.

BILE DUCT LIGATION SURGERY

The rats were anaesthetized with isoflurane (2-3%). The abdomen was shaved and cleaned. A midline abdominal incision was performed, and the common bile duct was isolated and cauterized between two ligatures as previously described^(3,4). Visual inspection of ascetic fluid in the peritoneal cavity was performed daily after surgery. Any rat showing morbidity or ascites of greater than 10% of the body weight was euthanized (Inactin 100 mg/kg ip). Sham rats received the same surgical procedure except their bile duct was not cauterized. Liver to body weight ratio was determined at the end of the study for verification of liver failure development.

PLASMA MEASUREMENTS

Trunk blood was collected from each rat after decapitation and plasma was collected for measuring plasma osmolality, hematocrit, copeptin, and estradiol concentration. Copeptin (CPP) is widely used as biomarker for AVP secretion⁽⁵⁾ and was measured in this study in addition to AVP. A 5 to 6 ml sample of blood was collected in Vacutainer tubes containing the anticoagulant, EDTA (12 mg). The proteinase inhibitor, aprotinin (0.6 TIU/ml of blood; Phoenix Pharmaceuticals, Inc, Burlingame, CA) was added to each sample. The samples were centrifuged at 1600 g for 15 minutes at 4° C. CPP and estradiol concentrations were measured in plasma samples by using specific ELISAs according to the manufacturer's instructions (CPP: MBS724037, MyBioSource, Inc, San Diego, CA; Estradiol: BioVendor Research and Diagnostic Products, Asheville, NC). Four parametric logistic analysis (4-PL) was performed to quantify the concentration of CPP.

A separate 1 to 2 ml sample of blood was collected in 2 ml microcentrifuge tube and prepared for measuring plasma osmolality and hematocrit as previously described^(6,7). Two heparinized

capillary tubes (Fisher Scientific, Hampton, NH) were filled with blood for measuring hematocrit using Micro-Hematocrit capillary tube reader (Lancer, St. Louis, MO). The remaining blood sample was centrifuged at 1600 g for 5-10 minutes and plasma was collected to measure plasma osmolality using vapor pressure osmometer (Wescor, Logan, UT).

IMMUNOHISTOCHEMISTRY

Four weeks after bile duct ligation surgery, rats were deeply anesthetized with inactin (100 mg/kg, ip.), perfused transcardially with phosphate-buffered saline (PBS) followed by 4% paraformaldehyde in PBS. After the perfusion, brains were extracted from the skull and placed in 30% sucrose until dehydrated. The brains were serial sectioned at a thickness of 40 μ m using a cryostat. Sections were processed for FosB and AVP using goat polyclonal FosB (Santa Cruz Biotechnology, Cat# sc-48-G Santa Cruz, CA; 1:1000), guinea pig polyclonal Anti-(Arg⁸)-VP (1:1000; Cat# T-5048 Peninsula Labs, San Carlos, CA). Sections were incubated in primary antibodies for two days at 4°C. Following primary antibody incubation, sections were then rinsed with PBS, followed by sequential incubation in respective secondary antibodies against host species. Biotinylated anti-goat secondary (1:1000, Jackson ImmunoResearch Laboratories, Inc. West Grove, PA) was used for FosB to visualize using 3,3'-diaminobenzidine hydrochlorides. The Cy3 fluorophores (Cy3-conjugated anti-guinea pig IgG (1:10000; Cat 706-165-148, Jackson ImmunoResearch Laboratories, Inc) was used for AVP. Sections were rinsed again in PBS, mounted on gelatin coated slides, and cover slipped with Vectashield (Vecta Labs, Burlingame, CA) mounting media. Sections were examined for co-localization of the FosB with AVP immunofluorescence to determine the activation of AVP neurons.

ADRENAL GLAND STEROID MEASUREMENTS

After four weeks of bile duct ligation surgery, the adrenal glands from ovariectomized female rats were collected and flash frozen using dry ice. The frozen (-80°C) adrenal tissue was thawed, weighed, and homogenized using acetonitrile. The steroids were extracted from tissue samples by organic phase extraction using acetonitrile to solubilize the steroid and hexane to remove fat and lipid that may be present in the sample. The steroid separated in acetonitrile phase was evaporated to dryness using vacuum centrifugal concentrator (8). The dried extracted samples were diluted in ethanol: assay buffer mixture (1:10). The reconstituted samples were used to measure DHEA, testosterone and estradiol concentration using specific ELISAs according to the manufacturer's instructions (DHEA: Enzo Life Sciences, Inc., Farmingdale, NY; Testosterone: BioVendor Research and Diagnostic Products).

EXPERIMENTAL GROUPS AND STATISTICAL ANALYSIS

The male, female and OVX rats were subdivided into two groups in these experiments: 1) Sham ligation and 2) BDL. The adrenal steroid concentration data from OVX sham and BDL rat was analyzed using Student's t-test. All other data were analyzed using two-way ANOVA with treatment (sham vs. BDL) as first factor and sex (male vs. female vs. OVX) as second factor followed by Bonferroni post-hoc comparisons using Sigma Plot 12.0. Figures were assembled using the 'magick' package in RStudio. The group sizes were determined by power analysis and effect size calculated from our previously published work^(4, 6, 9) and preliminary data using Sigma plot 12.0. The minimal n's per group for each experiment was decided to have an appropriately powered study with the effect size of approximately 0.7 (70%).

RESULTS

EFFECT OF BDL IN MALE AND FEMALE RATS

CHANGES IN LIVER TO BODY WEIGHT RATIO

The liver weight was measured four weeks after BDL/ sham ligation surgery. The increase in liver weight is widely used as a biomarker to verify the liver failure animal model^(4, 10). The liver to body weight ratio was increased in both male and female BDL rats compared to their respective sham ligated groups. The increase in liver to body weight ratio indicates that both the male and female BDL rats develop liver failure. Two- way ANOVA indicates significant difference between the groups ($F(2, 45) = 3.36, p < 0.05$). Bonferroni post hoc analysis indicates that the liver weight was significantly increased in male BDL rats compared to the male sham rats (Bonferroni $t = 5.703; p < 0.001$; Figure 1A). Similar increase was in female BDL rats compared to the female sham rats (Bonferroni $t = 11.517; p < 0.001$; Figure 1A). The liver weights were not significantly different between male and female BDL groups. This data shows that there was no sex difference in the development of liver failure disease with the bile duct ligation.

CHANGES IN PLASMA OSMOLALITY, VOLUME AND COPEPTIN

Plasma osmolality, hematocrit, and CPP concentration were measured four weeks after BDL/ sham ligation surgery. The decrease in plasma osmolality and hematocrit values in BDL rats indicates development of hyponatremia with bile duct ligation. The statistical analysis using two-way ANOVA shows that the first factor treatment is significantly different between some of the groups (Osmolality: $F(1, 44) = 8.671, p < 0.05$; Hematocrit: $F(1, 46) = 16.754, p < 0.05$; CPP: $F(1, 32) = 13.219$). The second factor sex did not have any significant effect on the osmolality

and hematocrit. The plasma CPP concentration was significantly different between male and female rats in both sham and BDL groups ($F(2, 32) = 40.489$; Bonferroni t tests, all $p < 0.05$).

Bonferroni multiple comparisons indicate that the male BDL rats had significantly decreased plasma osmolality and hematocrit values as compared to male Sham rats (Osmolality: Bonferroni $t = 2.890$; $p < 0.05$; Hematocrit: Bonferroni $t = 3.096$; $p < 0.05$; Figure 1B & 1C). Similar decreases were not observed between female BDL and sham (Figure 1B & 1C). Similarly, the concentration of CPP in male BDL rats was significantly increased compared to the male sham rats (Bonferroni $t = 3.096$; $p < 0.05$; Figure 1D). This increase in plasma CPP values was not seen in the female BDL rats (Figure 1D).

FosB AND AVP EXPRESSION IN SON NEURONS

FosB expression was measured in the SON of male and female sham and BDL rats (Figure 2A). It is well established that the increase in FosB expression indicates neuronal activation⁽⁴⁾. The neurons were double labeled with AVP to record AVP expression (Figure 2B) and localize FosB expression in AVP neurons (Figure 2C). The co-localization of FosB in the AVP neurons was measured in the sections from male sham and BDL rats. FosB expression in SON AVP neurons was increased in both male and female BDL rats compared to their respective shams. In male BDL rats, 59% of the FosB positive cells were vasopressinergic compared with 14% in sham ligated controls. The FosB expression was co-localized in AVP neurons in male BDL rats whereas in female BDL rats the FosB was not co-localized in AVP neurons. The 24% of the FosB positive neurons were colocalized with AVP compared with 19% in sham rats. The number of FosB and AVP co-localized neurons in female BDL rats was not significantly increased compared to the female shams (Figure 2D).

EFFECT OF BDL IN OVARIECTOMIZED FEMALE RATS

The following experiments were performed in ovariectomized rats to understand the role of estradiol in development of hyponatremia and increase in AVP secretion during liver failure. The male and female group data are represented again in the following sections along with the OVX groups for easier comparison.

CHANGES IN LIVER TO BODY WEIGHT RATIO

Two weeks later ovariectomy, the OVX rats undergo BDL/sham surgery. After four weeks of BDL/ sham ligation, the liver weight was measured. The increase in liver weight indicates the bile duct ligation surgery was successful and the rats develop liver failure^(4, 10). The liver to body weight ratio was very high in OVX BDL rats compared to their sham rats. The increase in liver to body weight ratio indicates the OVX BDL rats develop liver failure similar to the male and female BDL rats. The two-way ANOVA followed by post-hoc analysis indicates that the liver weight was significantly increased in OVX BDL rats compared to the OVX sham rats (Bonferroni $t = 9.995$; $p < 0.001$; Figure 3A). The liver to body weight of OVX BDL rats was similar to the male and female BDL rats.

PLASMA ESTRADIOL CONCENTRATION

Plasma estradiol concentration was measured in the OVX sham and BDL rats to compare the values with intact female sham and BDL rats and verify the efficiency of ovariectomy procedures. Plasma estradiol concentration was minimal in OVX sham rats compared to the intact female sham rats. This indicates the ovariectomy procedures were successful. However, the bile duct ligation in OVX rats increased the circulating estradiol concentration. Two-way ANOVA indicates significant difference between the groups ($F(1,29) = 42.706$; $p < 0.05$).

Bonferroni comparisons indicates that plasma estradiol concentration was significantly decreased with ovariectomy in sham rats compared to the intact female shams (Bonferroni $t = 2.345$; $p < 0.05$; Figure 3B). The OVX BDL rats showed significant increase in circulating estradiol concentration compared to the OVX sham rats (Bonferroni $t = 6.253$; $p < 0.05$; Figure 3B).

CHANGES IN PLASMA OSMOLALITY, VOLUME AND COPEPTIN

Plasma parameters were measured four weeks after BDL/sham surgery. Unlike the male BDL rats, OVX BDL rats did not develop hyponatremia. The plasma osmolality and hematocrit values were not decreased in OVX BDL rats compared to the OVX sham rats. Also, the OVX BDL rats did not had increase in plasma CPP concentration compared to the OVX sham rats.

The comparison of OVX sham and OVX BDL rats using two-way ANOVA and Bonferroni analysis shows that the plasma osmolality and hematocrit values were not significantly different between OVX sham and OVX BDL rats (Osmolality: Bonferroni $t = 1.350$; $p = 0.184$; Hematocrit: Bonferroni $t = 1.669$; $p = 0.102$; Figure 3C & 3D). The statistical analysis did not show significant increase in plasma CPP concentration in OVX BDL rats compared to the OVX sham rats (Bonferroni $t = 1.519$; $p = 0.139$; Figure 3E). The circulating CPP concentration was significantly different in OVX sham rats compared to male and female sham rats. Also, the CPP concentration in OVX BDL rats was significantly different compared to female rats but not to male rats (Bonferroni t tests, all $p < 0.05$). These data show that bile duct ligation did not affect the plasma parameters of OVX rats similar to that observed in intact female rats.

CHANGES IN ADRENAL STEROID CONCENTRATION

The adrenal steroid was extracted to measure the concentration of estradiol, testosterone and DHEA. Bile duct ligation increased adrenal estradiol concentration in OVX rats compared to the

sham rats. This increase in adrenal estradiol concentration might be contributing to the observed increase in circulating estradiol. In contrast, the concentration of estradiol precursors, testosterone and DHEA were decreased in adrenal glands of OVX BDL rats compared to the OVX sham rats. The decrease in substrates of estradiol synthesis pathway with the increase in the product renders the possibility of increase in enzyme activity.

Student's t-test showed significant increase in adrenal estradiol concentration in OVX BDL rats compared to the OVX sham rats ($t = -5.632$; d.f. = 11; $p < 0.001$; Figure 4A). The adrenal testosterone and DHEA were significantly decreased in the OVX BDL rats compared to the OVX sham rats (Testosterone: $t = 4.685$; d.f. = 11; $p < 0.001$; Figure 4B. DHEA: $t = 2.783$; d.f. = 11; $p < 0.05$; Figure 4C). This data suggests increase in aromatase transcription or activity in the adrenal glands.

REFERENCES

1. Zou W. Ovariectomy (Oophorectomy). 2011.
2. Khajuria DK, Razdan R, Mahapatra DR. Descrição de um novo método de ooforectomia em ratas. *Revista Brasileira de Reumatologia*. 2012; 52: 466-70.
3. Carreño FR, Ji LL, Cunningham JT. Altered central TRPV4 expression and lipid raft association related to inappropriate vasopressin secretion in cirrhotic rats. *American Journal of Physiology - Regulatory, Integrative and Comparative Physiology*. 2009; 296: R454-R66.
4. Cunningham JT, Nedungadi TP, Walch JD, Nestler EJ, Gottlieb HB. Δ FosB in the supraoptic nucleus contributes to hyponatremia in rats with cirrhosis. *American Journal of Physiology - Regulatory, Integrative and Comparative Physiology*. 2012; 303: R177-R85.
5. Balanescu S, Kopp P, Gaskill MB, Morgenthaler NG, Schindler C, Rutishauser J. Correlation of Plasma Copeptin and Vasopressin Concentrations in Hypo-, Iso-, and Hyperosmolar States. *The Journal of Clinical Endocrinology & Metabolism*. 2011; 96: 1046-52.
6. Nedungadi TP, Cunningham JT. Differential regulation of TRPC4 in the vasopressin magnocellular system by water deprivation and hepatic cirrhosis in the rat. *American Journal of Physiology - Regulatory, Integrative and Comparative Physiology*. 2014; 306: R304-R14.
7. Balapattabi K, Little JT, Farmer GE, Cunningham JT. High salt loading increases brain derived neurotrophic factor in supraoptic vasopressin neurones. *J Neuroendocrinol*. 2018; 30: e12639.
8. Rosario ER, Chang L, Head EH, Stanczyk FZ, Pike CJ. Brain levels of sex steroid hormones in men and women during normal aging and in Alzheimer's disease. *Neurobiology of aging*. 2011; 32: 604-13.

9. Choe KY, Han SY, Gaub P, Shell B, Voisin DL, Knapp BA, Barker PA, Brown CH, Cunningham JT, Bourque CW. High salt intake increases blood pressure via BDNF-mediated downregulation of KCC2 and impaired baroreflex inhibition of vasopressin neurons. *Neuron*. 2015; 85: 549-60.
10. Walch JD, Carreño FR, Cunningham JT. Intracerebroventricular losartan infusion modulates angiotensin type 1 receptor expression in the subfornical organ and drinking behaviour in bile duct ligated rats. *Experimental physiology*. 2013; 98: 922-33.

FIGURES

APPENDIX I - Figure I-1 – Parameters of male and female sham/BDL rats

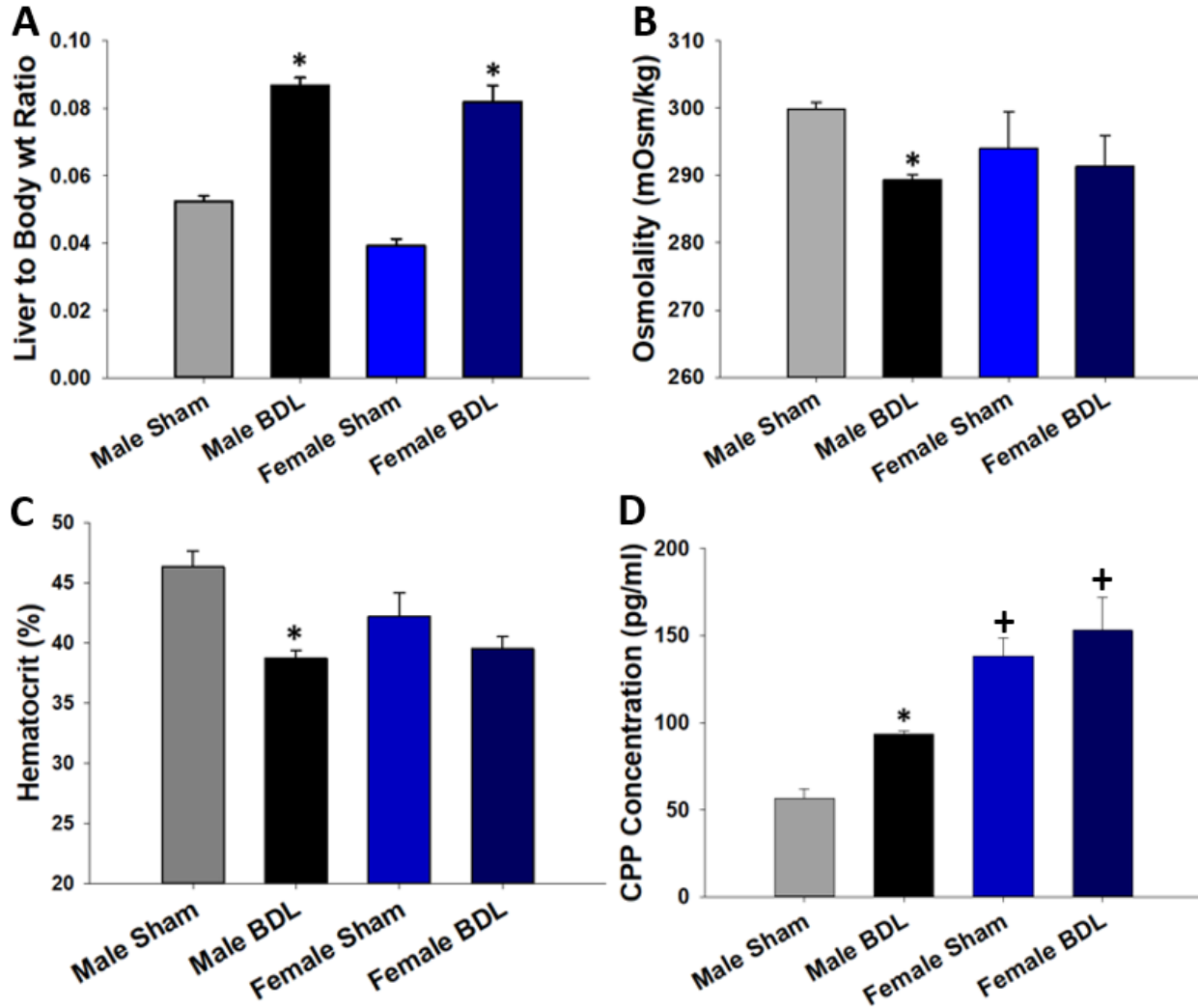


Figure 1: Effect of BDL in male and female rats on **A:** Liver to body weight ratio. **B:** Plasma osmolality. **C:** Hematocrit values. **D:** Plasma CPP concentration. Data are mean \pm SEM.*p < 0.05 vs. respective sham. +p < 0.05 vs. respective male group. Groups: Male Sham (n = 6-7); Male BDL (n = 6); Female Sham (n = 11); Female BDL (n = 9).

APPENDIX I - Figure I-2 – Immunohistochemistry of FosB and AVP expression in SON

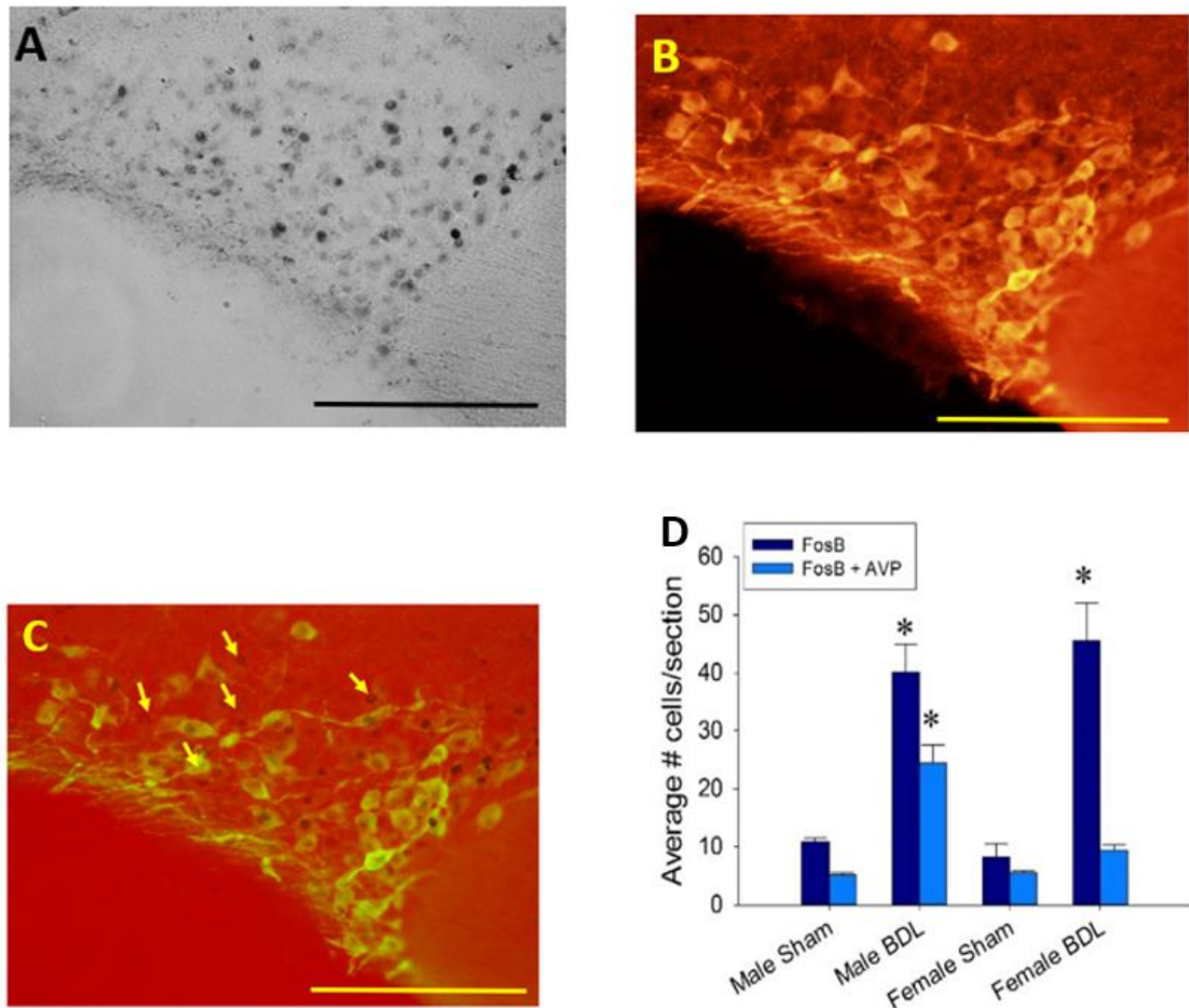


Figure 2: Immunohistochemistry in the SON. **A:** FosB expression in female BDL rats **B:** AVP expression in the same SON section from female BDL rats **C:** Double labelling of FosB and AVP obtained from the merge of A and B. Arrows indicate co-localization of FosB and AVP in female BDL rats **D:** Quantification graph indicating average no. of neurons expressing FosB and FosB+AVP in male sham, male BDL, female sham, female BDL. Data are mean \pm SEM.* $p < 0.05$ vs. respective sham. Groups: Male Sham (n = 7); Male BDL (n = 6); Female Sham (n = 9); Female BDL (n = 9).

APPENDIX I - Figure I-3 – Parameters of female and OVX sham/BDL rats

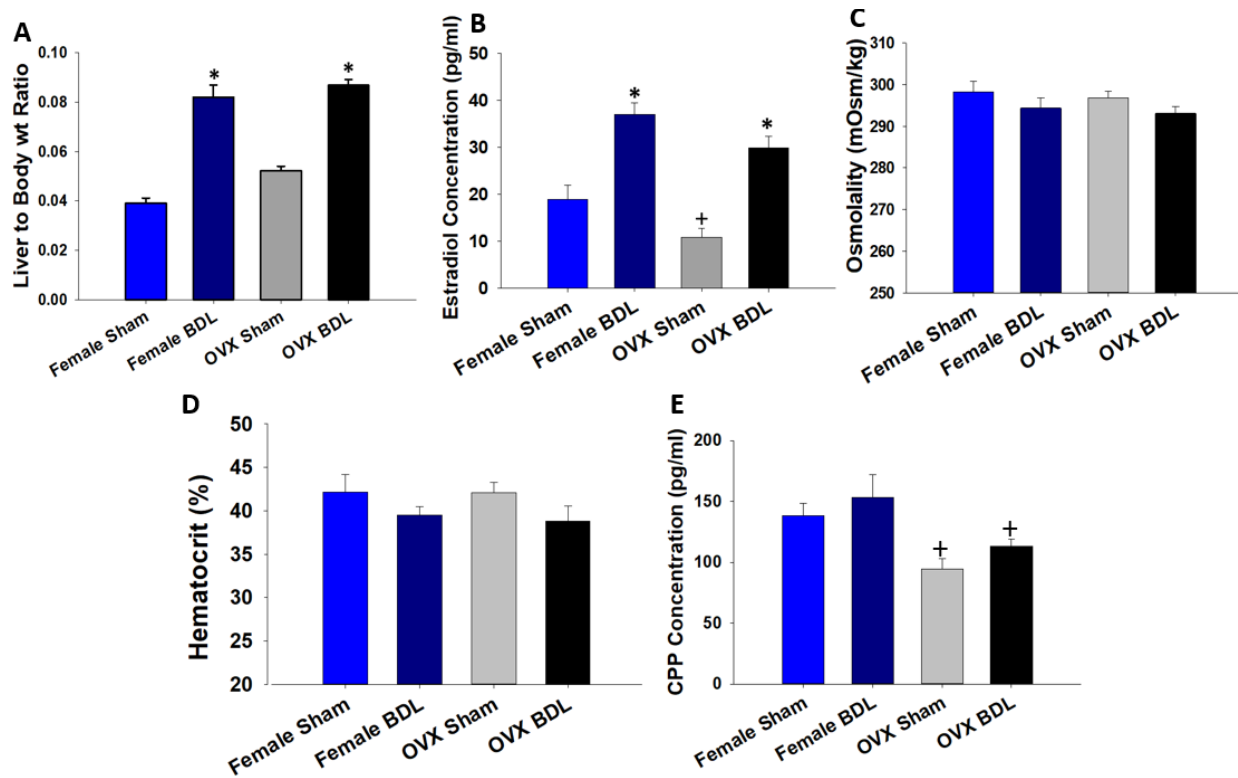


Figure 3: Effect of BDL in female and OVX rats on **A:** Liver to body weight ratio. **B:** Plasma estradiol concentration. **C:** Hematocrit values. **D:** Plasma CPP concentration. **E:** Plasma osmolality. Data are mean \pm SEM. * $p < 0.05$ vs. respective sham. + $p < 0.05$ vs. respective female group. Groups: Female Sham (n = 11); Female BDL (n = 9); OVX Sham (n = 6-9); OVX BDL (n = 6-11). The female sham and BDL rat data shown in this figure 3 are replicated from figure 1 to provide easier visual comparison between female and OVX groups.

APPENDIX I - Figure I-4 – Adrenal steroid concentration in OVX sham/BDL rats

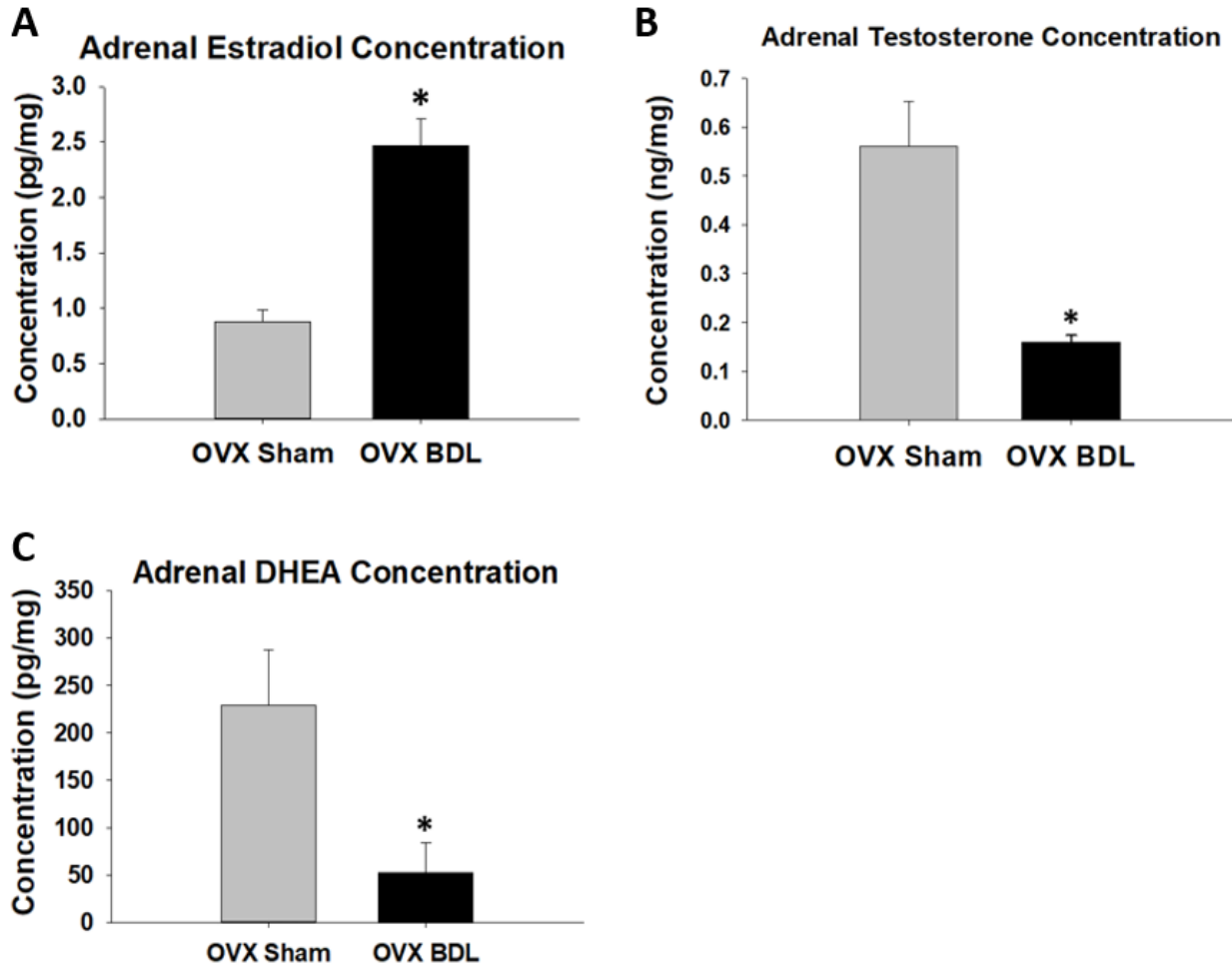


Figure 4: Effect of BDL in adrenal glands of OVX rats. **A:** Adrenal estradiol concentration. **B:** Adrenal testosterone concentration. **C:** Adrenal DHEA concentration. Data are mean \pm SEM.* $p < 0.05$ vs. OVX sham. Groups: OVX Sham (n = 7) and OVX BDL (n = 5).